

# Non-classical heat conduction and the associated thermal stress analysis

by

Wenzhi Yang

A thesis submitted in partial fulfillment of the requirements for the degree of

Doctor of Philosophy

Department of Mechanical Engineering  
University of Alberta

© Wenzhi Yang, 2020

## Abstract

Classical thermoelastic analysis within the framework of classical elasticity and Fourier's heat conduction cannot meet the increasing demand with the rapid development of new technologies and new materials. Fourier heat conduction theory indicates the speed of thermal propagation is infinite, and any disturbance should be felt everywhere instantaneously, which is obviously unphysical as heat dispersion will indeed require a certain time to propagate in the material. The classical Fourier heat conduction is inapplicable particularly for heat conduction involving a very small characteristic length ( $10^{-8}\sim 10^{-6}$  m), very short time scale ( $10^{-11}\sim 10^{-15}$  s), or very low temperature (1-10 K), where the time lag between the heat flux and temperature rise becomes significant. Therefore, non-Fourier heat conduction models have been proposed to account for the time lag between heat dispersion and temperature change, such as the hyperbolic heat conduction theory, dual-phase-lag (DPL) model. Besides, with the wider applications of soft materials, the viscous effect should be taken into consideration in the thermoelastic analysis of the cracked media to characterize the thermal stress concentration induced fracture of the material. Moreover, in the past decades, advanced materials or devices have been downsized to micrometer/nanometer scales. In these scales, the effective thermal and mechanical properties differ significantly than bulk materials, and neither the Fourier heat conduction nor classical continuum mechanics can explain these discrepancies.

Taking the aforementioned, unclassical problems into account, the non-Fourier heat conduction, nonlocal heat conduction, and nonlocal elasticity are introduced in the thermoelastic analysis in this thesis. The main contributions are summarized as follows:

(1) A thermo-viscoelastic model is developed for the crack problem in an infinite, functionally graded half plane under a thermal shock.

(2) A thermoelastic analytical model is established for a functionally graded half-plane containing a crack under a thermal shock in the framework of hyperbolic heat conduction theory.

(3) By extending the fractional calculus to DPL heat conduction theory, the transient thermal-mechanical response in cracked viscoelastic materials under thermal shock is analyzed.

(4) A modified nonlocal DPL theory is formulated to account for the heat conduction at the nanoscale. Both the temporally and spatially nonlocal effects are considered in heat conduction, which are verified experimentally by the size-dependent thermal conductivity of silicon nano-films and the transient temperature variation during the femtosecond laser heating of gold films. A generalized, uncoupled, nonlocal thermoviscoelastic theory is hence proposed.

(5) The interface crack problem between a functionally graded coating and the homogenous substrate is analyzed within the framework of the nonlocal continuum theory. The nonlocal elasticity is extended to interface crack problems under thermal loading for the first time to eliminate the stress singularities at the crack tips and address size effects on the thermoelastic response.

## Preface

This thesis is organized in a paper-based format.

A version of Chapter 2 of this thesis has been published as:

Yang, W. and Chen, Z., 2019. Thermo-viscoelastic response of a cracked, functionally graded half-plane under a thermal shock. *Engineering Fracture Mechanics*, 206, pp.267-277.

A version of Chapter 3 of this thesis has been published as:

Yang, W. and Chen, Z., 2019. Investigation of the thermal-elastic problem in cracked semi-infinite FGM under thermal shock using hyperbolic heat conduction theory. *Journal of Thermal Stresses*, 42(8), pp.993-1010.

A version of Chapter 4 of this thesis has been published as:

Yang, W. and Chen, Z., 2020. Investigation of transient thermal-mechanical behavior of a cracked viscoelastic material using time-fractional dual-phase-lag theory. *Theoretical and Applied Fracture Mechanics*, 106, p.102500.

A version of Chapter 5 of this thesis has been published as:

Yang, W. and Chen, Z., 2020. Nonlocal dual-phase-lag heat conduction and the associated nonlocal thermal-viscoelastic analysis. *International Journal of Heat and Mass Transfer*, 156, p.119752.

A version of Chapter 6 of this thesis is submitted as:

Yang, W. and Chen, Z., 2020. Nonlocal fracture analysis of an interface crack between a functionally graded coating and homogenous substrate under thermal loading.

## Acknowledgements

I would like to express my deepest appreciation and sincere thanks to my supervisor, Dr. Zengtao Chen, for his careful guidance, valuable suggestions, unparalleled support, and excellent supervision during the past four years. His extensive knowledge, enthusiasm and kindly patience will benefit me all my life.

Special thanks to Dr. Xiaodong Wang and Dr. James Hogan for the helpful suggestions you offered, which helps deepen my understanding and get a wider perspective of the research of solid mechanics.

Many thanks to Dr. Xueyang Zhang, Dr. Zhangna Xue, Dr. Amin Pourasghar for your constructive ideas and valuable discussions in the mathematical skills and coding the program.

Above all, I am extremely grateful to my family and all my friendships. Thanks for your long-lasting support and encouragement throughout all these years.

# Table of Contents

Abstract .....	ii
Preface.....	iv
Acknowledgements.....	v
List of Table.....	ix
List of Figures.....	x
Chapter 1: Introduction.....	1
1.1 Motivations.....	1
1.2 Statement of non-classical problems .....	3
1.2.1 Non-Fourier heat conduction.....	3
(1) Hyperbolic (single-phase-lag) heat conduction.....	4
(2) Dual-phase-lag heat conduction.....	5
(3) Fractional heat conduction .....	6
(4) Nonlocal heat conduction.....	7
1.2.2 Thermoviscoelasticity.....	8
1.2.3 Nonlocal Elasticity.....	9
1.3 Methods and Objectives.....	11
1.4 Organization of the thesis .....	12
Chapter 2: Thermo-viscoelastic response of a cracked, functionally graded half-plane under a thermal shock.....	13
2.1 Introduction.....	13
2.2 Statement of the problem and basic equations.....	15
(1) Heat conduction.....	16
(2) Thermal-viscoelastic field equations.....	16
2.3 Thermal stress .....	19
2.4 Numerical results and discussions .....	23
2.5 Conclusions.....	29
2.6 Appendix.....	30
Chapter 3: Investigation of the thermal-elastic problem in cracked semi-infinite FGM under thermal shock using hyperbolic heat conduction theory.....	31
3.1 Introduction.....	31
3.2 Formulation of the problem and basic equations.....	34
(1) Heat conduction equations .....	35

(2) Thermal stress field equations .....	36
3.3 Solution of the temperature field .....	37
3.4 Solution of thermal stress field .....	40
3.5 Numerical results and discussions .....	43
3.6 Conclusions.....	51
3.7 Appendix.....	52
Chapter 4: Investigation of transient thermal-mechanical behavior of a cracked viscoelastic material using time-fractional dual-phase-lag theory .....	53
4.1 Introduction.....	53
4.2 Problem formulation and basic equations.....	56
4.3 Theoretical solutions.....	61
4.3.1 Solutions of temperature field.....	61
4.3.2 Intensity factors of temperature gradient .....	63
4.3.3 Solutions of viscoelastic stresses field.....	64
4.4 Numerical results and discussions .....	67
4.5 Conclusion .....	77
4.6 Appendix.....	78
Chapter 5: Nonlocal dual-phase-lag heat conduction and the associated nonlocal thermal-viscoelastic analysis .....	80
5.1 Introduction.....	80
5.2 Nonlocal DPL model .....	82
5.2.1 Effective thermal conductivity of nanofilms .....	83
5.2.2 Femtosecond laser heating of gold films .....	86
5.3 Generalized nonlocal thermoviscoelasticity .....	89
5.3.1 Formulation of the problem .....	90
5.3.2 Analytical solutions by Laplace transform .....	92
5.4 Results and discussions.....	95
5.5 Conclusions.....	101
Chapter 6: Nonlocal fracture analysis of an interface crack between functionally graded coating and homogenous substrate under thermal loading.....	102
6.1 Introduction.....	102
6.2 Mathematical formulation of the problem .....	104
6.3 Solution procedures .....	109

6.3.1 Solutions of temperature field.....	109
6.3.2 Solutions of the thermal stress field.....	111
6.4 Numerical results and discussions .....	118
6.5 Conclusions.....	126
6.6 Appendix.....	127
Chapter 7: Conclusions and Future Perspectives.....	128
7.1 Conclusions.....	128
7.2 Future Perspectives .....	129
References.....	130

## List of Table

Table 5.1 Material parameters of polymethyl methacrylate.....	95
---	----

## List of Figures

Figure 2.1 Crack geometry and coordinates .....	15
Figure 2.2 Comparison of SIFs in viscoelastic and elastic materials .....	24
Figure 2.3 Variation of the cleavage stress versus angle $\theta$ at time $t = 0.5, t = 2.0$ in elastic and viscoelastic nonhomogeneous materials when $(\beta, \delta, \gamma) = (1, 1, 0.1)$ .....	25
Figure 2.4 Variation of the maximum of cleavage stress versus time in elastic and viscoelastic nonhomogeneous materials when $(\beta, \delta, \gamma) = (1, 1, 0.1)$ .....	25
Figure 2.5 The effect of the graded parameter $\beta$ on the SIFs (a) $K_I$ (b) $K_{II}$ .....	26
Figure 2.6 The effect of the graded parameter $\delta$ on the SIFs (a) $K_I$ (b) $K_{II}$ .....	27
Figure 2.7 The effect of the graded parameter $\gamma$ on the SIFs (a) $K_I$ (b) $K_{II}$ .....	27
Figure 2.8 Comparison of SIFs for two different viscoelastic relaxation functions.....	29
Figure 3.1 Crack geometry and coordinates .....	34
Figure 3.2 The effect of parameter B on the dimensionless temperature variation versus dimensionless time.....	43
Figure 3.3 Dimensionless temperature on crack faces and extension line, with material constant $\delta = 1$ and $\delta = 2$ under different time instants.....	45
Figure 3.4 The effect of parameter B on the variations of SIFs with time .....	46
Figure 3.5 Variation of the cleavage stress versus angle $\theta \in (-\pi, \pi)$ .....	47
Figure 3.6 The effect of parameter B on variation of the maximum of cleavage stress versus time .....	49
Figure 3.7 The effect of the gradient parameter $\gamma$ on the SIFs.....	49
Figure 3.8 The effect of the gradient parameter $\delta$ on the SIFs .....	50
Figure 3.9 The effect of the gradient parameter $\beta$ on the SIFs .....	50
Figure 3.10 The variation of peak values of stress intensity factors with: (1) the gradient parameter $\beta \in (-2, 2)$ when $\delta = 1, \gamma = 0.1$ . (2) the gradient parameter $\delta \in (-2, 2)$ when $\beta = 1, \gamma = 0.1$ .....	51
Figure 4.1 Geometry of the crack problem.....	57

Figure 4.2 Non-dimensional temperature distributions on crack faces and the extension line based on different Non-Fourier heat conduction models at different time instants.....	68
Figure 4.3 Non-dimensional temperature's variation of the midpoints of crack faces under influence of the ratio between two thermal relaxation lags, when time fractional order $\alpha = 1$ ..	69
Figure 4.4 Non-dimensional temperature's variation of the midpoints of crack faces under influence of the ratio between two thermal relaxation lags, when time fractional order $\alpha = 0.75$ .	73
Figure 4.5 Non-dimensional temperature's variation of the midpoints of crack faces under influence of the ratio between two thermal relaxation lags, when time fractional order $\alpha = 0.5$ .	73
Figure 4.6 The temperature distribution along $x = 0$ at time instant (a) $t=1$ ; (b) $t=2$ ; (c) $t=3$ under the influence of the ratio of thermal lags $\tau_r / \tau_q$ in fractional DPL model when $\alpha = 0.5$ ..	75
Figure 4.7 The dynamic IFTGs for different heat conduction models .....	75
Figure 4.8 The parametric investigation of dynamic SIFs.....	76
Figure 4.9 Transient SIFs under the influence of the ratio of two thermal lags .....	76
Figure 4.10 Transient SIFs under the influence of the ratio of two thermal lags, when the fractional order $\alpha = 0.75$ .	77
Figure 4.11 Transient SIFs under the influence of the ratio of two thermal lags, when the fractional order $\alpha = 0.5$ .	77
Figure 5.1 Schematic diagram of nanofilms .....	83
Figure 5.2 Comparison of thermal conductivity models and experimental data .....	86
Figure 5.3 Normalized temperature change in the femtosecond heating of gold films.....	89
Figure 5.4 Schematic diagram of a viscoelastic plate under transient thermal shock .....	91
Figure 5.5 Temperature distributions along the thickness direction at $t=0.05$ .....	96
Figure 5.6 Distributions of the non-dimensional nonlocal stress $t_{xx}$ .....	96
Figure 5.7 The evolutions of non-dimensional nonlocal stress $t_{xx}$ profile .....	97
Figure 5.8 The time history of non-dimensional nonlocal stress $t_{xx}$ at the right end ( $x=L$ ).....	97
Figure 5.9 Distributions of the non-dimensional nonlocal stress $t_{yy}$ along $x$ coordinate at $t=0.05$ .....	99
Figure 5.10 The time history of non-dimensional nonlocal stress $t_{yy}$ at the right end ( $x=L$ ).....	99

Figure 5.11 Distributions of the non-dimensional displacement $u$ along x coordinate at $t=0.05$ .....	100
Figure 5.12 Distributions of the non-dimensional strain $\varepsilon_{xx}$ along x coordinate at $t=0.05$ .....	100
Figure 6.1 Geometry of the interface crack between FGM coating and homogeneous substrate .....	105
Figure 6.2 Dimensionless temperature distributions on crack faces and the extension line with the variation of nonhomogeneous parameter in thermal conductivity when $k^*=0.1$ . ....	118
Figure 6.3 Dimensionless temperature distributions on crack faces and the extension line varied with partially insulations parameter when $\delta = -1$ . ....	119
Figure 6.4 Dimensionless stresses: (a) $t_{xy}$ (b) $t_{yy}$ along crack faces and the extension line when $\chi = 0.001, \beta = \delta = \gamma = -0.5, k^* = 0.1$ .....	121
Figure 6.5 Dimensionless stresses: (a) $t_{xy}$ (b) $t_{yy}$ along crack faces and the extension line when $\chi = 0.0005, \beta = \delta = \gamma = -1, k^* = 0$ .....	121
Figure 6.6 Dimensionless thermal stress distributions: (a) $t_{xy}$ (b) $t_{yy}$ around the crack tip (1,0) when $\chi = 0.0005, \beta = \delta = \gamma = -1, k^* = 0$ . ....	122
Figure 6.7 Dimensionless stress distributions (a) $t_{xy}$ (b) $t_{yy}$ along the crack line varied with.....	122
Figure 6.8 Dimensionless stress distributions (a) $t_{xy}$ (b) $t_{yy}$ along the crack line varied with.....	123
Figure 6.9 Dimensionless stress distributions (a) $t_{xy}$ (b) $t_{yy}$ along the crack line.....	124
Figure 6.10 Dimensionless stress distributions (a) $t_{xy}$ (b) $t_{yy}$ along the crack line.....	124
Figure 6.11 Dimensionless stress distributions (a) $t_{xy}$ (b) $t_{yy}$ along the crack line.....	125
Figure 6.12 Peak values of the stresses along the crack line with the variation of $\beta$ . ....	125
Figure 6.13 Peak values of the stresses along the crack line with the variation of $\delta$ . ....	126
Figure 6.14 Peak values of the stresses along the crack line with the variation of $\gamma$ . ....	126

# Chapter 1: Introduction

## 1.1 Motivations

Thermoelastic analysis is a classical fundamental branch in solid mechanics, which investigates the heat conduction within various solid materials and the resulting stress/strain fields [1-3]. As an extension of classical elasticity, thermoelasticity takes the effect of thermal expansions into account via adding a temperature relating term to the stress-strain constitutive law. Classical thermoelastic analyses are usually based on the classical elasticity and Fourier's heat conduction law [4-5], which offers the fundamental understandings in many industrial applications in aerospace, mechanical, civil and nuclear engineering.

Many machine components working in the high temperature environment, like thermal shielding components in the aerospace industry, would suffer from intense thermal stresses, which may lead to the failure of the material. In order to assure the lifetime, safety and reliability of these components, the analyses of heat transfer and internal thermal stress distributions are of importance. Particularly, microcracks may develop in the manufacturing of materials or during the thermal or mechanical loading process, and the concentration of thermal stresses and high temperature gradients would occur around the cracks. As to the thermoelastic analysis of crack problems in various materials, there have been extensive theoretical researches. Based on classical Fourier's heat conduction and assuming the properties of the nonhomogeneous material following an exponential law, Noda and Jin [4-8] conducted a series of theoretical analysis of the thermoelastic behaviors of functionally graded materials containing a Griffith crack and presented the influence of nonhomogeneity on both thermal and thermal stress responses. Utilizing the finite difference method, the coupled, thermoelastic problem of an infinite solid containing a penny-shaped crack was solved by Noda et. al. [9]. In a separate study, Nied and Erdogan [10] solved the dynamic thermoelastic problem for a circumferential edge crack in a hollow cylinder cooled from inside. Nabavi and Ghajar [11] derived a general weight function to evaluate the thermal stress intensity factors for elastic cylinders containing circumferential cracks. Wang et. al. [12] investigated the dynamic response of noncollinear cracks in a graded composite material plate subject to dynamic thermal loading. Bao and Wang [13] studied the crack driving force for multiple

cracks in functionally graded ceramic/metal coatings. Ueda [14-19] performed a series of investigations into thermo-electro-mechanical fracture behavior of cracked piezoelectric materials. All these works were based on Fourier's law and neglected the effect of thermal wave speed.

With the rapid development of new technologies, fast-growing usage of new materials, and increasing demand for high accuracy in engineering problems, the thermoelastic analysis within the framework of classical elasticity and Fourier's heat conduction cannot meet these requirements and the unclassical effects should not be neglected anymore. Some examples are listed here. (1) With the rapid development of ultrafast laser heating technology, the processing time of heating is shortened to the level of femtoseconds or picoseconds [20-22], where the classical Fourier heat conduction breaks down. (2) Due to the advanced nanotechnologies, micro-electromechanical systems (MEMS) and nano-electromechanical systems (NEMS) have been widely applied in engineering. In these highly integrated devices, high thermal density would be generated and accurate analysis of the heat conduction and thermal stress distributions becomes a necessity. Under these circumstances, the scale effect would become significant, and both the classical continuum mechanics and Fourier heat conduction are inapplicable [20]. (3) In the past several decades, many soft materials, such as polymer matrix composites, nanocomposites hydrogels and soft elastomers, have been invented and used extensively in a broad range of applications. Classical elasticity does not apply to the new, synthetic composite materials and cannot describe the creep or stress relaxation phenomena caused by the rheological properties. In the fracture risk of these materials, the viscoelastic properties need to be concerned.

This thesis work was motivated by the existing challenges in dealing with non-classical, thermomechanical behavior of advanced materials. It focuses on introducing non-Fourier heat conduction theory in thermal analysis, as well as time-dependent, viscoelasticity theory and non-local theory into the mechanical analysis to facilitate a comprehensive framework for advanced thermal stress analysis of materials. It can be used to deal with the thermomechanical behavior of materials and structures with heterogeneous microstructure or soft matter under extreme thermal loading conditions, and other non-classical problems.

## 1.2 Statement of non-classical problems

In this section, the non-classical theories considered in this thesis are presented in detail.

### 1.2.1 Non-Fourier heat conduction

As a very general internal energy transfer in various solids, liquids, and gas, heat conductions are usually taken place by numerous microstructure collisions of energy carriers, like molecules, phonons, or free electrons. Heat always flows spontaneously from hotter areas to cold areas and the flow rate varies with the temperature difference (temperature gradient). The relationship between the flow rate and the temperature gradient within a material can be described by an empirical law, which was formulated by Fourier in 1822. In most classical engineering problems with the macro spatial and temporal scales, the Fourier Law performs satisfactorily [20], which is shown as:

$$\mathbf{q}(\mathbf{x}, t) = -k\nabla T(\mathbf{x}, t) \quad (1.1)$$

where  $\mathbf{q}$  is the heat flux vector,  $T$  is the temperature,  $t$  is time,  $\mathbf{x}$  is the position, and  $k$  is the thermal conductivity. When the inner heat source is negligible, the conservation of local energy is expressed by:

$$-\nabla \cdot \mathbf{q} = \rho c_p \frac{\partial T}{\partial t} \quad (1.2)$$

where  $c_p$  is the specific heat, and  $\rho$  is the mass density. Incorporate Eq. (1.1) and (1.2), there is the governing PDE:

$$\nabla^2 T = \frac{1}{\kappa} \frac{\partial T}{\partial t} \quad (1.3)$$

where  $\kappa$  is the thermal diffusivity. However, this parabolic heat conduction theory implies thermal waves can propagate in the media at an infinite speed [23], and any thermal disturbances can be felt at infinity instantaneously. Obviously, this indication contradicts physical facts and admits the heat signal travel faster than light, which is inadmissible in the framework of relativity. In some applications with micro/nano spatial and temporal scales, this unphysical deficiency becomes more pronounced and the classical analysis cannot satisfy the requirement of the accuracy anymore.

Typical examples include, but not limited to, heat conduction (1) at very low temperature [20]; (2) under intense heat flux or very high temperature gradient [20-22]; (3) within materials with micro/nano scales inner structures [20]. Actually, experimental evidence has shown the failure of Fourier's Law at some specific applications. Peshkov [24] investigated the heat conduction in helium at very low temperatures (down to 0.38 K) and confirmed the finite thermal wave speed. Narayanamurti [25] measured the second-sound velocity in the semimetal bismuth in the temperature range of 1.2 to 4 K. By experiments performed in the thin gold films under femtosecond laser irradiation, Brorson et. al. [26] found the heat transport speed is close to the Fermi velocity of electrons in Au.

From the microscopic viewpoint, this non-Fourier effect in heat transfer can be attributed to the approaching of the characteristic physical length or processing time to the level of the mean free path or mean free time of energy carriers, respectively [20]. The mean free path is defined by the averaged distance over sufficient collisions of the energy carrier, and the mean free time is defined by the averaged time for each collision. Usually, the mean free time of energy carriers is in the order of  $10^0$  femtosecond to  $10^1$  picosecond, and the mean free path is in the order of  $10^1$  to  $10^2$  nanometer [20]. For the widely applied ultrafast laser heating techniques, the processing time can be shortened to the level of femtoseconds, where the finite speed of thermal waves and the time-lagging behaviors cannot be neglected anymore. As to the heat conduction in helium at extremely low temperatures, the delayed responses are very obvious since the finite time required to activate the inert energy carriers to an energy level for efficient heat conduction [20].

### **(1) Hyperbolic (single-phase-lag) heat conduction**

In order to avoid this unphysical deficiency and incorporate the finite speed of thermal wave into heat conduction, the thermal wave model (or C-V model) was proposed by Cattaneo and Vernotte [27-28] through introducing the "thermal relaxation time  $\tau_q$ ", which denotes the time lag in the thermal wave propagation, as follows:

$$\mathbf{q}(\mathbf{x}, t) + \tau_q \frac{\partial \mathbf{q}(\mathbf{x}, t)}{\partial t} = -k \nabla T(\mathbf{x}, t). \quad (1.4)$$

The relaxation time,  $\tau_q$  is a material constant, usually related to the collision frequency of the molecules within the material, and the finite thermal wave speed can be calculated as  $C_T = \sqrt{k / (\rho c_p \tau_q)}$ , where  $c_p$  is the specific heat, and  $\rho$  is the mass density. When the finite speed is neglected,  $\tau_q$  will equal zero and the Eq. (1.4) will be degenerated to the classical Fourier's Law. Consider the conservation of local energy in Eq. (1.2), there is the hyperbolic-type governing PDE:

$$\nabla^2 T = \frac{1}{\kappa} \frac{\partial T}{\partial t} + \frac{\tau}{\kappa} \frac{\partial^2 T}{\partial t^2} \quad (1.5)$$

If the relaxation time is regarded as the time lag between the temperature gradient and heat flux, Eq. (1.4) can be expressed as:

$$\mathbf{q}(\mathbf{x}, t + \tau_q) = -k \nabla T(\mathbf{x}, t) \quad (1.6)$$

which indicates the temperature gradient at one material point will proceed the resulting heat flux by a time lag  $\tau_q$ . Mathematically, the Eq. (1.4) can be obtained by the Taylor series expansion of Eq. (1.6) to its first order.

## (2) Dual-phase-lag heat conduction

Following the hyperbolic heat conduction theory, Tzou [20] proposed a more generalized dual-phase-lag (DPL) model as:

$$\mathbf{q}(\mathbf{x}, t + \tau_q) = -k \nabla T(\mathbf{x}, t + \tau_r) \quad (1.7)$$

where  $\tau_r$  is the time lag of the temperature gradient. Unlike the assumption that the temperature gradient always proceeds the heat flux in single-phase lag theory, for  $\tau_r > \tau_q$ , DPL theory indicates the heat flux at one point will proceed the temperature gradient, which means the heat flux could be the cause and the temperature gradient is the result. This more generalized model can capture the transient effect when the response time is comparable to the thermalization time needed for the microstructural interaction to build the thermodynamic equilibrium [20-21]. According to Tzou [20], the two thermal lags are intrinsic thermal properties of the materials. As to the composites with complex internal structures like porous media, which always require finite

times for the material to reach thermal equilibrium, the thermal lags could become the structural properties. Unlike the thermal wave model, which is the macroscopic description over many grains, the DPL model considering the more pronounced microstructural effect which requiring finite time to achieve local thermal equilibrium. For metals under the ultrafast laser heating, the thermal lags are caused by phonon–electron interactions. As to the porous media or composites, the energy carriers will follow the more conducting path and dissipate the energy to the neighbor phases, which is the cause of thermal lags. Due to these advantages, the DPL model has a satisfactory performance in small-scale and fast transient processes and agrees well with the ultrafast laser heating experiments in metal films [22].

### (3) Fractional heat conduction

As an extension of the integer order in partial differential equations, fractional calculus has been widely discussed in various applications like fluid mechanics, viscoelasticity and biological engineering [29-32]. Mainardi [33] extended the fractional calculus into the study of some basic physical phenomena like relaxation, diffusion, oscillation and wave propagation. Unlike the integer order, the most important aspect of time fractional differential is their nonlocal properties and memory effects, which implies the next state of a system depends on both the current input as well as the historical states. Povstenko [34] proposed the quasi-static uncoupled thermoelasticity theory based on the heat conduction equation with a time-fractional derivative. Sherief et. al. [35] introduce the fractional calculus into the thermal wave model, shown as:

$$\mathbf{q}(\mathbf{x}, t) + \tau_q \frac{\partial^\alpha \mathbf{q}(\mathbf{x}, t)}{\partial t^\alpha} = -k \nabla T(\mathbf{x}, t) \quad (1.8)$$

where

$$\frac{\partial^\alpha f(\mathbf{x}, t)}{\partial t^\alpha} = \begin{cases} \frac{1}{\Gamma(1-\alpha)} \int_0^t (t-\tau)^{-\alpha} \frac{\partial f(\mathbf{x}, \tau)}{\partial \tau} d\tau, & 0 < \alpha < 1 \\ \frac{\partial f(\mathbf{x}, t)}{\partial t}, & \alpha = 1 \end{cases}$$

Using the Taylor series expansion of Eq. (1.6) to its fractional order of  $\alpha$ , Ezzat and EI-Karamany [36-37] proposed the fractional single-phase heat conduction theory:

$$\mathbf{q}(\mathbf{x}, t) + \frac{\tau_q^\alpha}{\alpha!} \frac{\partial^\alpha \mathbf{q}(\mathbf{x}, t)}{\partial t^\alpha} = -k \nabla T(\mathbf{x}, t) \quad (1.9)$$

The extension of fractional calculus to heat conduction theory has yielded promising results [36-37]. The sharp thermal wavefront which implies infinite thermal gradient in hyperbolic heat conduction theory was eliminated [38] using fractional models, and the enhanced fractional heat conduction theory fits very well with the experiment and shows the fractional order is a powerful characteristic parameter for non-continuous materials like composites [39]. Similar, introducing the fractional calculus into the DPL model, the fractional order DPL heat conduction law is studied by Ezzat [40] and Xu [41] with the form as:

$$\mathbf{q} + \frac{\tau_q^\alpha}{\alpha!} \frac{\partial^\alpha \mathbf{q}}{\partial t^\alpha} + \frac{\tau_q^{2\alpha}}{(2\alpha)!} \frac{\partial^{2\alpha} \mathbf{q}}{\partial t^{2\alpha}} = -k(\nabla T + \frac{\tau_T^\alpha}{\alpha!} \frac{\partial^\alpha}{\partial t^\alpha} \nabla T), 0 < \alpha \leq 1 \quad (1.10)$$

#### (4) Nonlocal heat conduction

The aforementioned part focuses on the lagging behaviors in time to account for non-Fourier heat conduction. Moreover, the classical Fourier's Law cannot meet the requirement spatially for heat conduction within nano sized materials or devices. Experimental measurements of the thermal conductivity of nano-structural materials such as silicon nanofilm or nanowires, graphene sheets, is size-dependent, which is remarkably different from bulk materials [42]. These findings show the spatially nonlocal effect in heat conduction of nano size and the Fourier Law breaks down to describe these steady-state heat conduction.

To incorporate the spatially nonlocal effect in heat conduction, different mathematical models have been proposed. Based on the linearized Boltzmann equation for the pure phonon field, the well-known Guyer-Krumhansl model was proposed in [43-44]. Considering the mass, pressure, and inertial force of the phonon gas [45], the thermomass model can also characterize the nonlocal effect in heat transport. Stemming from the analogy with the integral form of the nonlocal elasticity, an integro-differential equation governing the nonlocal effect was proposed by Xu [46-47]. Obviously, there is still no common agreement on the spatial nonlocality in heat conduction [48-49]. Parallel to these works, Tzou et. al. extended their DPL model by introducing a nonlocal length to accommodate the spatially nonlocal effect [50-51], shown as:

$$\mathbf{q}(\mathbf{x} + \boldsymbol{\xi}, t + \tau_q) = -k \nabla T(\mathbf{x}, t + \tau_q) \quad (1.11)$$

in which  $\boldsymbol{\xi}$  is the vector relating to the spatial nonlocality of the heat flux vector. The advantage of this theory is the macroscopic unification of both the temporally and spatially nonlocal effects in a simple form, especially for some engineering analyses without sufficient knowledge of the phonon dynamics. By Taylor series expansion to the first order of space dimension, and neglecting all terms involving time, the steady state form of this theory:

$$(1 + \boldsymbol{\xi} \cdot \nabla) \mathbf{q}(\mathbf{x}) = -k \nabla T(\mathbf{x}) \quad (1.12)$$

was verified by the experimental results of thin nanowires as it captured the linear dependence of the effective thermal conductivity on their radiuses [50].

## 1.2.2 Thermoviscoelasticity

In the past decades, with the developments of advanced manufacturing techniques, more and more advanced soft materials like hydrogel, elastomers, and polymers-based composites are designed and put into engineering applications. Unlike elastic materials, these materials always exhibit significant creep and stress relaxation under room temperatures and the stress and strain depend on their time variations. Moreover, these behaviors always become more severe in the high temperature environments. Thermoviscoelasticity offers the basis for studying these complicated phenomenological behaviors and designing the flexible materials. The constitutive law of thermoviscoelasticity can be formulated as [52-53]:

$$\begin{aligned} s_{ij} &= \int_0^t G_1(x, y, t - \tau) \frac{de_{ij}}{d\tau} d\tau \\ \sigma_{kk} &= \int_0^t G_2(x, y, t - \tau) \frac{d\varepsilon_{kk}}{d\tau} d\tau - 3 \int_0^t \varphi(x, y, t - \tau) \frac{dT}{d\tau} d\tau \end{aligned} \quad (1.13)$$

with

$$s_{ij} = \sigma_{ij} - \frac{1}{3} \sigma_{kk} \delta_{ij}, \quad e_{ij} = \varepsilon_{ij} - \frac{1}{3} \varepsilon_{kk} \delta_{ij}$$

where  $s_{ij}, e_{ij}$  are deviatoric components of the stress and strain tensors,  $T$  is temperature,  $G_1(x, y, t)$  and  $G_2(x, y, t)$  are the shear and the bulk relaxation functions,  $\varphi(x, y, t)$  is the thermal relaxation

function. Recently, there has been some work focusing on thermoviscoelasticity. Ezzat et. al. extended heat conduction with the memory-dependent derivatives [54] and fractional relaxation operators [55] into thermoviscoelasticity and calculated the responding temperature variations and thermal stresses distributions in one-dimensional cases. Li et. al. [56] considered the effect of fractional order strain in the thermomechanical analysis of a thick viscoelastic plate. With the help of mapping of Kirchhoff's transformation, the thermoviscoelastic analysis of an infinitely long hollow cylinder with variable thermal conductivity was conducted by Ezzat and Ei-Bary [57]. However, these works were only focused on the one-dimensional heat transfer in uncracked materials. There are very few works investigating the thermal fracture behavior of viscoelastic materials. As to cracked viscoelastic materials, the heat conduction would always be two-dimensional since the existence of a crack could disturb the temperature field. The transient fracture behavior in viscoelastic materials under non-Fourier heat conduction remains unknown. With the increasing application of soft composites, the viscoelastic fracture analysis under thermal loading has become an important topic

### **1.2.3 Nonlocal Elasticity**

Considerable progress has been made in nanotechnology during the past decades. Since the discovery of carbon-nanotubes, much attention has been attracted to nano-structural materials owing to their excellent multifunctional performance in mechanical, electric and optical applications [58-59]. Some high-performance nanostructures like nanowires, nanotubes, nanofibers, are believed to be promising materials to build nanodevices, such as nanoelectromechanical systems (NEMS) [60-61]. In the design or safe operation process of sophisticated, expensive NEMS, accurate analysis of inherent stress, strain, and heat conduction becomes an inevitable necessity. However, many experimental evidences have shown the intrinsic properties of nano-structural materials differ notably with that in bulk materials [62], which is greatly attributed to the scale effects, such as the diameter of nanowires or the thickness of thin films [62]. Due to the very small characteristic dimensions, mechanics in these nano-structural materials or systems will be significantly affected by the forces in molecular or atomic scales, where the applicability of classical continuum models is questioned [63].

In order to bridge the gap between the classical continuum mechanics and the mechanics at the nanoscale, several modified, size dependent, continuum theories have been proposed, such

as the strain gradient elasticity theory, couple stress theory, and nonlocal elasticity theory [64–69], of which the nonlocal theory has been widely applied to research at the nanoscale. Initiated by Eringen et al. [65-66], the stress-strain relation is expressed in an integral form:

$$t_{ij}(X) = \int_{\Omega} \alpha(|X - X'|) \sigma_{ij}(X') d\Omega(X') \quad (1.14)$$

In which  $t_{ij}$  is the nonlocal stress,  $\sigma_{ij}$  is the classical local stress,  $\alpha(|X - X'|)$  is the kernel function characterizing the long-range interactions between molecules or atoms. Compared with the classical continuum, nonlocal theory indicates the stress of one spatial point does not depend uniquely only on the strain at that point, but also on the strains in a surrounding space, and thus building the connections between macroscopic mechanical behaviors with the microscopic, molecular or atomic interactions. In 1983, the equivalent, partial differential form of nonlocal theory was proposed by Eringen et al. [70] for some specific, physically admissible kernels expressed as:

$$(1 - (e_0 a)^2 \nabla^2) t_{ij} = \sigma_{ij} \quad (1.15)$$

where  $e_0$  is a constant depending on materials,  $a$  is an internal characteristic length, and  $\nabla^2$  is the Laplacian operator. Compared to the integral form, the differential form of nonlocal theory has gained more popularity among researchers due to its simplicity [71]. Until now, the nonlocal continuum has been widely applied in various areas [72-75], such as fracture mechanics, dislocation mechanics, wave propagation in composites, etc. Nonlocal theory has seen many applications in fracture mechanics. Using nonlocal theory, Eringen [72,77-78] obtained the non-singular stress fields around the tip of a Griffith crack under uniform tension, shear, or anti-plane shear. As the nonlocal theory leads to a finite stress field around the crack tip, fracture criteria based on the maximum stress can be built to simplify the application of fracture mechanics in mechanical design. Many researchers further extended the application of nonlocal theory in various crack problems under different loading conditions. For example, Zhou et al. [79-83] employed Schmidt's method to investigate various crack problems based on nonlocal theory. Using nonlocal theory, Liu et al. [84-85] studied the three-dimensional crack problem in piezoelectric and magneto-electro-elastic materials. Jamia et al. [86-87] studied the crack problem

of a functionally graded, magneto-electro-elastic and piezoelectric material, respectively, using nonlocal theory.

Until now, all research works on the application of nonlocal theory in fracture mechanics were only focused on the crack problem under mechanical loading, and the nonlocal analysis of crack problems under thermal loading has yet been reported. The thermoelastic investigation of cracked media by nonlocal theory will be introduced in this thesis.

### **1.3 Methods and Objectives**

The objective of this thesis is to obtain a comprehensive understanding of the non-classical problem's influence on the thermoelastic response by mathematical modelling related to the following issues:

- (1) Non-Fourier heat conduction in cracked viscoelastic media and related thermal stress analysis.
- (2) Nonlocal heat conduction and the associated thermoviscoelastic response.
- (3) Extension of nonlocal elasticity in dealing with thermoelastic response of cracked media under thermal loading.

The main theoretical methods of integral transform and singular integral equations, are utilized to deal with the governing equations of both the transient thermal fields and dynamic stress fields. In order to solve the unclassical thermoelastic problems in cracked media, Fourier transform is used to convert the partial differential equations to ordinary differential equations, while Laplace transform is efficient in avoiding the time dependence by analyzing the mathematical problem in Laplace domain. With the help of boundary conditions, the problems are finally reduced to singular integral equations or dual integral equations, and then solved numerically to display the concentration of thermal stresses and high temperature gradients around the cracks.

## 1.4 Organization of the thesis

This thesis is organized as follows. After this brief introduction to the topics, a thermoviscoelastic analysis is conducted for a cracked, functionally graded half-plane under a thermal shocking load. In the third chapter, the non-Fourier, CV heat conduction equation is introduced in the thermal analysis of a cracked half-plane to reflect the influence of thermal waves on the thermomechanical, fracture behavior of functionally graded materials under thermal shock loading. In chapter 4, the time-dependent, viscoelastic behavior is combined with the non-Fourier, fractional dual-phase lag heat conduction model for thermal stress analysis of soft materials under transient thermal loading. In chapter 5, the non-local, dual-phase-lag theory is verified by experimental data based on thermal conductivity of silicon nanofilms and femtosecond laser heating of gold films, and a generalized nonlocal thermoviscoelastic theory is built to analyze the thermomechanical response of a thin film. In chapter 6, non-local thermal stress analysis is further extended to an interface crack problem to illustrate the influence of microstructure heterogeneity on interface debonding. Conclusions and some perspectives for future work are provided in chapter 7.

## **Chapter 2: Thermo-viscoelastic response of a cracked, functionally graded half-plane under a thermal shock**

A thermo-viscoelastic model is developed for the crack problem in an infinite, functionally graded half plane under a thermal shock. The moduli are assumed to be separable forms of both spatial coordinates and time, and two types of relaxation function of viscoelasticity are considered in this chapter. By employing the Fourier transform and Laplace transform, coupled with the singular integral equations, the governing partial differential equations under mixed thermo-mechanical boundary conditions are solved numerically. The results show that the variations of stress intensity factors (SIFs) in viscoelastic functionally graded materials (FGMs) are significantly different than those in the elastic ones, which cannot be neglected in designing FGMs.

### **2.1 Introduction**

Over the last few decades, with the aid of developed manufacturing techniques like 3D printing, various soft materials such as hydrogels, elastomers, polymers and other composites [88-89] have been invented and put into use in a broad range of applications such as biomedical, aerospace, tissue, automotive, mechanical, drug delivery, civil, and nuclear engineering. Among them, polymer-based functionally graded materials (FGMs) are currently receiving much attention. To avoid severe thermal stresses and improve the structural integrity, FGMs always possess gradual change in composition and microstructure so as to achieve continuous variations in physical and mechanical properties spatially.

For polymer-based FGMs, materials may exhibit significant creep and stress relaxation even under room temperature. Unlike elastic materials, deformation in viscoelastic FGMs is a time-dependent process, and both stress and strain depend on their time variation. Moreover, in the framework of classical, linear viscoelasticity, materials will show more significant creep and stress relaxation under elevated temperature, and therefore, viscoelasticity cannot be neglected in designing polymer-based FGMs.

FGMs can help reduce mechanical and thermal stresses to avoid catastrophic failure of structures, especially for the stresses around the cracks. There has been extensive research about

the crack problems in FGMs under mechanical or thermal loading [6, 13, 90-95]. Noda and Jin [96] pointed out that the stress intensity factors are still applicable in fracture problems of FGMs and their singularity and angular distribution in crack tip fields are the same with the homogenous materials. Following these works, a number of analytical or semi-analytical models are introduced to solve the crack problems, such as the piecewise linear or exponential models [97-98]. However, compared with the elastic problems, there are only a few investigations focusing on the crack problem in viscoelastic FGMs. For example, by solving the governing equations directly, Schovanec et al. [99-103] studied the stationary and dynamic mode I and mode III crack problems in nonhomogeneous, viscoelastic materials. In a separate study, Paulino and Jin [104-107] extended the elastic-viscoelastic correspondence principle to FGMs under the assumption that the relaxation functions can be written in separable forms of space and time, which greatly simplified the analytical solutions. Using this correspondence, they analyzed a crack problem in viscoelastic FGMs strip under in-plane loading and anti-plane loading. Wang et al. [108] solved the viscoelastic crack problem using their piecewise-exponential model. However, the correspondence principle can only be used in simple problems, in which one can turn the final elastic solutions to viscoelastic ones directly by corresponding substitutions. When the problems become complex, such as the thermal-viscoelastic problems, or when dimensionless variables exist, it is difficult to get the correct solutions by this correspondence.

In this chapter, we aim to establish a thermo-viscoelastic analytical model for a cracked half-plane under a thermal shock in FGMs. By employing Laplace transform, the convolution in viscoelastic constitutive equation is avoided to simplify the derivation process. The partial differential equations are solved by Fourier transform, and the boundary conditions on crack faces are reduced to a set of singular integral equations. The Lobatto-Chebyshev method [109] is employed to solve the singular integral equations numerically, and the Laplace inversion [110] is used to get the results in the time domain.

## 2.2 Statement of the problem and basic equations

As illustrated in Figure 2.1, a semi-infinite, nonhomogeneous, viscoelastic plane containing a crack of length  $2c$  under plane stress condition is considered. The crack is parallel to the free boundary, and is assumed to remain completely thermally insulated, so the temperature field will be disturbed by the presence of this crack. The whole temperature is set to be zero initially, and a thermal shock is suddenly applied on the free boundary at time  $t = 0$ . Inertia and body forces are neglected.

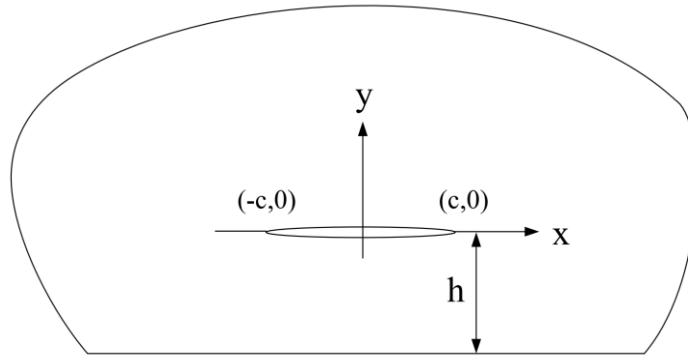


Figure 2.1 Crack geometry and coordinates

In viscoelastic, nonhomogeneous materials, the moduli are functions of both spatial coordinates and time. To simplify the theoretical derivation, separable forms of the properties are assumed as:

$$\begin{aligned}
 E &= E_0 \exp(\beta y) m_1(t) \\
 \mu &= \mu_0 (1 + \varepsilon y) \exp(\beta y) m_2(t) \\
 \alpha &= \alpha_0 \exp(\gamma y) m_3(t) \\
 k &= k_0 \exp(\delta y) \\
 \kappa &= \kappa_0
 \end{aligned} \tag{2.1}$$

where  $\beta, \varepsilon, \gamma, \delta$  are material constants;  $E, \mu, \alpha, k$  and  $\kappa$  are the Young's modulus, Poisson's ratio, thermal expansion coefficient, heat conductivity and thermal diffusivity;  $m_i(t)$  ( $i = 1, 2, 3$ ) are the relaxation functions in viscoelasticity with no loading applied on the material before  $t = 0$ . In the present work, two classical relaxation functions [111] are employed as:

$$m_1(t) = m_2(t) = m_3(t) = m(t) = \left( \frac{E_\infty}{E_0} + \left(1 - \frac{E_\infty}{E_0}\right) e^{-\frac{t}{t_0}} \right) \quad (2.2)$$

$$m_1(t) = m_2(t) = m_3(t) = m(t) = \left( \frac{t_0}{t} \right)^q, \quad 0 < q < 1$$

## (1) Heat conduction

The heat conduction when the heat generation is negligible is:

$$\nabla^2 T + \frac{1}{k} \nabla k \cdot \nabla T = \frac{1}{\kappa} \frac{\partial T}{\partial t} \quad (2.3)$$

By introducing the following dimensionless variables,

$$\bar{T} = T / T_0, \quad \bar{t} = t / (c^2 / \kappa), \quad (\bar{x}, \bar{y}, \bar{h}) = (x, y, h) / c, \quad \bar{\delta} = \delta \cdot c \quad (2.4)$$

Considering the material properties in equation (2.1), the governing equation for heat conduction can be reduced to:

$$\nabla^2 T + \delta \frac{\partial T}{\partial y} = \frac{\partial T}{\partial t} \quad (2.5)$$

Here and after, the hat of the dimensionless variables has been omitted for simplicity. The initial and boundary conditions for heat conduction in dimensionless forms are:

$$\begin{aligned} T = 0, \quad \frac{\partial T}{\partial t} = 0, \quad (t = 0) \\ T(x, -h) = 1, \quad (t > 0, |x| < \infty) \\ T = 0, \quad (y \rightarrow \infty) \\ \frac{\partial T}{\partial y} = 0, \quad (y = 0, |x| \leq 1) \\ T(x, 0^+) = T(x, 0^-), \quad (|x| > 1) \\ \frac{\partial T(x, 0^+)}{\partial y} = \frac{\partial T(x, 0^-)}{\partial y}, \quad (|x| > 1) \end{aligned} \quad (2.6)$$

## (2) Thermal-viscoelastic field equations

The equilibrium equations for plane stress problems without considering the inertia effect are:

$$\frac{\partial \sigma_x}{\partial x} + \frac{\partial \sigma_{xy}}{\partial y} = 0, \quad \frac{\partial \sigma_{xy}}{\partial x} + \frac{\partial \sigma_y}{\partial y} = 0 \quad (2.7)$$

The strain-displacement relations are:

$$\varepsilon_x = \frac{\partial u}{\partial x}, \quad \varepsilon_y = \frac{\partial v}{\partial y}, \quad \varepsilon_{xy} = \frac{1}{2} \left( \frac{\partial u}{\partial y} + \frac{\partial v}{\partial x} \right) \quad (2.8)$$

The compatibility equation for two-dimensional problems is:

$$\frac{\partial^2 \varepsilon_x}{\partial y^2} + \frac{\partial^2 \varepsilon_y}{\partial x^2} = 2 \frac{\partial^2 \varepsilon_{xy}}{\partial x \partial y} \quad (2.9)$$

The constitutive law of viscoelasticity can be expressed as:

$$\begin{aligned} s_{ij} &= \int_0^t G_1(x, y, t - \tau) \frac{de_{ij}}{d\tau} d\tau \\ \sigma_{kk} &= \int_0^t G_2(x, y, t - \tau) \frac{d\varepsilon_{kk}}{d\tau} d\tau - 3 \int_0^t \varphi(x, y, t - \tau) \frac{dT}{d\tau} d\tau \end{aligned} \quad (2.10)$$

with

$$s_{ij} = \sigma_{ij} - \frac{1}{3} \sigma_{kk} \delta_{ij}, \quad e_{ij} = \varepsilon_{ij} - \frac{1}{3} \varepsilon_{kk} \delta_{ij}$$

where  $s_{ij}, e_{ij}$  are deviatoric components of the stress and strain tensors,  $T$  is temperature,  $G_1(x, y, t)$  and  $G_2(x, y, t)$  are the shear and the bulk relaxation functions,  $\varphi(x, y, t)$  is the thermal relaxation function.

The relations between these functions and the relaxation function of Young's modulus  $E^*$  and Poisson's ratio  $\mu^*$  in the Laplace domain are expressed as [52]:

$$G_1^* = \frac{E^*}{1 + p\mu^*}, \quad G_2^* = \frac{E^*}{1 - 2p\mu^*}, \quad \varphi^* = pG_2^* \alpha^* \quad (2.11)$$

where  $p$  is the Laplace transform variable. Here and after, the superscript “\*” denotes the variables in Laplace domain. By using the Laplace transform, the above equations can be reduced to:

$$\begin{aligned}
\varepsilon_x^* &= \frac{1}{pE^*}(\sigma_x^* - p\mu^* \sigma_y^*) + p\alpha^* T^* \\
\varepsilon_y^* &= \frac{1}{pE^*}(\sigma_y^* - p\mu^* \sigma_x^*) + p\alpha^* T^* \\
\varepsilon_{xy}^* &= \frac{1+p\mu^*}{pE^*} \sigma_{xy}^*
\end{aligned} \tag{2.12}$$

Combined with equation (2.1), the following equations are obtained as:

$$\begin{aligned}
\frac{\partial u^*}{\partial x} &= \frac{1}{pE_0 m_1^*(p) \exp(\beta y)} [\sigma_x^* - p\mu_0 m_2^*(p)(1+\varepsilon y) \exp(\beta y) \sigma_y^*] + p\alpha_0 m_3^*(p) \exp(\gamma y) T^* \\
\frac{\partial v^*}{\partial y} &= \frac{1}{pE_0 m_1^*(p) \exp(\beta y)} [\sigma_y^* - p\mu_0 m_2^*(p)(1+\varepsilon y) \exp(\beta y) \sigma_x^*] + p\alpha_0 m_3^*(p) \exp(\gamma y) T^* \\
\frac{\partial u^*}{\partial y} + \frac{\partial v^*}{\partial x} &= \frac{2(1+p\mu_0(1+\varepsilon y) \exp(\beta y) m_2^*(p))}{pE_0 \exp(\beta y) m_1^*(p)} \sigma_{xy}^*
\end{aligned} \tag{2.13}$$

where  $m_i^*(p)$  ( $i=1,2,3$ ) are the Laplace transform of  $m_i(t)$  ( $i=1,2,3$ ).

Let  $U^*$  is the Airy stress function, in terms of which the stress can be expressed as:

$$\sigma_x^* = \frac{\partial^2 U^*}{\partial y^2}, \sigma_y^* = \frac{\partial^2 U^*}{\partial x^2}, \sigma_{xy}^* = -\frac{\partial^2 U^*}{\partial x \partial y} \tag{2.14}$$

Substitute the above equations into equation (2.9) and (2.13), the governing equation is obtained:

$$\nabla^2 \nabla^2 U^* - 2\beta \frac{\partial}{\partial y} (\nabla^2 U^*) + \beta^2 \frac{\partial^2 U^*}{\partial y^2} + E_0 \alpha_0 p^2 m_1^*(p) m_3^*(p) \exp((\beta + \gamma)y) (\nabla^2 T^* + 2\gamma \frac{\partial T^*}{\partial y} + \gamma^2 T^*) = 0 \tag{2.15}$$

Besides (2.4), we introduce the following dimensionless variables,

$$\begin{aligned}
\bar{\sigma}_{ij} &= \sigma_{ij} / (E_0 \alpha_0 T_0), \quad \bar{U} = U / (E_0 \alpha_0 T_0 c^2) \\
(\bar{u}, \bar{v}) &= (u, v) / (c \alpha_0 T_0), \quad \bar{\varepsilon}_{ij} = \varepsilon_{ij} / (\alpha_0 T_0) \\
(\bar{x}, \bar{y}, \bar{h}) &= (x, y, h) / c, \quad (\bar{\beta}, \bar{\varepsilon}, \bar{\gamma}) = (\beta, \varepsilon, \gamma) \cdot c
\end{aligned} \tag{2.16}$$

The governing equation can be reduced to:

$$\nabla^2 \nabla^2 U^* - 2\beta \frac{\partial}{\partial y} (\nabla^2 U^*) + \beta^2 \frac{\partial^2 U^*}{\partial y^2} + p^2 m_1^*(p) m_3^*(p) \exp((\beta + \gamma)y) (\nabla^2 T^* + 2\gamma \frac{\partial T^*}{\partial y} + \gamma^2 T^*) = 0 \quad (2.17)$$

And the dimensionless constitutive equations are reduced to:

$$\begin{aligned} \frac{\partial u^*}{\partial x} &= \frac{1}{pm_1^*(p)} [\exp(-\beta y) \sigma_x^* - p\mu_0 m_2^*(p)(1 + \varepsilon y) \sigma_y^*] + pm_3^*(p) \exp(\gamma y) T^* \\ \frac{\partial v^*}{\partial y} &= \frac{1}{pm_1^*(p)} [\exp(-\beta y) \sigma_y^* - p\mu_0 m_2^*(p)(1 + \varepsilon y) \sigma_x^*] + pm_3^*(p) \exp(\gamma y) T^* \\ \frac{\partial u^*}{\partial y} + \frac{\partial v^*}{\partial x} &= \frac{2(\exp(-\beta y) + p\mu_0(1 + \varepsilon y)m_2^*(p))}{pm_1^*(p)} \sigma_{xy}^* \end{aligned} \quad (2.18)$$

Similar with equation (2.5), the hat of the dimensionless variables has been omitted for simplicity.

In this problem, the mechanical boundary conditions can be expressed as:

$$\begin{aligned} \sigma_{xy}(x, -h) &= \sigma_y(x, -h) = 0, \quad (|x| < \infty) \\ \sigma_{xy}(x, 0) &= \sigma_y(x, 0) = 0, \quad (|x| \leq 1) \\ \sigma_{xy}(x, 0^+) &= \sigma_{xy}(x, 0^-), \quad (|x| > 1) \\ \sigma_y(x, 0^+) &= \sigma_y(x, 0^-), \quad (|x| > 1) \\ u(x, 0^+) &= u(x, 0^-), \quad (|x| > 1) \\ v(x, 0^+) &= v(x, 0^-), \quad (|x| > 1) \end{aligned} \quad (2.19)$$

## 2.3 Thermal stress

We assume the thermal-viscoelastic coupling effect can be neglected, and the stress field will not influence the temperature field. By employing Laplace transform, the solution of (2.5) subjected to conditions (2.6) are given as [6]:

$$\begin{aligned} T^*(x, y, p) &= \int_{-\infty}^{\infty} D(\xi, p) \exp(-\mu_2 y - ix\xi) d\xi + \frac{1}{p} \exp(-\lambda(y+h)); \quad y > 0 \\ T^*(x, y, p) &= \int_{-\infty}^{\infty} \frac{\mu_2 D(\xi, p)}{\mu_1 - \mu_2 \exp(-2\mu h)} \{1 - \exp(-2\mu(h+y))\} \exp(-\mu_1 y - ix\xi) d\xi \\ &\quad + \frac{1}{p} \exp(-\lambda(y+h)); \quad y < 0 \end{aligned} \quad (2.20)$$

Where

$$\mu_1 = \frac{\delta}{2} - \mu, \quad \mu_2 = \frac{\delta}{2} + \mu, \quad \mu = \sqrt{p + \xi^2 + \frac{\delta^2}{4}}, \quad \lambda = \frac{\delta}{2} + \sqrt{p + \frac{\delta^2}{4}}$$

$\xi$  is the Fourier transform variable and  $D(\xi, p)$  is associated with the density function of temperature, which can be calculated from the singular integral equation in [6]. In the Laplace domain, substituting the solution of temperature distribution (2.18) into the following governing equation for thermal stresses:

$$\nabla^2 \nabla^2 U^* - 2\beta \frac{\partial}{\partial y} (\nabla^2 U^*) + \beta^2 \frac{\partial^2 U^*}{\partial y^2} = -p^2 m_1^*(p) m_3^*(p) \exp((\beta + \gamma)y) (\nabla^2 T^* + 2\gamma \frac{\partial T^*}{\partial y} + \gamma^2 T^*) \quad (2.21)$$

the general solution of Eq. (2.21) can be expressed as:

$$\begin{aligned} U^*(x, y, p) &= \int_{-\infty}^{\infty} (B_1 + B_2 y) \exp(-s_2 y - ix\xi) d\xi - \int_{-\infty}^{\infty} C_1 \exp[(\beta + \gamma - \mu_2)y - ix\xi] d\xi, & y > 0 \\ U^*(x, y, p) &= \int_{-\infty}^{\infty} \{(A_1 + A_2 y) + (A_3 + A_4 y) \exp(-2sy)\} \exp(-s_1 y - ix\xi) d\xi \\ &\quad - \int_{-\infty}^{\infty} \{C_{21} + C_{22} \exp(-2\mu y) \exp[(\beta + \gamma - \mu_1)y - ix\xi]\} d\xi, & y < 0 \end{aligned} \quad (2.22)$$

where  $A_1, A_2, A_3, A_4, B_1, B_2$  can be derived from the boundary conditions (2.19), and

$$s_1 = -\frac{\beta}{2} - s, \quad s_2 = -\frac{\beta}{2} + s, \quad s = \sqrt{\xi^2 + \frac{\beta^2}{4}}$$

and the following equations can be obtained by the particular solution of (2.20),

$$\begin{aligned} C_1(\xi, p) &= [(\beta + \gamma - \mu_2)(\gamma - \mu_2) - \xi^2]^{-2} [\gamma^2 + p - (2\gamma - \delta)\mu_2] D(\xi, p) p^2 m_1^*(p) m_3^*(p) \\ C_{21}(\xi, p) &= [(\beta + \gamma - \mu_1)(\gamma - \mu_1) - \xi^2]^{-2} [\gamma^2 + p - (2\gamma - \delta)\mu_1] \frac{\mu_2 D(\xi, p)}{\mu_1 - \mu_2 \exp(-2\mu a)} p^2 m_1^*(p) m_3^*(p) \\ C_{22}(\xi, p) &= [(\beta + \gamma - \mu_2)(\gamma - \mu_2) - \xi^2]^{-2} [(2\gamma - \delta)\mu_2 - \gamma^2 - p] \frac{\mu_2 D(\xi, p) \exp(-2\mu a)}{\mu_1 - \mu_2 \exp(-2\mu a)} p^2 m_1^*(p) m_3^*(p) \end{aligned} \quad (2.23)$$

From constitutive equation (2.18) and the corresponding boundary conditions, the jumps of the displacement on the line  $y = 0$  are:

$$\begin{aligned}\frac{\partial[u^*]}{\partial x} &= \frac{1}{pm_1^*(p)}[\sigma_x^*] + pm_3^*(p)[T^*] \\ \frac{\partial^2[v^*]}{\partial x^2} &= -\frac{1}{pm_1^*(p)}\left[\frac{\partial}{\partial y}\{\exp(-\beta y)\sigma_y^*\}\right] - pm_3^*(p)\gamma[T^*]\end{aligned}\quad (2.24)$$

The stress components can be obtained from solution (2.22) combined with equation (2.14). Substituting the stresses and temperature jump into (2.24), we have:

$$\begin{aligned}\frac{\partial[u^*]}{\partial x} &= \int_{-\infty}^{\infty} \frac{1}{pm_1^*(p)} \left\{ -2s_2(B_2 - A_4) + s_2^2(B_1 - A_3) + (2s_1A_2 - s_1^2A_1) + \right. \\ &\quad \left. (\beta + \gamma - \mu_1)^2C_{21} + (\beta + \gamma - \mu_2)^2(C_{22} - C_1) \right\} \exp(-ix\xi)d\xi \\ &\quad + \int_{-\infty}^{\infty} pm_3^*(p)D(\xi) \frac{\mu_1 - \mu_2}{\mu_1 - \mu_2 e^{-2\mu a}} \exp(-ix\xi)d\xi \\ \frac{\partial[v^*]}{\partial x} &= \int_{-\infty}^{\infty} \left(-\frac{i}{\xi}\right) \frac{1}{pm_1^*(p)} \left\{ \begin{aligned} &-(\beta + s_2)[s_2^2(B_1 - A_3) - 2s_2(B_2 - A_4)] + s_2^2(B_2 - A_4) \\ &+ (\beta + s_1)(-2s_1A_2 + s_1^2A_1) - s_1^2A_2 + (\beta + \gamma - \mu_1)^2(\gamma - \mu_1)C_{21} \\ &+ (\beta + \gamma - \mu_2)^2(\gamma - \mu_2)(C_{22} - C_1) \end{aligned} \right\} \exp(-ix\xi)d\xi \\ &\quad + \int_{-\infty}^{\infty} \left(-\frac{i}{\xi}\right) pm_3^*(p)D(\xi) \frac{\mu_1 - \mu_2}{\mu_1 - \mu_2 e^{-2\mu a}} \exp(-ix\xi)d\xi\end{aligned}\quad (2.25)$$

Following the procedure in [109], introducing two dislocation density functions as:

$$\psi_1^*(x, p) = \frac{\partial[u^*(x, p)]}{\partial x}, \quad \psi_2^*(x, p) = \frac{\partial[v^*(x, p)]}{\partial x} \quad (2.26)$$

By applying the second mechanical boundary condition on crack faces in equation (2.19), the following singular integral equations can be obtained as:

$$\int_{-1}^1 \sum_{j=1}^2 \left[ \frac{\delta_{ij}}{\tau - x} + k_{ij}(x, \tau) \right] \psi_j^*(\tau, p) d\tau = 4\pi pm_3^*(p)W_i^*(x, p), \quad i=1,2 \quad -1 \leq x \leq 1 \quad (2.27)$$

With

$$\int_{-1}^1 \psi_i^*(x, p) dx = 0, \quad i=1,2 \quad (2.28)$$

The kernels are given by:

$$\begin{aligned}
k_{11}(x, \tau) &= \int_0^{\infty} [1 - 4\xi f_{11}(\xi)] \sin[(x - \tau)\xi] d\xi \\
k_{22}(x, \tau) &= \int_0^{\infty} [1 - 4\xi^2 f_{22}(\xi)] \sin[(x - \tau)\xi] d\xi \\
k_{12}(x, \tau) &= \int_0^{\infty} -4\xi f_{12}(\xi) \cos[(x - \tau)\xi] d\xi \\
k_{21}(x, \tau) &= \int_0^{\infty} -4\xi^2 f_{21}(\xi) \cos[(x - \tau)\xi] d\xi
\end{aligned} \tag{2.29}$$

and

$$\begin{aligned}
W_1^*(x, p) &= 2 \int_0^{\infty} \xi w_1(\xi, p) \sin(x\xi) d\xi \\
W_2^*(x, p) &= -2 \int_0^{\infty} \xi^2 w_2(\xi, p) \cos(x\xi) d\xi \\
w_1^*(\xi, p) &= -\frac{h_{11}(\beta g_1 + 2g_2) + 2sh_{12}(s_2 g_1 - g_2)}{8s^3} - g_3 \\
w_2^*(\xi, p) &= -\frac{h_{21}(\beta g_1 + 2g_2) + 2sh_{22}(s_2 g_1 - g_2)}{8s^3} - g_4
\end{aligned} \tag{2.30}$$

Where the expressions of  $f_{ij}$ ,  $g_1$ ,  $h_{ij}$  can be found in the Appendix.

Using the Lobatto-Chebyshev method [109], the above singular integral equations can be transformed to algebraic equations:

$$\begin{aligned}
\sum_{i=1}^n A_i \left[ \frac{1}{\tau_i - x_k} + k_{11}(x_k, \tau_i) \right] F_1^*(\tau_i, p) + \sum_{i=1}^n A_i k_{12}(x_k, \tau_i) F_2^*(\tau_i, p) &= 4\pi p m_3(p) W_1^*(x_k, p) \\
\sum_{i=1}^n A_i F_1^*(\tau_i, p) &= 0 \\
\sum_{i=1}^n A_i k_{21}(x_k, \tau_i) F_1^*(\tau_i, p) + \sum_{i=1}^n A_i \left[ \frac{1}{\tau_i - x_k} + k_{22}(x_k, \tau_i) \right] F_2^*(\tau_i, p) &= 4\pi p m_3(p) W_2^*(x_k, p) \\
\sum_{i=1}^n A_i F_2^*(\tau_i, p) &= 0
\end{aligned} \tag{2.31}$$

where

$$\psi_i^*(\tau, p) = \frac{F_i^*(\tau, p)}{\sqrt{1 - \tau^2}}, \quad (i = 1, 2), \quad |\tau| \leq 1 \tag{2.32}$$

$$\begin{aligned}
\tau_i &= \cos \frac{(i-1)\pi}{n-1}, \quad i = 1, 2, \dots, n; \\
x_k &= \cos \frac{(2k-1)\pi}{2(n-1)}, \quad k = 1, 2, \dots, n-1; \\
A_i &= \frac{\pi}{2(n-1)}, \quad i = 1, n; \quad A_i = \frac{\pi}{n-1}, \quad i = 2, 3, \dots, n-1.
\end{aligned} \tag{2.33}$$

The stress intensity factors (SIFs) are defined as:

$$K_I^*(p) = -\frac{\pi}{4} F_2^*(1, p), \quad K_{II}^*(p) = -\frac{\pi}{4} F_1^*(1, p) \tag{2.34}$$

To get the SIFs in time domain, the inverse Laplace transformation has to be employed for above solutions. Since analytical inversion is difficult, the numerical inversion by Miller and Guy [110] will be used.

## 2.4 Numerical results and discussions

The SIFs in the time domain can be obtained after the inverse Laplace transform. To begin with, the following standard linear viscoelastic relaxation function:

$$m(t) = \frac{E_\infty}{E_0} + \left(1 - \frac{E_\infty}{E_0}\right) e^{-\frac{t}{t_0}}, \quad \text{with } \frac{E_\infty}{E_0} = 0.5, t_0 = 1 \tag{2.35}$$

is considered [111], and the results of SIFs are shown in comparison with the corresponding elastic solutions. The elastic solution for the same thermal shock and same boundary conditions can be obtained when we assume the relaxation function to be  $m(t) = 1$ . In the following figures, the SIFs for comparison of elastic and viscoelastic materials and a series of parametric investigations are plotted versus dimensionless time. In all the cases, the distance between the boundary and crack faces,  $h$ , is assumed to be 1. It is worth noting the nonhomogeneous parameter  $\varepsilon$  has no influence on the SIFs since it has been eliminated in the governing equations. Besides, from the singular integral equations (2.27), It's easy to find that only the relaxation function  $m_3(t)$  in the thermal expansion coefficient will affect the results of SIFs. From a physical standpoint, this can be explained by the space independence of relaxation functions. All three relaxation functions are assumed to be independent with space coordinates, however,  $\delta T$  (change of temperature) is a

variable dependent on the space coordinates in this problem, which leads to the fact only the relaxation function of thermal expansion will heighten the nonhomogeneity of thermal stresses, thus bringing the variation of SIFs.

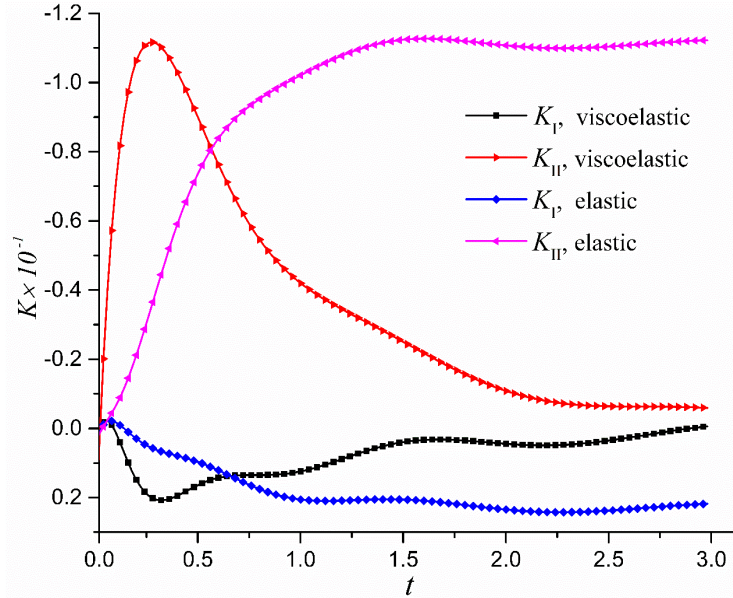


Figure 2.2 Comparison of SIFs (a)  $K_I$  (b)  $K_{II}$  in viscoelastic and elastic materials, when  $(\beta, \delta, \gamma) = (1, 1, 0.1)$ .

As shown in the Figure 2.2,  $K_I$  is positive while  $K_{II}$  is negative in the select values of the nonhomogeneous material parameter. Compared to  $K_I$ , the magnitudes of  $K_{II}$  are much higher in both elastic and viscoelastic materials, more than five times of  $K_I$ , which implies Mode II fracture plays a predominant role under thermal shock in both elastic and viscoelastic FGMs. Significant discrepancies are shown between elastic and viscoelastic results: the elastic SIFs increase from 0 at  $t=0$  to a steady state around  $t=1.5$ , while the viscoelastic SIFs increase from 0 at  $t=0$  to a peak value around  $t=0.3\sim 0.5$ , after which the SIFs start to decrease dramatically, even approaching 0 at  $t=3.0$ , which indicates that although there is no much difference in the maximum of SIFs, the fracture may occur at a much more earlier stage in viscoelastic FGMs under thermal shock if the stress intensity factors exceed the fracture toughness.

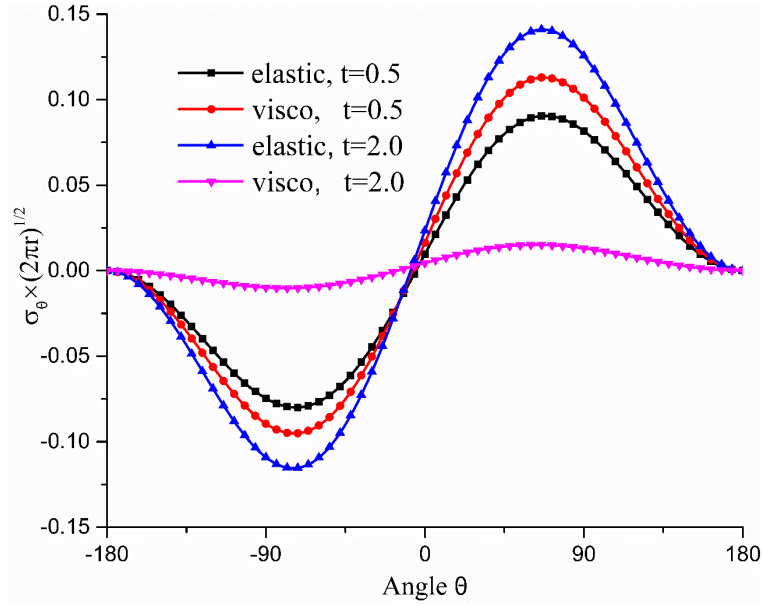


Figure 2.3 Variation of the cleavage stress versus angle  $\theta$  at time  $t = 0.5, t = 2.0$  in elastic and viscoelastic nonhomogeneous materials when  $(\beta, \delta, \gamma) = (1, 1, 0.1)$ .

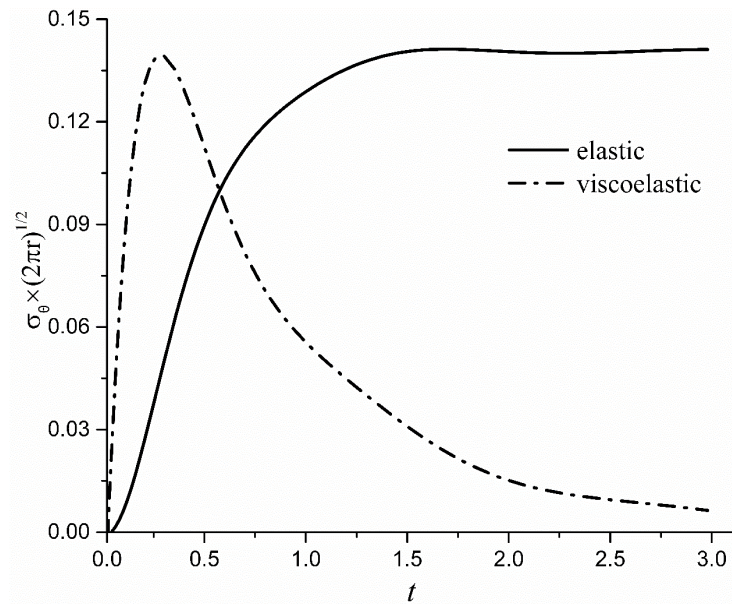


Figure 2.4 Variation of the maximum of cleavage stress versus time in elastic and viscoelastic nonhomogeneous materials when  $(\beta, \delta, \gamma) = (1, 1, 0.1)$ .

To give a clearer comparison and illustrate the dynamic stress field around the crack tip, the variation of cleavage stresses  $\sigma_\theta$  :

$$\sigma_{\theta} = \frac{1}{\sqrt{2\pi r}} \left\{ K_I \left[ \frac{3}{4} \cos\left(\frac{\theta}{2}\right) + \frac{1}{4} \cos\left(\frac{3\theta}{2}\right) \right] + K_{II} \left[ -\frac{3}{4} \sin\left(\frac{\theta}{2}\right) - \frac{3}{4} \sin\left(\frac{3\theta}{2}\right) \right] \right\} \quad (2.36)$$

versus angle  $\theta$  are shown in Figure 2.3 when the nonhomogeneous material parameters  $(\beta, \delta, \gamma) = (1, 1, 0.1)$ . Two different times  $t = 0.5, t = 2.0$  are considered for both elastic and viscoelastic materials. All curves show the cleavage stresses reach their maximum at the same angle, no matter the materials are elastic and viscoelastic, which indicates the crack propagation direction will keep the same at different times. Compared with elastic materials, the cleavage stresses in viscoelastic materials in later stage will be significant decreased. In fracture mechanics, the maximum of cleavage stresses can characterize the crack initiation under mixed mode failure, and their variations with time are depicted in Figure 2.4. The results show that the main difference between elastic and viscoelastic materials are the maximum of cleavage stress reach its peak value at a much earlier time than the elastic one.

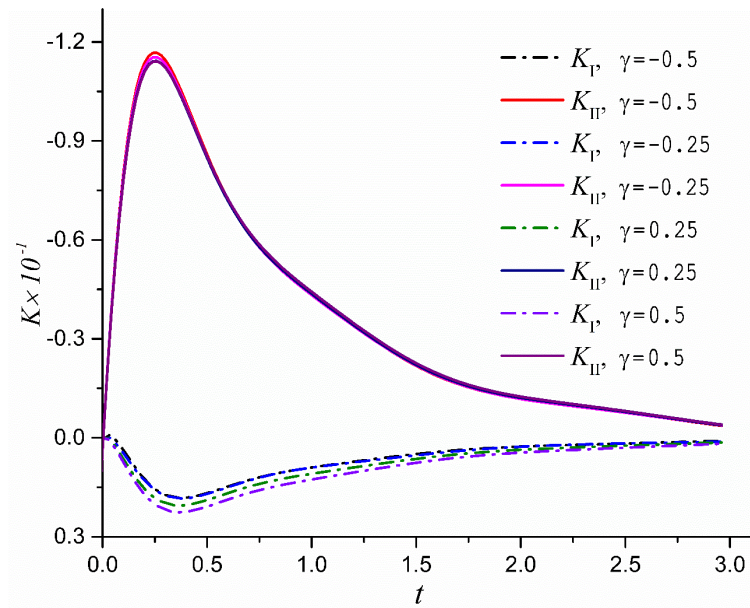


Figure 2.5 The effect of the graded parameter  $\beta$  on the SIFs (a)  $K_I$  (b)  $K_{II}$  when  $\delta = 1, \gamma = 0.1$ .

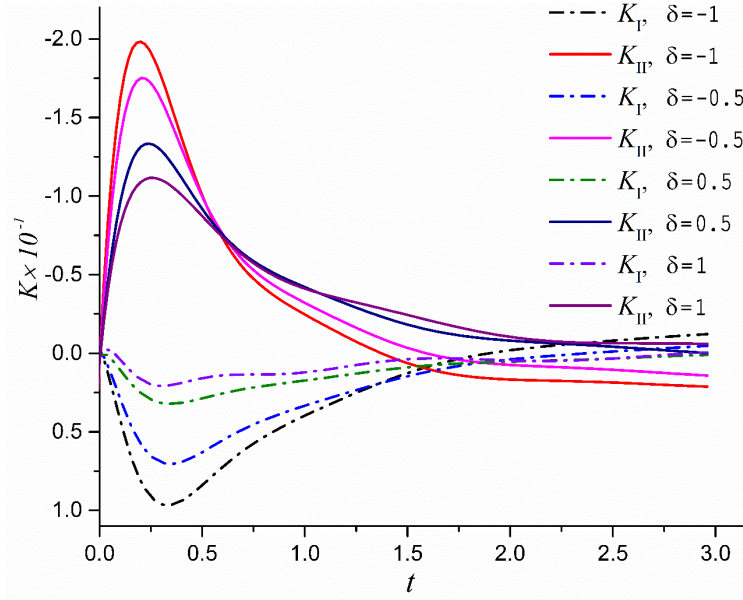


Figure 2.6 The effect of the graded parameter  $\delta$  on the SIFs (a)  $K_I$  (b)  $K_{II}$  when  $\beta = 1, \gamma = 0.1$ .

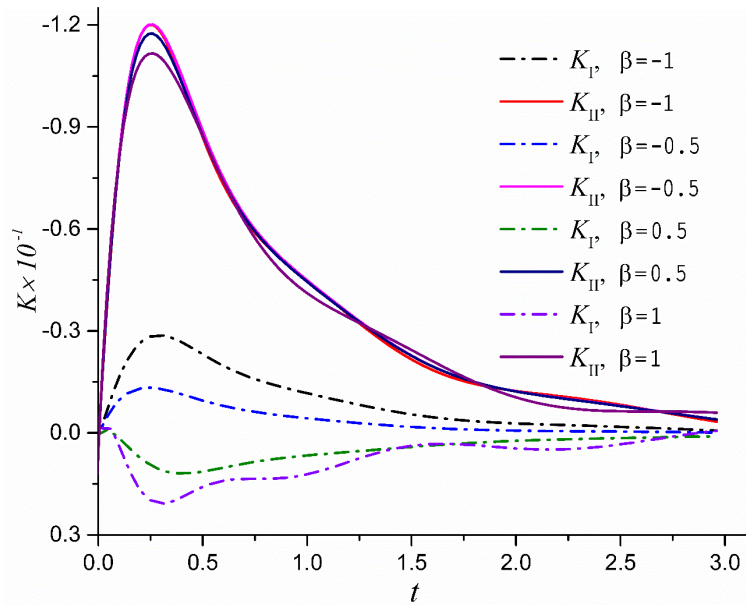


Figure 2.7 The effect of the graded parameter  $\gamma$  on the SIFs (a)  $K_I$  (b)  $K_{II}$  when  $\beta = 1, \delta = 1$ .

In the Figure 2.5, 2.6 and 2.7, parametric investigations are conducted to illustrate the nonhomogeneous parameters' influence on SIFs. Figure 2.5 shows the effect of the graded parameter  $\beta$  on the SIFs when  $\delta = 1, \gamma = 0.1$ . It's obvious that  $\beta$  has very little influence on  $K_{II}$  but has a great impact on  $K_I$ . When  $\beta = 1$ , the  $K_I$  is positive, which means the crack faces are

under tension. When  $\beta = -1$ , the  $K_I$  is negative, which indicates the contact of crack faces would occur. As mentioned above, the Mode II fracture would play a predominant role in this article. It seems the variation of  $K_I$  will have limited effect on the fracture behaviors, however, the contact of crack faces will increase the friction and make the heat transfer easier [6], besides, the crack contact also influence on the Mode II fracture as reported by [112-114]. Therefore, a detailed discussion considering crack contact problem in nonhomogeneous viscoelastic material may be considered in future work.

The effect of the graded parameter  $\delta$  on the SIFs is illustrated in Figure 2.6.  $\delta$  has a great influence on both  $K_I$  and  $K_{II}$ . When  $\delta$  is decreased from 1 to -1, the peak value of  $K_I$  increases to fourfold, while the peak value of  $K_{II}$  is doubled, which greatly heighten the fracture risk. Therefore, an increase of the gradient of thermal conductivity in viscoelastic FGMs can significantly lower the thermal stresses and stress intensity factors. Compared with the nonhomogeneous parameters  $\beta$  and  $\delta$ , the graded parameter  $\gamma$  in thermal expansion has almost no influence on the fracture behaviors, which can be found in Figure 2.7.

Another power law relaxation function is also considered as

$$m(t) = \left(\frac{t_0}{t}\right)^q, \quad q = \frac{1}{2}, \quad t_0 = 1. \quad (2.37)$$

Variations of SIFs with dimensionless time are compared with the standard linear viscoelastic material under the same nonhomogeneous parameters, as shown in Figure 2.8. For  $K_I$ , the magnitude of peak values in viscoelastic material with power law's relaxation is a little higher than that in standard linear one, and the rate of decay is slower. Compared with  $K_I$ , significant difference is illustrated for  $K_{II}$ . For Mode II fracture, the magnitude of peak values in viscoelastic material with power law's relaxation is much higher than that in standard linear one, and the decay of rate would be much slower. At time  $t = 3.0$ , the value of  $K_{II}$  in standard linear viscoelastic material has approached to zero, while the one in viscoelastic material with power law's relaxation is still much higher than zero. All these results indicate the detailed type of relaxation function is vitally important for designing the viscoelastic FGMs.

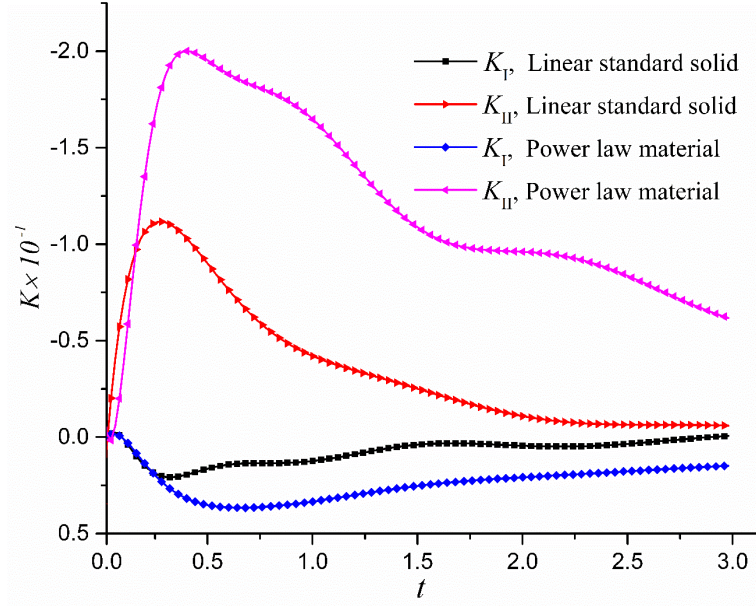


Figure 2.8 Comparison of SIFs for two different viscoelastic relaxation functions when  $\beta = 1, \delta = 1, \gamma = 0.1$ .

## 2.5 Conclusions

In this chapter, the transient SIFs and the thermal stresses under a thermal shock in FGMs are investigated when the crack is parallel to the free boundary of infinite half plane. Two classical types of relaxation function of linear viscoelasticity are considered and the moduli of FGMs are assumed to be forms of both spatial coordinates and time. By employing the Fourier transform and Laplace transform, coupled with the singular integral equations, the governing partial differential equations under mixed thermo-mechanical boundary conditions are solved numerically. The results show that significant discrepancies of transient SIFs exist between nonhomogeneous elastic and viscoelastic materials. The fracture risk occurs at a much earlier stage in viscoelastic FGMs under thermal shock than the elastic ones. An increase of the gradient of thermal conductivity in viscoelastic FGMs can lower the thermal stresses and fracture risks. The materials' intrinsic viscoelastic relaxation properties are vitally important for designing the viscoelastic FGMs. All the results show that the viscoelastic properties should be concerned in designing FGMs, especially the “soft” polymer-based FGMs.

## 2.6 Appendix

$$h_{11}(\xi) = -s_1 + \exp[(s_1 - s_2)h][s_1 + hs_2(s_2 - s_1)]$$

$$h_{12}(\xi) = 1 - \exp[(s_1 - s_2)h][1 - h(s_2 - s_1)(1 - hs_2)]$$

$$h_{21}(\xi) = 1 - \exp[(s_1 - s_2)h][1 + h(s_2 - s_1)]$$

$$h_{22}(\xi) = h^2(s_2 - s_1) \exp[(s_1 - s_2)h]$$

$$f_{11}(\xi) = [-\beta h_{11} + s_2(s_1 - s_2)h_{12}](s_1 - s_2)^{-3}$$

$$f_{12}(\xi) = [-2\xi h_{11} - \xi(s_1 - s_2)h_{12}](s_1 - s_2)^{-3}$$

$$f_{21}(\xi) = [-\beta h_{21} + s_2(s_1 - s_2)h_{22}](s_1 - s_2)^{-3}$$

$$f_{22}(\xi) = [-2\xi h_{21} - \xi(s_1 - s_2)h_{22}](s_1 - s_2)^{-3}$$

$$g_1(\xi) = -s_2^2 f_3 - 2s_2 f_4 + f_5$$

$$g_2(\xi) = -(2s_2 + \beta)s_2^2 f_3 - (3s_2 + 2\beta)s_2 f_4 - f_6$$

$$g_3(\xi) = \exp(-s_2 h)[(1 - hs_2)f_2 - hs_2^2 f_1] - (\beta + \gamma - \mu_1)I_{21} - (\beta + \gamma - \mu_2)I_{22}$$

$$g_4(\xi) = \exp(-s_2 h)[(1 + hs_2)f_1 + hf_2] - I_{21} - I_{22}$$

$$I_1(\xi, p) = \frac{1}{p^2 m_1^*(p) m_3^*(p)} C_1(\xi, p)$$

$$I_{21}(\xi, p) = \frac{1}{p^2 m_1^*(p) m_3^*(p)} C_{21}(\xi, p)$$

$$I_{22}(\xi, p) = \frac{1}{p^2 m_1^*(p) m_3^*(p)} C_{22}(\xi, p)$$

$$f_1(\xi) = I_{21} \exp[-(\beta + \gamma - \mu_1)h] + I_{22} \exp[-(\beta + \gamma - \mu_2)h]$$

$$f_2(\xi) = (\beta + \gamma - \mu_1)I_{21} \exp[-(\beta + \gamma - \mu_1)h] + (\beta + \gamma - \mu_2)I_{22} \exp[-(\beta + \gamma - \mu_2)h]$$

$$f_3(\xi) = I_1 - I_{21} - I_{22}$$

$$f_4(\xi) = -(\beta + \gamma - \mu_1)I_{21} - (\beta + \gamma - \mu_2)(I_{22} - I_1)$$

$$f_5(\xi) = (\beta + \gamma - \mu_1)^2 I_{21} + (\beta + \gamma - \mu_2)^2 (I_{22} - I_1) + \frac{\mu_1 - \mu_2}{\mu_1 - \mu_2 e^{-2\mu h}} D(\xi)$$

$$f_6(\xi) = (\beta + \gamma - \mu_1)^2 (\gamma - \mu_1) I_{21} + (\beta + \gamma - \mu_2)^2 (\gamma - \mu_2) (I_{22} - I_1) + \frac{\mu_1 - \mu_2}{\mu_1 - \mu_2 e^{-2\mu h}} D(\xi) \gamma$$

# **Chapter 3: Investigation of the thermal-elastic problem in cracked semi-infinite FGM under thermal shock using hyperbolic heat conduction theory**

A thermo-elastic analytical model is established for a functionally gradient half-plane containing a crack under a thermal shock in the framework of hyperbolic heat conduction theory. The moduli of FGMs are assumed to vary exponentially with the coordinates. By employing the Fourier transform and Laplace transform, coupled with singular integral equations, the governing partial differential equations under mixed, thermo-mechanical boundary conditions are solved numerically. For both the temperature distribution and transient stress intensity factors (SIFs) in FGMs, the results of hyperbolic heat conduction model are significantly different than those of Fourier's Law, which should be considered carefully in designing FGMs.

## **3.1 Introduction**

Over the past decades, considerable researches have been conducted on FGMs due to their increasing application in heat engineering, such as high temperature chambers, heat exchanger tubes, thermoelectric generators, gas turbines etc. Compared to homogenous composite materials, FGMs possess gradual changes in composition and microstructure with spatially continuous variations in physical and mechanical properties. Invented as a thermal shield to sustain very high temperature gradients in thin structures [115], one primary advantage of FGMs is their excellent performance in improving bonding strength and reducing residual and thermal stresses. Fracture failure of cracked material may occur when the crack propagation is induced by the external high thermal load, such as thermal shock. To investigate the thermal stress concentration around cracks and the potential fracture failure in high temperature environment, numerous studies have been devoted to the crack problem under thermal loading in FGMs [4-9, 116].

However, in the previous studies, almost all the analyses of heat conduction are based on the classical Fourier's Law,

$$\mathbf{q}(\mathbf{X}, t) = -k\nabla T(\mathbf{X}, t), \quad (3.1)$$

where  $\mathbf{q}$  is the heat flux vector,  $T$  is temperature,  $t$  is time,  $\mathbf{X}$  is position and  $k$  is thermal conductivity. Fourier's Law implies the thermal wave can propagate instantaneously in the media at an infinite speed, which contradicts physical facts. Although Fourier's Law is practical in many engineering applications, the negligence of the finite speed of heat propagation would be unacceptable with the increasing demanding of accuracy in engineering problems, especially under some extreme conditions, such as the heat conduction in micro or nano scale, or the extremely low or high temperature conditions etc. [109]. In these situations, the measured results showed significant discrepancy with the temperature predicted by Fourier's Law [109, 117], which indicates that the finite speed of thermal wave has to be taken into consideration. To incorporate the finite speed of thermal wave into heat conduction, the hyperbolic heat conduction model was proposed by Cattaneo and Vernotte [22-28] by introducing the "thermal relaxation time  $\tau_q$ ", which denotes the time lag in the thermal wave propagation, as follows

$$\mathbf{q}(\mathbf{X}, t) + \tau_q \frac{\partial \mathbf{q}(\mathbf{X}, t)}{\partial t} = -k \nabla T(\mathbf{X}, t). \quad (3.2)$$

The relaxation time,  $\tau_q$  is a material constant, usually related to the collision frequency of the molecules within the material, and the finite thermal wave speed can be calculated as  $C_T = \sqrt{k / (\rho c_p \tau_q)}$ , where  $c_p$  is the specific heat, and  $\rho$  is the mass density.

For crack problems, application of the hyperbolic heat conduction model on homogeneous material has been reported in some recent literature. Chen and Hu [109, 118] analyzed the transient SIFs around a crack parallel to the free surface under a thermal shock impact in an infinite half plate, and a cracked substrate bonded to a coating. Hu and Chen [119] investigated a partially, thermal insulated crack in a strip under a thermal shock. When the crack is perpendicular to the surface of the strip, the temperature field will not be disturbed, as reported by Chang et al [120] and Wang et al. [121]. By assuming the time-varying temperature field and stress field will not be affected by the existence of crack, with the help of weight function, they investigated the crack problem by both maximum local stress criterion and maximum stress intensity factors criterion. The fracture behavior of a thermoelastic solid cylinder subjected to a sudden temperature change on its outer surface using hyperbolic heat conduction model are investigated by Fu et. al. [122] for a circumferential crack and Wang [123] for an infinitesimal penny-shaped crack. Zhang and Li

[124] introduced the fractional calculus into the hyperbolic heat conduction model and investigated the fracture problem for a circumferential crack in a hollow cylinder under thermal shock.

The material-dependent thermal relaxation time  $\tau_q$  plays a vital role in the hyperbolic heat conduction theory, usually in the order of picoseconds for most engineering materials [123], which means this theory cannot be neglected only in extreme engineering problems like extremely high rate heating. However, the relaxation time  $\tau_q$  can be up to the order of  $10\text{ s}$  in some functionally graded materials as reported the experiment results in [125], and the order of  $10^2\text{ s}$  in some biology materials [122], where non-Fourier effect would play a significant role in the thermoelastic behavior even under no extreme conditions. With the increasing application of FGMs, especially the polymer-based FGMs in bio-medical engineering, it is necessary to extend the hyperbolic heat conduction to thermoelastic study of FGMs. For example, the hyperbolic heat conduction in a functionally graded sphere and cylinder is investigated by Babaei and Chen [115, 126], where all material properties except for the thermal relaxation time vary continuously along the radius of the structures in a power law. In a separate study, Keles and Conker [127] analyzed the non-Fourier hyperbolic heat conduction analysis for heterogeneous hollow cylinders and spheres made of functionally graded material (FGM) with exponentially-varying properties.

To the authors' best knowledge, the transient crack problem in FGMs under thermal loading using hyperbolic heat conduction model has only been investigated by Eshraghi et al [128]. They assumed the circumferential crack does not disturb the temperature field and studied the fracture behavior in a functionally graded hollow cylinder with the help of weight function. In this article, we aim to build a thermo-elastic, analytical model for an FGM half-plane containing a crack under a thermal shock impact using the hyperbolic heat conduction theory. The crack is parallel to the free surface and assumed to be thermally insulated, so its disturbance to the temperature field could not be neglected. By employing both Fourier transform and Laplace transform, the governing, partial differential equations subjected to thermal-mechanical boundary conditions are reduced to a set of singular integral equations, which is solved numerically by the technique from [129] and Lobatto-Chebyshev method [109]. Finally, the numerical, inverse Laplace transform [110] are performed to obtain the results of temperature field and SIFs in the time domain.

### 3.2 Formulation of the problem and basic equations

As shown in Figure 3.1, assume a crack of length  $2c$  parallel to the free surface is located in a nonhomogeneous, functionally graded half-plane and is subjected to a thermal shock impact  $T_0H(t)$  on the free surface at time  $t = 0$ , where  $H(t)$  is the Heaviside step function. The crack is assumed to be completely, thermally insulated so the redistribution of temperature field must be taken into consideration. At time  $t = 0$ , the temperature of the entire half-plane is initially a constant, without loss of generality, which is set as zero. For simplicity, inertia effect and body forces are neglected.

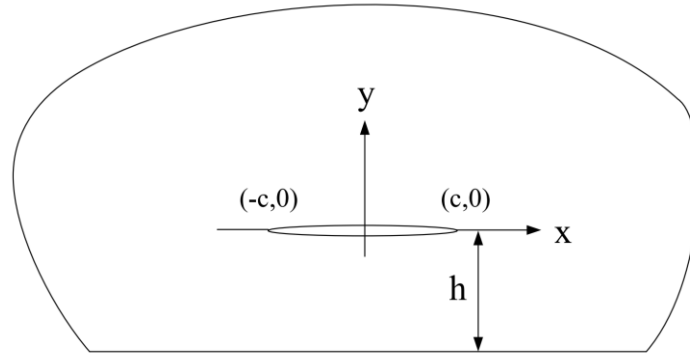


Figure 3.1 Crack geometry and coordinates

The nonhomogeneous properties of the FGM are assumed to vary exponentially with  $y$ -coordinate, expressed as:

$$\begin{aligned}
 E &= E_0 \exp(\beta y), \\
 \nu &= \nu_0 (1 + \varepsilon y) \exp(\beta y), \\
 \alpha &= \alpha_0 \exp(\gamma y), \\
 k &= k_0 \exp(\delta y), \\
 \kappa &= \kappa_0,
 \end{aligned} \tag{3.3}$$

where  $\beta$  is graded material constant for Young's modulus and Poisson's ratio,  $\varepsilon$  is graded material constant for Poisson's ratio,  $\gamma$  is graded material constant for thermal expansion coefficient and  $\delta$  is graded material constant for thermal conductivity;  $E, \nu, \alpha, k$  and  $\kappa$  are the Young's modulus, Poisson's ratio, thermal expansion coefficient, heat conductivity and thermal diffusivity, respectively.

## (1) Heat conduction equations

Usually the heat conduction is assumed to be governed by the classical, parabolic, Fourier's law, in which the speed of heat propagation is infinite. In this article, as described in equation (3.2), the thermal relaxation time  $\tau_q$  is introduced for the hyperbolic the heat conduction model. When the inner heat source is negligible, the conservation of local energy is expressed by:

$$-\nabla \cdot \mathbf{q} = \rho c_p \frac{\partial T}{\partial t}. \quad (3.4)$$

Considering the gradient of thermal conductivity in equation (3.3), coupled with (3.2) and (3.4), the governing equation of the temperature field in FGMs can be obtained as:

$$\nabla^2 T + \delta \frac{\partial T}{\partial y} = \frac{1}{\kappa} \frac{\partial T}{\partial t} + \frac{\tau}{\kappa} \frac{\partial^2 T}{\partial t^2}. \quad (3.5)$$

By introducing the following dimensionless variables,

$$\bar{T} = T / T_0, \quad \bar{t} = t / (c^2 / \kappa), \quad (\bar{x}, \bar{y}, \bar{h}) = (x, y, h) / c, \quad \bar{\delta} = \delta \cdot c, \quad (3.6)$$

then equation (3.5) is converted into the following dimensionless form:

$$\nabla^2 T + \delta \frac{\partial T}{\partial y} = \frac{\partial T}{\partial t} + \frac{\kappa \tau}{c^2} \frac{\partial^2 T}{\partial t^2}. \quad (3.7)$$

Here and after, the hats of the dimensionless variables have been omitted for simplicity. The dimensionless initial and boundary conditions for temperature field are:

$$\begin{aligned} T = 0, \quad \frac{\partial T}{\partial t} = 0, \quad (t = 0), \\ T(x, -h) = 1, \quad (t > 0, |x| < \infty), \\ T = 0, \quad (y \rightarrow \infty), \\ \frac{\partial T}{\partial y} = 0, \quad (y = 0, |x| \leq 1), \\ T(x, 0^+) = T(x, 0^-), \quad (|x| > 1), \\ \frac{\partial T(x, 0^+)}{\partial y} = \frac{\partial T(x, 0^-)}{\partial y}, \quad (|x| > 1). \end{aligned} \quad (3.8)$$

## (2) Thermal stress field equations

In the following, we assume the functionally graded half plane is under plane stress condition. Thus,  $\sigma_{zz} = \sigma_{zx} = \sigma_{zy} = 0$ . Without considering the body force and inertia effect, the equilibrium equations are:

$$\frac{\partial \sigma_x}{\partial x} + \frac{\partial \sigma_{xy}}{\partial y} = 0, \quad \frac{\partial \sigma_{xy}}{\partial x} + \frac{\partial \sigma_y}{\partial y} = 0, \quad (3.9)$$

the strain-displacement relations are:

$$\varepsilon_x = \frac{\partial u}{\partial x}, \quad \varepsilon_y = \frac{\partial v}{\partial y}, \quad \varepsilon_{xy} = \frac{1}{2} \left( \frac{\partial u}{\partial y} + \frac{\partial v}{\partial x} \right), \quad (3.10)$$

the compatibility equation is:

$$\frac{\partial^2 \varepsilon_x}{\partial y^2} + \frac{\partial^2 \varepsilon_y}{\partial x^2} = 2 \frac{\partial^2 \varepsilon_{xy}}{\partial x \partial y}, \quad (3.11)$$

and the thermal-elastic constitutive equations are:

$$\begin{aligned} \varepsilon_x &= \frac{1}{E} (\sigma_x - \nu \sigma_y) + \alpha T, \\ \varepsilon_y &= \frac{1}{E} (\sigma_y - \nu \sigma_x) + \alpha T, \\ \varepsilon_{xy} &= \frac{1+\nu}{E} \sigma_{xy}. \end{aligned} \quad (3.12)$$

Let  $U$  be the Airy stress function, thus the plane stresses can be expressed as:

$$\sigma_x = \frac{\partial^2 U}{\partial y^2}, \quad \sigma_y = \frac{\partial^2 U}{\partial x^2}, \quad \sigma_{xy} = -\frac{\partial^2 U}{\partial x \partial y}. \quad (3.13)$$

Incorporating equations (3.11), (3.12), (3.13), considering material properties in equation (3.3), the governing equation of elastic stress field in FGMs can be obtained as:

$$\nabla^2 \nabla^2 U - 2\beta \frac{\partial}{\partial y} (\nabla^2 U) + \beta^2 \frac{\partial^2 U}{\partial y^2} + E_0 \alpha_0 \exp((\beta + \gamma)y) (\nabla^2 T + 2\gamma \frac{\partial T}{\partial y} + \gamma^2 T) = 0. \quad (3.14)$$

Besides (3.6), introducing the other following dimensionless variables,

$$\begin{aligned}\bar{\sigma}_{ij} &= \sigma_{ij} / (E_0 \alpha_0 T_0), \quad \bar{U} = U / (E_0 \alpha_0 T_0 c^2), \\ (\bar{u}, \bar{v}) &= (u, v) / (c \alpha_0 T_0), \quad \bar{\varepsilon}_{ij} = \varepsilon_{ij} / (\alpha_0 T_0), \\ (\bar{\beta}, \bar{\varepsilon}, \bar{\gamma}) &= (\beta, \varepsilon, \gamma) \cdot c,\end{aligned}\tag{3.15}$$

then the governing equations can be reduced to dimensionless forms:

$$\nabla^2 \nabla^2 U - 2\beta \frac{\partial}{\partial y} (\nabla^2 U) + \beta^2 \frac{\partial^2 U}{\partial y^2} + \exp((\beta + \gamma)y) (\nabla^2 T + 2\gamma \frac{\partial T}{\partial y} + \gamma^2 T) = 0.\tag{3.16}$$

Similarly, the hat of the dimensionless variables is omitted for simplicity. And the boundary conditions for mechanical conditions are:

$$\begin{aligned}\sigma_{xy}(x, -h) &= \sigma_y(x, -h) = 0, \quad (|x| < \infty), \\ \sigma_{xy}(x, 0) &= \sigma_y(x, 0) = 0, \quad (|x| \leq 1), \\ \sigma_{xy}(x, 0^+) &= \sigma_{xy}(x, 0^-), \quad (|x| > 1), \\ \sigma_y(x, 0^+) &= \sigma_y(x, 0^-), \quad (|x| > 1), \\ u(x, 0^+) &= u(x, 0^-), \quad (|x| > 1), \\ v(x, 0^+) &= v(x, 0^-), \quad (|x| > 1).\end{aligned}\tag{3.17}$$

### 3.3 Solution of the temperature field

The Laplace transform is employed against time variable, thus the governing equation (3.7) and the corresponding boundary conditions can be transformed to:

$$\nabla^2 T^* + \delta \frac{\partial T^*}{\partial y} = p T^* + \frac{\kappa \tau}{c^2} p^2 T^*,\tag{3.18}$$

$$\begin{aligned}
T^*(x, -h) &= 1/p, \quad (|x| < \infty), \\
T^* &= 0, \quad (y \rightarrow \infty), \\
\frac{\partial T^*}{\partial y} &= 0, \quad (y = 0, |x| \leq 1), \\
T^*(x, 0^+) &= T^*(x, 0^-), \quad (|x| > 1), \\
\frac{\partial T^*(x, 0^+)}{\partial y} &= \frac{\partial T^*(x, 0^-)}{\partial y}, \quad (|x| > 1).
\end{aligned} \tag{3.19}$$

Here and after, the superscript “\*” denotes the variables in the Laplace domain, and  $p$  is the Laplace transform variable.

By applied Fourier transform to (3.18), the solution of temperature field subjected to (3.19) in the Laplace domain can be obtained as:

$$\begin{aligned}
T^*(x, y, p) &= \int_{-\infty}^{\infty} D(\xi, p) \exp(-m_2 y - i x \xi) d\xi + \frac{1}{p} \exp(-q(y+h)), \quad y > 0, \\
T^*(x, y, p) &= \int_{-\infty}^{\infty} \frac{m_2 D(\xi, p)}{m_1 - m_2 \exp(-2mh)} \{1 - \exp(-2m(h+y))\} \exp(-m_1 y - i x \xi) d\xi \\
&\quad + \frac{1}{p} \exp(-q(y+h)), \quad y < 0,
\end{aligned} \tag{3.20}$$

where  $m_1 = \frac{\delta}{2} - m$ ,  $m_2 = \frac{\delta}{2} + m$ ,  $m = \sqrt{p + \xi^2 + \frac{\delta^2}{4} + Bp^2}$ ,  $q = \frac{\delta}{2} + \sqrt{p + \frac{\delta^2}{4} + Bp^2}$ ,  $B = \frac{\kappa\tau}{c^2}$ ,

and  $D(\xi, p)$  is unknown and will be determined by the following density function:

$$\phi^*(x, p) = \frac{\partial T^*(x, 0^+, p)}{\partial x} - \frac{\partial T^*(x, 0^-, p)}{\partial x}. \tag{3.21}$$

Incorporating equations (3.20) and (3.21), by employing Fourier inverse transform, there is

$$D(\xi, p) = -\frac{i[m_1 - m_2 \exp(-2mh)]}{4\pi\xi m} \int_{-1}^1 \phi^*(\tau, p) \exp(i\xi\tau) d\tau. \tag{3.22}$$

From the condition of continuity in (3.19), it is clear that

$$\int_{-1}^1 \phi^*(x, p) dx = 0, \quad (3.23)$$

$$\phi^*(x, p) = 0, \quad (|x| > 1). \quad (3.24)$$

Substituting equation (3.22) into the temperature distribution (3.20), by using the boundary condition on the crack faces in (3.19), the following singular integral equation is obtained:

$$\int_{-1}^1 \phi^*(\tau, p) \left[ \frac{1}{\tau - x} + k^*(x, \tau, p) \right] d\tau = \frac{2\pi q}{p} \exp(-qh), \quad |x| \leq 1, \quad (3.25)$$

and the kernel function is given as:

$$k^*(x, \tau, p) = \int_0^\infty \left\{ 1 + \frac{m_2 [m_1 - m_2 \exp(-2mh)]}{m\xi} \right\} \sin[(x - \tau)\xi] d\xi. \quad (3.26)$$

The numerical technique in [129] is employed to solve the integral equations (3.23) and (3.25), and the following algebraic equation is obtained:

$$\sum_{k=1}^n \frac{1}{n} F^*(\tau_k, p) \left[ \frac{1}{\tau_k - x_r} + k^*(x_r, \tau_k, p) \right] = \frac{2\pi q}{p} \exp(-qh), \quad |x| \leq 1, \quad (3.27)$$

$$\sum_{k=1}^n \frac{\pi}{n} F^*(\tau_k, p) = 0. \quad (3.28)$$

where  $\tau_k = \cos \frac{(2k-1)\pi}{2n}$ ,  $k = 1, 2, \dots, n$ ;  $x_r = \cos \frac{r\pi}{n}$ ,  $r = 1, 2, \dots, n-1$  and

$$F^*(x, p) = \frac{\phi^*(x, p)}{\sqrt{1-x^2}}, \quad |x| \leq 1. \quad (3.29)$$

Once the integral equations are solved, the temperature field in the Laplace domain can be obtained. The numerical technique in [110] is used for the Laplace inverse transform, thus the temperature field in the time domain is obtained.

### 3.4 Solution of thermal stress field

Once the temperature field in the Laplace domain is obtained, the general solution of equation (3.16) satisfying the regular condition at infinity can be obtained as:

$$\begin{aligned}
 U^*(x, y, p) &= \int_{-\infty}^{\infty} (B_1 + B_2 y) \exp(-s_2 y - ix\xi) d\xi - \int_{-\infty}^{\infty} C_1 \exp[(\beta + \gamma - m_2)y - ix\xi] d\xi, \\
 & \qquad \qquad \qquad y > 0, \\
 U^*(x, y, p) &= \int_{-\infty}^{\infty} \{(A_1 + A_2 y) + (A_3 + A_4 y) \exp(-2sy)\} \exp(-s_1 y - ix\xi) d\xi \\
 & \quad - \int_{-\infty}^{\infty} \{C_{21} + C_{22} \exp(-2\mu y) \exp[(\beta + \gamma - m_1)y - ix\xi]\} d\xi, \qquad y < 0,
 \end{aligned} \tag{3.30}$$

where  $A_1, A_2, A_3, A_4, B_1, B_2$  can be derived from the boundary conditions (3.17), and

$$s_1 = -\frac{\beta}{2} - s, \quad s_1 = -\frac{\beta}{2} + s, \quad s = \sqrt{\xi^2 + \frac{\beta^2}{4}},$$

and

$$\begin{aligned}
 C_1(\xi, p) &= [(\beta + \gamma - m_2)(\gamma - m_2) - \xi^2]^{-2} [\gamma^2 + p - (2\gamma - \delta)m_2] D(\xi, p), \\
 C_{21}(\xi, p) &= [(\beta + \gamma - m_1)(\gamma - m_1) - \xi^2]^{-2} [\gamma^2 + p - (2\gamma - \delta)m_1] \frac{m_2 D(\xi, p)}{m_1 - m_2 \exp(-2mh)}, \\
 C_{22}(\xi, p) &= [(\beta + \gamma - m_2)(\gamma - m_2) - \xi^2]^{-2} [(2\gamma - \delta)m_2 - \gamma^2 - p] \frac{m_2 D(\xi, p) \exp(-2mh)}{m_1 - m_2 \exp(-2mh)}.
 \end{aligned} \tag{3.31}$$

Then the plane stresses can be obtained easily from equation (3.13) and (3.30) by taking some derivatives. Similar to the density function (3.21) in the solution of temperature field, two dislocation density functions are introduced here:

$$\psi_1^*(x, p) = \frac{\partial[u^*(x, p)]}{\partial x}, \quad \psi_2^*(x, p) = \frac{\partial[v^*(x, p)]}{\partial x}, \tag{3.32}$$

where  $[u^*(x, p)]$ , and  $[v^*(x, p)]$  are the displacement jumps across the crack faces. Considering the mechanical boundary condition on crack faces in equation (3.17), the following singular integral equations can be obtained as:

$$\int_{-1}^1 \sum_{j=1}^2 \left[ \frac{\delta_{ij}}{\tau-x} + k_{ij}(x, \tau) \right] \psi_j^*(\tau, p) d\tau = 4\pi W_i^*(x, p), \quad i=1,2, \quad -1 \leq x \leq 1, \quad (3.33)$$

with

$$\int_{-1}^1 \psi_i^*(x, p) dx = 0, \quad i=1,2. \quad (3.34)$$

The Fredholm-type kernels are given by:

$$\begin{aligned} k_{11}(x, \tau) &= \int_0^\infty [1 - 4\xi f_{11}(\xi)] \sin[(x-\tau)\xi] d\xi, \\ k_{22}(x, \tau) &= \int_0^\infty [1 - 4\xi^2 f_{22}(\xi)] \sin[(x-\tau)\xi] d\xi, \\ k_{12}(x, \tau) &= \int_0^\infty -4\xi f_{12}(\xi) \cos[(x-\tau)\xi] d\xi, \\ k_{21}(x, \tau) &= \int_0^\infty -4\xi^2 f_{21}(\xi) \cos[(x-\tau)\xi] d\xi, \end{aligned} \quad (3.35)$$

and

$$\begin{aligned} W_1^*(x, p) &= 2 \int_0^\infty \xi w_1^*(\xi, p) \sin(x\xi) d\xi, \\ W_2^*(x, p) &= -2 \int_0^\infty \xi^2 w_2^*(\xi, p) \cos(x\xi) d\xi, \\ w_1^*(\xi, p) &= -\frac{h_{11}(\beta g_1 + 2g_2) + 2sh_{12}(s_2 g_1 - g_2)}{8s^3} - g_3, \\ w_2^*(\xi, p) &= -\frac{h_{21}(\beta g_1 + 2g_2) + 2sh_{22}(s_2 g_1 - g_2)}{8s^3} - g_4, \end{aligned} \quad (3.36)$$

where the expressions of  $f_{ij}(\xi)$ ,  $h_{ij}(\xi)$  ( $i, j=1, 2$ ) and  $g_i(\xi)$  ( $i=1, 2, 3, 4$ ) can be found in the Appendix. The solutions of the above integral equations can be expressed as:

$$\psi_i^*(x, p) = \frac{G_i^*(x, p)}{\sqrt{1-x^2}}, \quad (i=1, 2), \quad |x| \leq 1. \quad (3.37)$$

Using the Lobatto-Chebyshev method, the above singular integral equations can be transformed to algebraic equations:

$$\begin{aligned}
\sum_{i=1}^n A_i \left[ \frac{1}{\tau_i - x_k} + k_{11}(x_k, \tau_i) \right] G_1^*(\tau_i, p) + \sum_{i=1}^n A_i k_{12}(x_k, \tau_i) G_2^*(\tau_i, p) &= 4\pi W_1^*(x_k, p), \\
\sum_{i=1}^n A_i G_1^*(\tau_i, p) &= 0, \\
\sum_{i=1}^n A_i k_{21}(x_k, \tau_i) G_1^*(\tau_i, p) + \sum_{i=1}^n A_i \left[ \frac{1}{\tau_i - x_k} + k_{22}(x_k, \tau_i) \right] G_2^*(\tau_i, p) &= 4\pi W_2^*(x_k, p), \\
\sum_{i=1}^n A_i G_2^*(\tau_i, p) &= 0,
\end{aligned} \tag{3.38}$$

where

$$\begin{aligned}
\tau_i &= \cos \frac{(i-1)\pi}{n-1}, \quad i = 1, 2, \dots, n, \\
x_k &= \cos \frac{(2k-1)\pi}{2(n-1)}, \quad k = 1, 2, \dots, n-1, \\
A_i &= \frac{\pi}{2(n-1)}, \quad i = 1, n; \quad A_i = \frac{\pi}{n-1}, \quad i = 2, 3, \dots, n-1.
\end{aligned} \tag{3.39}$$

From reference [6], the stress intensity factors (SIFs) in the Laplace domain can be obtained as:

$$K_I^*(p) = -\frac{\sqrt{\pi}}{4} G_2^*(1, p), \quad K_{II}^*(p) = -\frac{\sqrt{\pi}}{4} G_1^*(1, p). \tag{3.40}$$

The dynamic stress intensity factors in the time domain can be obtained by the Laplace inverse transform via equation (3.40),

$$\begin{aligned}
K_I(t) &= \frac{1}{2\pi i} \int_{Br} -\frac{\sqrt{\pi}}{4} G_2^*(1, p) \exp(pt) dp, \\
K_{II}(t) &= \frac{1}{2\pi i} \int_{Br} -\frac{\sqrt{\pi}}{4} G_1^*(1, p) \exp(pt) dp,
\end{aligned} \tag{3.41}$$

where ‘‘Br’’ stands for the Bromwich path. In the following section, the numerical algorithm of Laplace inverse transform proposed by Miller and Guy [110] will be used to obtain the SIFs in the time domain.

### 3.5 Numerical results and discussions

The temperature field distribution in the time domain can be obtained after taking the inverse Laplace transform of equation (3.20). Since the crack is assumed to be thermally insulated, the existence of crack parallel to the free surface will disturb the temperature field. At the beginning, the temperature variations of the mid-points of crack faces versus dimensionless time are investigated under the influence of  $B = \frac{\kappa\tau}{c^2}$ , which plays a vital role in the hyperbolic heat conduction theory.

From [125], the thermal relaxation time for nonhomogeneous FGMs could be up to the order of  $10\text{ s}$ . If we take the typical crack size as  $1\text{ mm}$ , the parameter  $B$  can be up to 10 according the experiment results, which is much larger than that in homogenous materials,

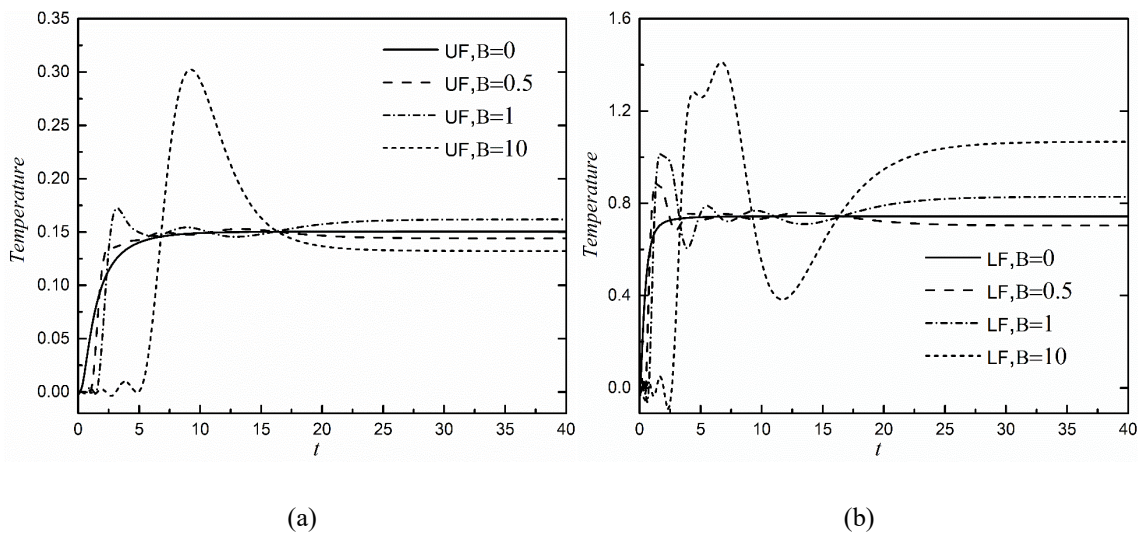
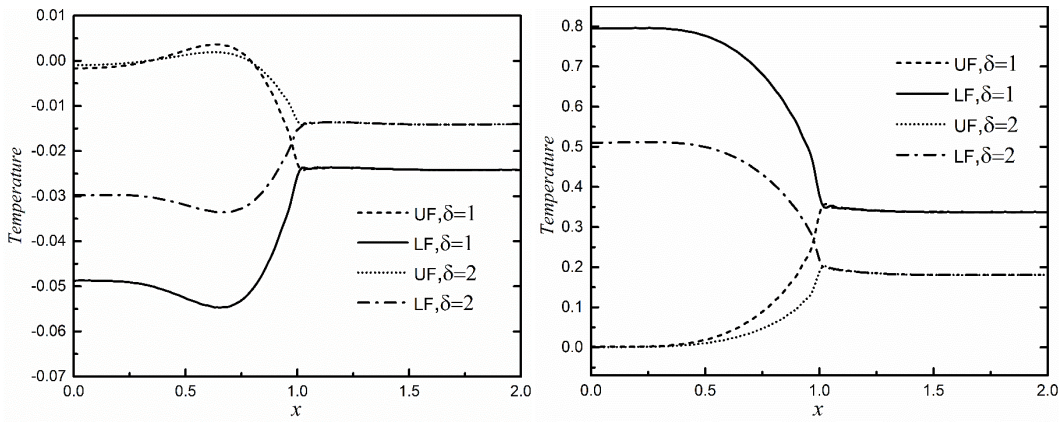


Figure 3.2 The effect of parameter  $B$  on the dimensionless temperature variation versus dimensionless time for (a) mid-point of upper crack face; (b) mid-point of lower crack face.

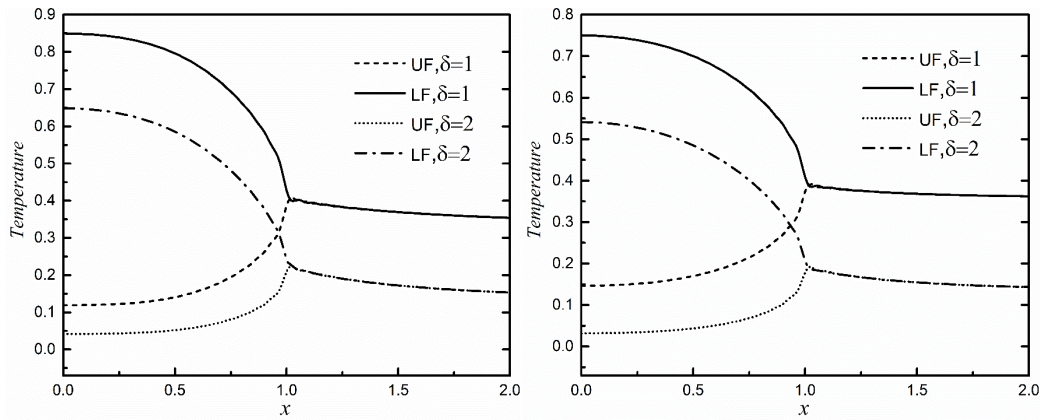
such as metals. As shown in Figure 3.2 (a) and (b), the “UF” and “LF” in these figures denote the temperature of mid-points of upper and lower crack faces, respectively. As expected, the temperature in the upper face is much lower than that of lower face due to thermal insulation of the crack. All curves increase from around zero at time  $t = 0$  till a steady value eventually. For the case of  $B = 0$ , when the hyperbolic heat conduction theory is reduced to the classical Fourier’s Law, the temperature of both “UF” and “LF” will increase gradually until approaching the steady

state values without any fluctuations. The introduction of thermal relaxation time brings fluctuations, and the temperatures for both crack faces need more time to reach the steady state values. With the increase of “B”, the oscillation amplitudes will also increase, so will the time to reach the peak value of temperature. At the lower crack face, the temperature of the mid-point may even reach 1.4 when B=10, which is much higher than the applied thermal shock on the free surface. This is the so-called overshooting phenomenon. Although FGMs have a good performance in reducing thermal gradient, the numerical results show the significant difference in transient temperature variation and the obvious temperature overshooting when the speed of heat transport



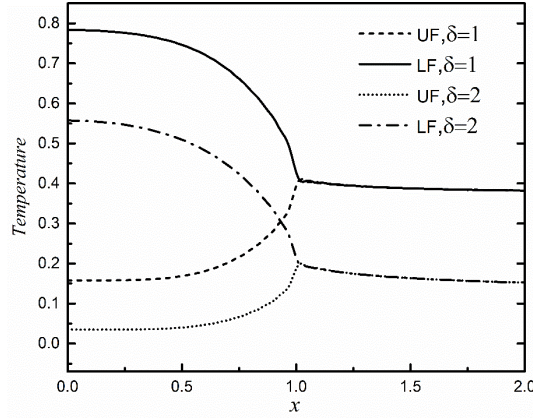
(a)  $t=0.5$

(b)  $t=1$



(c)  $t=2$

(d)  $t=5$



(e)  $t = \text{inf}$

Figure 3.3 Dimensionless temperature on crack faces and extension line, with material constant  $\delta = 1$  and  $\delta = 2$  under different time instants (a)  $t = 0.5$ ; (b)  $t = 1$ ; (c)  $t = 2$ ; (d)  $t = 5$ ; (e)  $t = \text{inf}$ ; while the parameter  $B = 0.5$ .

is considered. Therefore, extra consideration is required to accommodate this overshooting in designing FGMs structures for dynamic thermal disturbances.

The transient temperature distribution on crack faces and their extension line is shown in Figure 3.3 for hyperbolic heat conduction with the parameter  $B = 0.5$  at different time instants. The peak value of temperature always appears at the mid-point of crack faces except when  $t = 0.5$ , in which case the peak points are around the crack tips. The temperature jumps across the crack faces are evident for all cases; and the jump increases at first and then decrease after  $t = 1$ , until it reaches a steady state in case (e) (“inf” denotes a long enough time). From equation (3.20), it is easy to find that only the material parameter  $\delta$  has significant effect on the temperature distribution, and its influence is also shown in these figures. A larger  $\delta$ , i.e., increasing the gradient of thermal conductivity of FGMs, can always reduce the temperature jump across crack faces and lower the temperature along the crack extension line under a thermal shock except at the very early stage (such as that of  $t = 0.5$ ).

The effect of parameter “B” on the variations of SIFs is shown in Figure 3.4 when  $\beta = 1$ ,  $\delta = 1$ ,  $\gamma = 0.1$ . The curves of  $B = 0$  corresponds to the classical Fourier’s Law, where the thermal relaxation time,  $\tau_q = 0$ . Like the temperature variations in Figure 3.2, the SIFs show similar fluctuations. In the case of Fourier’s Law, the SIFs will increase smoothly till a steady

value in a short time, whereas the introduction of “B” brings significant oscillations in all SIF curves. A larger B, i.e. larger thermal relaxation time  $\tau_q$ , corresponds to more time needed to reach the steady-state value and a higher oscillation amplitude. Compared to  $K_I$ , the magnitudes of  $K_{II}$  are always much higher, around four times of  $K_I$ , which implies Mode II fracture would play a dominant role in FGMs under thermal shock. The fracture behavior under the framework of the hyperbolic conduction model would be highly dependent on the value of the parameter  $B = \frac{\kappa\tau}{c^2}$ . When “B” is large enough, like “B=10”, the peak value of  $K_{II}$  calculating from hyperbolic heat conduction model is twice of the steady value of Fourier’s Law, which implies a much higher risk of fracture failure. All results show that consideration of hyperbolic heat conduction model in FGMs brings not only significant temperature overshooting, but also much higher magnitudes of transient SIFs.

$$\sigma_\theta = \frac{1}{\sqrt{2\pi r}} \left\{ K_I \left[ \frac{3}{4} \cos\left(\frac{\theta}{2}\right) + \frac{1}{4} \cos\left(\frac{3\theta}{2}\right) \right] + K_{II} \left[ -\frac{3}{4} \sin\left(\frac{\theta}{2}\right) - \frac{3}{4} \sin\left(\frac{3\theta}{2}\right) \right] \right\} \quad (3.42)$$

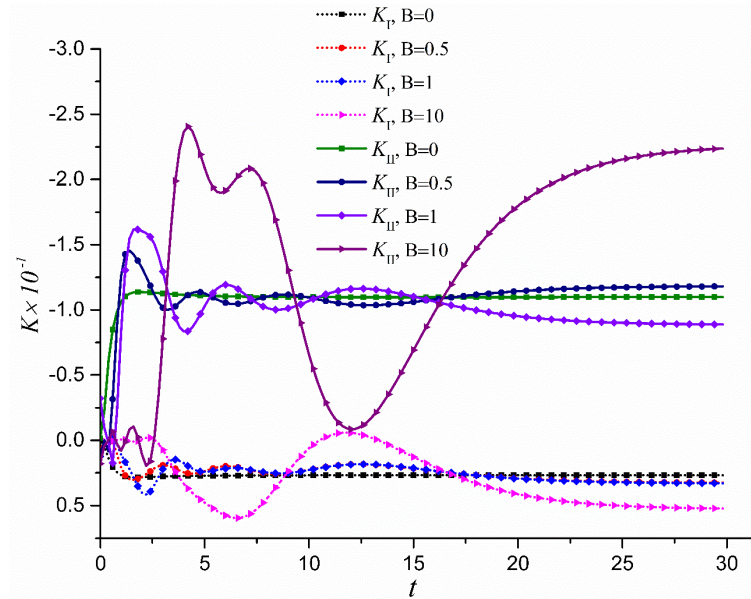


Figure 3.4 The effect of parameter B on the variations of SIFs with time

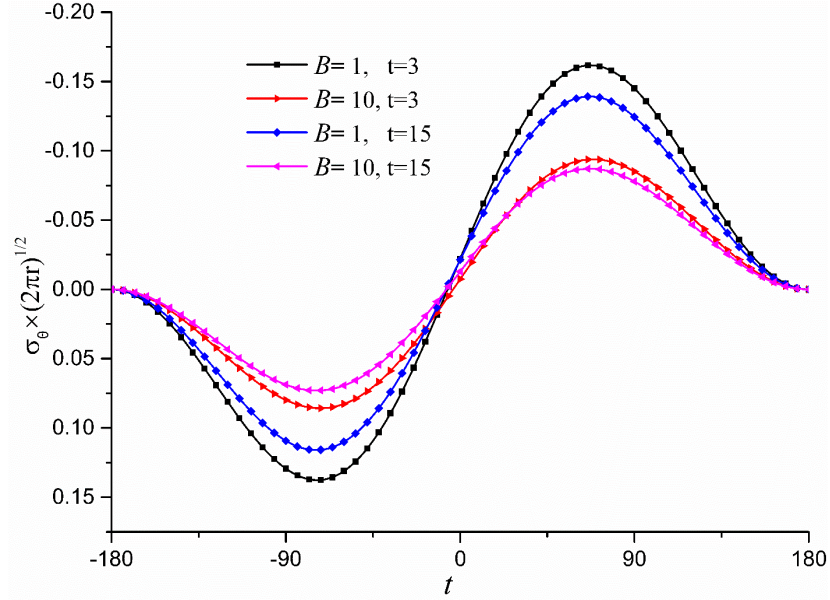


Figure 3.5 Variation of the cleavage stress versus angle  $\theta \in (-\pi, \pi)$  at time  $t = 3, t = 15$  when  $B = 1, B = 10$ .

To give a better illustration of the transient dynamic stress field around the crack tips, the variation of cleavage stresses (see equation (3.42)) versus angle  $\theta \in (-\pi, \pi)$  is shown in Figure 3.5. Two different time instants,  $t = 3, t = 15$  are considered when  $B = 1, B = 10$ . It can be easily found the cleavage stresses reach their maximum at the same angle, which means the direction of the possible crack propagation will always be the same at different time instants independent of the thermal relaxation time. In this premise, we give the time variation of the maximum cleavage stress under different thermal relaxation time. Similar to the variation of stress intensity factors, significant oscillations are observed when the thermal wave speed is considered, and the amplitudes of the oscillations increase with increasing  $B$ . In addition, the variation of the cleavage stress versus time may lead to fatigue failure of the structure. Therefore, it would always be conservative and necessary to take the hyperbolic heat conduction model into consideration in designing FGMs.

In FGMs, the nonhomogeneous material constants play a vital role as they affect the SIFs significantly according to the literature. As a result, the parametric investigations are conducted under the framework of hyperbolic heat conduction theory when  $B = 0.5$ . From the singular integral equation in thermal stress field, the Poisson's ratio would have no influence on the stress

intensity factors, only the material constants  $\beta, \gamma, \delta$  will affect the SIFs. The results of parametric investigations of  $\beta, \gamma, \delta$  are shown in Figure 3.7-3.10. Figure 3.7 shows the effect of the gradient parameter  $\gamma$  on the SIFs when  $\beta=1, \delta=1, B=0.5$ . The results show the parameter  $\gamma$  has almost no influence on  $K_{II}$ , whereas it has a very limited influence on  $K_I$ . An increase of the gradient of thermal expansion can reduce the peak value and the oscillation of  $K_I$ , but not significantly. Compared with  $\gamma$ ,  $\delta$  has a significant influence on both  $K_I$  and  $K_{II}$ , as shown in Figure 3.8. With the increasing gradient of thermal conductivity, the amplitude of stress intensity factors and the oscillation would decrease significantly. As to the gradient in Young's modulus, the value of  $\beta$  has little effect on  $K_{II}$ , but its influence on  $K_I$  could be significant. When  $\beta < 0$ ,  $K_I$  is negative, and when  $\beta > 0$ ,  $K_I$  is positive, which agrees with the result in [6]. With an increasing  $\beta$  in Young's modulus, the peak value of  $K_I$  would also be increased. Similar phenomena can be observed in Figure 3.10. To analyze the fracture risk, the most important aspect is the peak values of the stress intensity factors. From above analysis, it is  $\delta, \beta$  rather than  $\gamma$  that have a significant influence on the peak values of the SIFs. The variations of the peak values with the gradient parameters  $\delta \in (-2, 2)$  and  $\beta \in (-2, 2)$  are shown graphically in Figure 3.10. It is noted the negative values of  $K_I$  indicate crack faces would be under compression. The contact of the crack faces would make the heat transfer easier, and  $K_{II}$  would also be influenced by the crack closure [113-114], which is beyond the scope of this article. To make our discussion reasonable, the  $\beta$  was confined to be positive.

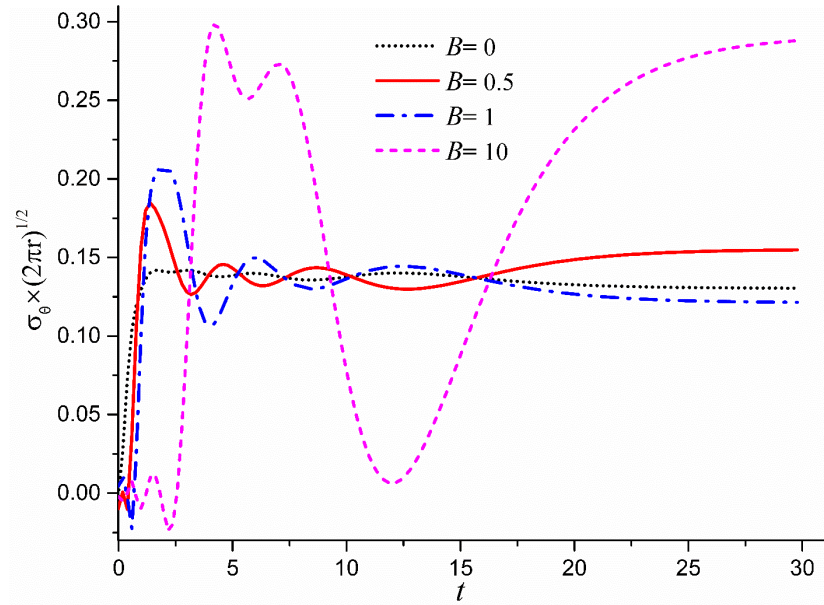


Figure 3.6 The effect of parameter B on variation of the maximum of cleavage stress versus time

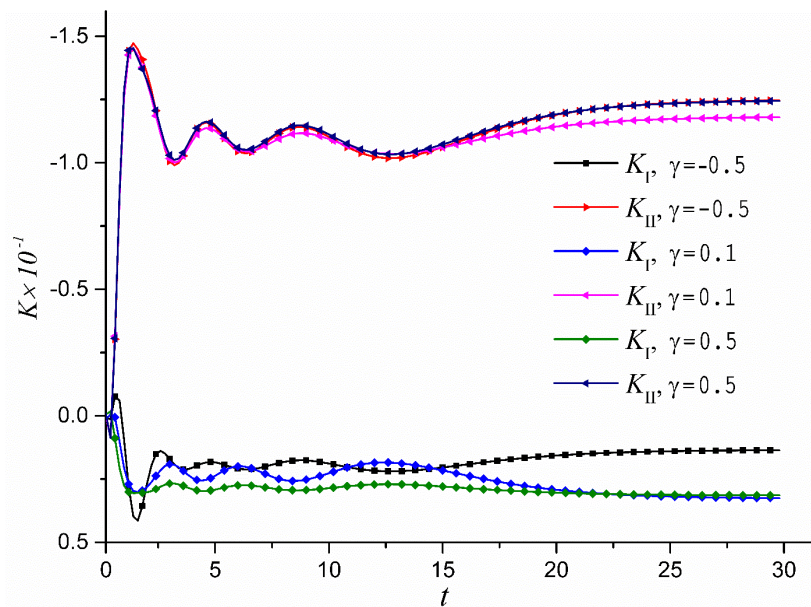


Figure 3.7 The effect of the gradient parameter  $\gamma$  on the SIFs when  $\beta=1, \delta=1, B=0.5$

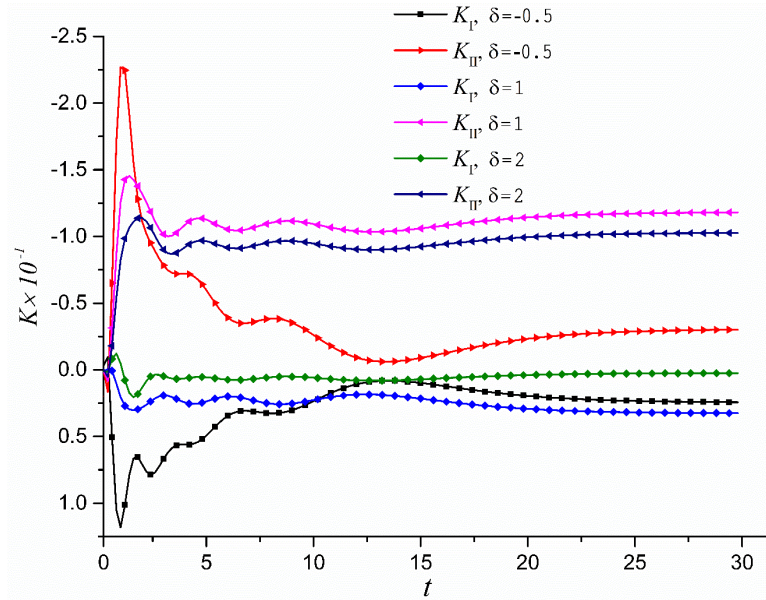


Figure 3.8 The effect of the gradient parameter  $\delta$  on the SIFs when  $\beta = 1, \gamma = 0.1, B = 0.5$

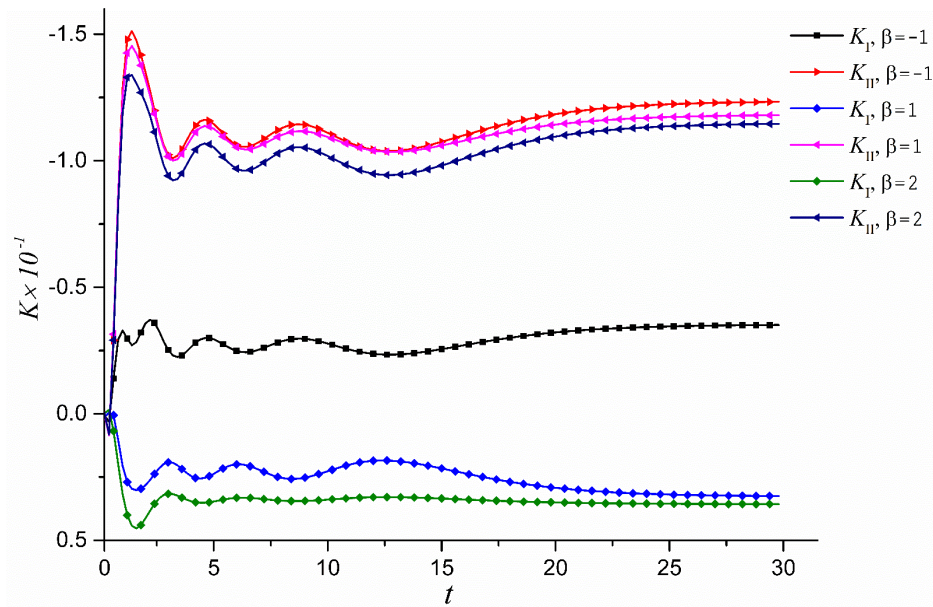


Figure 3.9 The effect of the gradient parameter  $\beta$  on the SIFs when  $\delta = 1, \gamma = 0.1, B = 0.5$

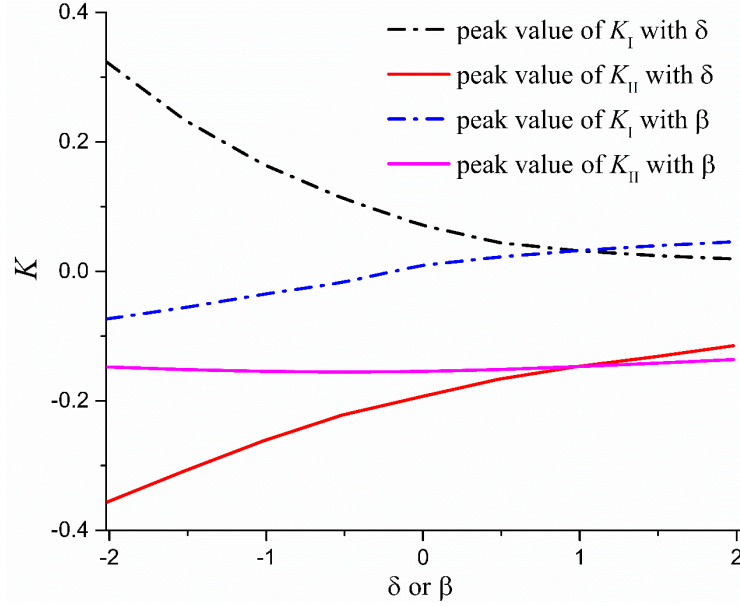


Figure 3.10 The variation of peak values of stress intensity factors with: (1) the gradient parameter  $\beta \in (-2, 2)$  when  $\delta = 1, \gamma = 0.1$ . (2) the gradient parameter  $\delta \in (-2, 2)$  when  $\beta = 1, \gamma = 0.1$ .

### 3.6 Conclusions

In this paper, the transient SIFs and the thermal stresses of an FGM half-space with a crack parallel to the surface have been investigated under a thermal shock in the framework of the hyperbolic heat conduction theory. By employing the Fourier transform and Laplace transform, coupled with the method of singular integral equations, the governing partial differential equations under mixed thermo-mechanical boundary conditions have been solved. The results show that significant discrepancies of both temperature distribution and transient SIFs exist between the hyperbolic heat conduction model and Fourier's Law. Although FGMs have good performance in reducing thermal gradient and thermal stresses, significant temperature overshooting and much higher transient SIFs are observed when the finite speed of heat wave is considered. The present work confirms that for FGMs with relatively high "thermal relaxation time" in the transient heat processes, hyperbolic-type heat conduction models should be employed in designing structural components to account for the dynamic overshooting in order to avoid potential fracture risk.

### 3.7 Appendix

$$\begin{aligned}
 h_{11}(\xi) &= -s_1 + \exp[(s_1 - s_2)h][s_1 + hs_2(s_2 - s_1)] \\
 h_{12}(\xi) &= 1 - \exp[(s_1 - s_2)h][1 - h(s_2 - s_1)(1 - hs_2)] \\
 h_{21}(\xi) &= 1 - \exp[(s_1 - s_2)h][1 + h(s_2 - s_1)] \\
 h_{22}(\xi) &= h^2(s_2 - s_1) \exp[(s_1 - s_2)h]
 \end{aligned}$$

$$\begin{aligned}
 f_{11}(\xi) &= [-\beta h_{11} + s_2(s_1 - s_2)h_{12}](s_1 - s_2)^{-3} \\
 f_{12}(\xi) &= [-2\xi h_{11} - \xi(s_1 - s_2)h_{12}](s_1 - s_2)^{-3} \\
 f_{21}(\xi) &= [-\beta h_{21} + s_2(s_1 - s_2)h_{22}](s_1 - s_2)^{-3} \\
 f_{22}(\xi) &= [-2\xi h_{21} - \xi(s_1 - s_2)h_{22}](s_1 - s_2)^{-3}
 \end{aligned}$$

$$\begin{aligned}
 g_1(\xi) &= -s_2^2 f_3 - 2s_2 f_4 + f_5 \\
 g_2(\xi) &= -(2s_2 + \beta)s_2^2 f_3 - (3s_2 + 2\beta)s_2 f_4 - f_6 \\
 g_3(\xi) &= \exp(-s_2 h)[(1 - hs_2)f_2 - hs_2^2 f_1] - (\beta + \gamma - \mu_1)C_{21} - (\beta + \gamma - \mu_2)C_{22} \\
 g_4(\xi) &= \exp(-s_2 h)[(1 + hs_2)f_1 + hf_2] - C_{21} - C_{22}
 \end{aligned}$$

$$\begin{aligned}
 f_1(\xi) &= C_{21} \exp[-(\beta + \gamma - \mu_1)h] + C_{22} \exp[-(\beta + \gamma - \mu_2)h] \\
 f_2(\xi) &= (\beta + \gamma - \mu_1)C_{21} \exp[-(\beta + \gamma - \mu_1)h] + (\beta + \gamma - \mu_2)C_{22} \exp[-(\beta + \gamma - \mu_2)h] \\
 f_3(\xi) &= C_1 - C_{21} - C_{22} \\
 f_4(\xi) &= -(\beta + \gamma - \mu_1)C_{21} - (\beta + \gamma - \mu_2)(C_{22} - C_1) \\
 f_5(\xi) &= (\beta + \gamma - \mu_1)^2 C_{21} + (\beta + \gamma - \mu_2)^2 (C_{22} - C_1) + \frac{\mu_1 - \mu_2}{\mu_1 - \mu_2 e^{-2\mu h}} D(\xi) \\
 f_6(\xi) &= (\beta + \gamma - \mu_1)^2 (\gamma - \mu_1)C_{21} + (\beta + \gamma - \mu_2)^2 (\gamma - \mu_2)(C_{22} - C_1) + \frac{\mu_1 - \mu_2}{\mu_1 - \mu_2 e^{-2\mu h}} D(\xi)\gamma
 \end{aligned}$$

## **Chapter 4: Investigation of transient thermal-mechanical behavior of a cracked viscoelastic material using time-fractional dual-phase-lag theory**

In the past decade, viscoelastic materials (like polymer composites, biological tissues, rubber, etc.) have been increasingly used in a variety of industries due to their excellent multifunctional properties. In this work, by extending the fractional calculus to DPL heat conduction theory, the transient thermal-mechanical response in cracked viscoelastic materials under thermal shock is analyzed. With the aids of Fourier and Laplace transform, the thermal-viscoelastic problem is converted into a system of singular integral equations with Cauchy kernels of the first kind, which are then solved numerically. The parametric study is performed and the numerical results of temperatures, intensity factors of temperature gradient (IFTG) and stress intensity factors (SIFs) around the crack tips, are shown graphically to illustrate the effects of time fractional order, thermal lags and viscoelastic relaxation on the thermoelastic response.

### **4.1 Introduction**

Due to the excellent multifunctional and rheological properties, viscoelastic materials [88-89], such as polymer matrix composites, biological tissues, rubber, composite propellant, nanocomposites hydrogels, soft elastomers, are becoming more and more popular and promising in many industrial applications, like aerospace, drug delivery, biomedical, mechanical, civil and nuclear engineering. Viscoelastic materials usually exhibit both elastic and viscous characteristics when undergoing deformation. In particular, the rheological property shares the time-dependent features in the mechanical response, which is functions of not only the current input but also the historical process [52-53]. To describe these specific characteristics, like delayed strain recovery or creep under constant loads, the linear viscoelastic response can usually be characterized by the hereditary integral [52].

One common but important aspect to evaluate the viscoelastic materials is their performance under thermal loading [54-55]. It is of great importance to figure out the detailed mechanism of thermo-viscoelasticity in some applications. In recent years, highly increasing attention has been paid to the generalized thermoviscoelasticity, in which a variety of Non-Fourier

heat conduction theories are concerned with. The classical Fourier law of heat conduction is the conventional approach which was extensively employed especially in engineering problems. However, one main drawback of this parabolic theory is the neglect of thermal wave speed, which implies the heat propagation speed is infinite [20]. To address this problem, the hyperbolic heat conduction theory, also known as C-V theory, is established by Cattaneo and Vernotte [27-28], who introduced a thermal relaxation time  $\tau_q$ , shown as  $\vec{q}(t + \tau_q) = -k\nabla T(t)$ , which indicates it requires a delay time  $\tau_q$  to build the heat flux after the temperature gradient of a point is built at time  $t$ . To some extent, this theory provides a promising tool to consider the effect of thermal inertia in heat conduction. However, it assumes a macroscopic thermal behavior averaged over many grains and discernible discrepancies are observed between theoretical predictions and experiment results [130], which leaves the model open for debate [131]. On the other hand, the phenomenological, two-step model proposed by Anisimov [132] achieved success in describing the temperatures of election gas and the metal lattice during short pulse laser treatment [133]. To incorporate the microscopic effects (like electron-phonon interaction) into a macroscopic description, Tzou [20] proposed the dual-phase-lag (DPL) model, shown as  $\vec{q}(t + \tau_q) = -k\nabla T(t + \tau_T)$ , where  $\tau_T$  is the thermal lag of temperature gradient. The DPL model can capture the transient effect when the response time is comparable to the thermalization time needed for the microstructural interaction to build the thermodynamic equilibrium. The generalized thermoviscoelasticity is of significant importance for some applications like the microfabrication of medical stent design using femtosecond laser, especially considering the thermal lags can reach the order of 1~10 second for some viscoelastic composites and biological tissues [122, 134]. Mohamed et. al. [135] proposed the generalized, thermo-viscoelastic plane wave theory with two relaxation times. The uniqueness and reciprocity theorems for generalized thermo-viscoelasticity with thermal relaxation were proved by Ezzat et al. [136]. The state space formulation for thermo-viscoelasticity with two relaxation times was introduced by Ezzat et al. [137]. Mohamed et al. [138] proposed the basic theory for generalized thermo-magneto-viscoelasticity in isotropic and electrically conductive space. The solution of generalized thermo-viscoelasticity for an isotropic medium with variable thermal conductivity and fractional-order heat transfer are given in [139]. Recently, a generalized, thermo-viscoelastic analysis with fractional strain in a thick plate is investigated by Li et al. [56].

The aforementioned research about thermo-viscoelasticity mainly focused on the transient, one-dimensional heat conduction and the governing equations were usually solved by Laplace transform. Non-Fourier heat conduction shares the wave-like behaviors and overshooting phenomena [109], which is believed as a result of interference of two thermal waves. Heat conduction would become more complicated in cracked media, considering the wave-like thermal propagation, interference of thermal waves, and the disturbance induced by the thermally insulated cracks. Besides, the overshooting temperature in cracked media raises more concerns about the safety of structures under thermal disturbances, especially for sophisticated microdevices. Overshooting temperature in cracked media may elevate the thermal stress to the level for crack propagation. Nowadays the Non-Fourier thermal-mechanical research in cracked media mainly focuses on elastic materials. Chen and Hu [109,119] firstly extend Non-Fourier heat conduction to crack problems in a half plane and a long strip, respectively. Chang et al. [120] and Wang et al. [121] investigate the transient crack problems in a half plane under thermal shock when the crack is perpendicular to the free surface, where the crack will not disturb the temperature field. Zhang et al. [124,140] extend the fractional, CV heat conduction theory to thermo-elasticity in cracked media. In these researches, the materials are assumed to be pure elastic and the viscoelastic relaxation is neglected. However, the viscous effect of many materials would become significant under elevated temperatures. For some viscoelastic materials, experiments show their fracture toughness is temperature-dependent and would decrease with the increase of work temperature [141-143]. With the wide applications of viscoelastic composites, the thermal-mechanical behavior of these materials under thermal shock and the associated safety problem becomes an essential necessity.

Although DPL heat conduction theory has been widely applied in the theoretical and numerical works, some unphysical results have been reported [144-146]. Similar unrealistic phenomena can be observed in the non-Fourier heat conduction in cracked media [147]. Take the results in [147] for example, when the initial dimensionless temperature was assumed to be dimensionless zero and the applied thermal temperature on the surface was all positive, negative temperatures were observed in the early stage of temperature history. Although the crack would disturb the heat flux and thermal waves may interfere with each other, the appearance of negative dimensionless temperatures indicates some heat flux flowed from cold areas to hot areas, which obviously violates the second law of thermodynamics. Compared with conventional integer

differential order, fractional calculus has been used successfully to modify many models of physical processes [29, 32]. The most important aspect of time fractional differential is their nonlocal properties and memory effects, which implies the next state of a system depends on both the current input as well as the historical states. The extension of fractional calculus to heat conduction theory has yielded promising results. The sharp thermal wavefront which implies infinite thermal gradient in hyperbolic heat conduction theory was eliminated [38] using fractional models, and the enhanced fractional heat conduction theory fits very well with the experiment and shows the fractional order is a powerful characteristic parameter for non-continuous materials like composites [39].

In this study, the time fractional differential is extended to DPL heat conduction model to investigate the heat transfer in a half-infinite space with an embedded crack which is parallel to the free surface under thermal shock. The viscoelastic relaxation is considered to analyze the mechanical response and fracture behavior of the cracked half-space. By using Laplace and Fourier transforms, the governing equations subjected to thermal-mechanical boundary conditions are reduced to singular integral equations, which are then solved numerically. Finally, the numerical inversion of Laplace transform is employed to present the results of temperature, IFTG and SIFs in the time domain.

## 4.2 Problem formulation and basic equations

As shown in Figure 4.1, consider a semi-infinite, isotropic, viscoelastic space with a Griffith crack heated by a sudden thermal shock. The crack of length  $2c$  is parallel to the free surface and assumed to be thermally insulated completely. Initially, the temperature of the space is assumed to be equal to  $T_1$  uniformly. The thermal shock  $T_0H(t)$  is applied on the free surface at  $t=0$  and keeps to be constant afterwards, where  $H(t)$  is the Heaviside step function. In this research, the uncoupled, thermo-viscoelasticity and quasi-static problem are assumed, in which only the temperature field influences the viscoelastic stresses, whilst the stress will not affect the temperature field. In addition, the inertia effect is neglected.

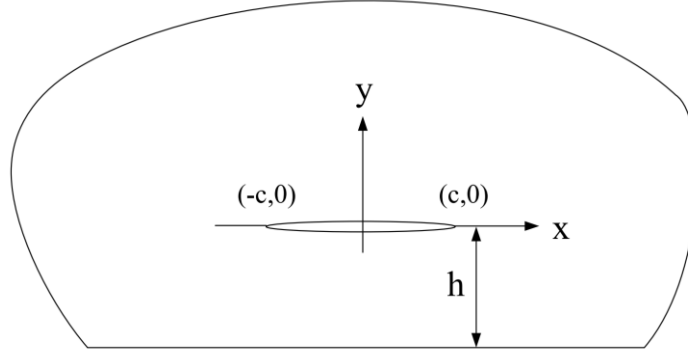


Figure 4.1 Geometry of the crack problem

Considering microstructural interaction, in order to eliminate the aforementioned negative effect coupled with integral order DPL model [147], the time fractional DPL model is employed to govern the heat conduction in this research, where the thermal lags in composites can be treated as structural properties. Using Taylor series expansion, the fractional DPL theory shows:

$$\mathbf{q} + \frac{\tau_q^\alpha}{\alpha!} \frac{\partial^\alpha \mathbf{q}}{\partial t^\alpha} + \frac{\tau_q^{2\alpha}}{(2\alpha)!} \frac{\partial^{2\alpha} \mathbf{q}}{\partial t^{2\alpha}} = -k(\nabla T + \frac{\tau_T^\alpha}{\alpha!} \frac{\partial^\alpha \nabla T}{\partial t^\alpha}), 0 < \alpha \leq 1 \quad (4.1)$$

where  $q$  is heat flux,  $T$  is temperature rise with respect to the reference temperature,  $\tau_q$  is the time lag of heat flux,  $\tau_T$  is the time lag of temperature rise,  $k$  is thermal conductivity,  $\nabla$  is gradient operator, and the Caputo fractional derivative of order  $\alpha$  is defined as:

$$\frac{\partial^\alpha f(X, t)}{\partial t^\alpha} = \begin{cases} \frac{1}{\Gamma(1-\alpha)} \int_0^t (t-\tau)^{-\alpha} \frac{\partial f(X, \tau)}{\partial \tau} d\tau, & 0 < \alpha < 1 \\ \frac{\partial f(X, t)}{\partial t}, & \alpha = 1 \end{cases} \quad (4.2)$$

Coupled with the energy conservation  $-\nabla \cdot \mathbf{q} = \rho c_p \cdot \partial T / \partial t$ , where  $\rho$  is the mass density and  $c_p$  is the specific heat, the governing equation of temperature field reads:

$$a[\nabla^2 T + \frac{\tau_T^\alpha}{\alpha!} \frac{\partial^\alpha \nabla^2 T}{\partial t^\alpha}] = \frac{\partial T}{\partial t} + \frac{\tau_q^\alpha}{\alpha!} \frac{\partial^{1+\alpha} T}{\partial t^{1+\alpha}} + \frac{\tau_q^{2\alpha}}{(2\alpha)!} \frac{\partial^{1+2\alpha} T}{\partial t^{1+2\alpha}} \quad (4.3)$$

where  $a = k / \rho c_p$  is the thermal diffusivity. For simplicity, some dimensionless variables, such as  $\bar{T} = (T - T_1) / (T_0 - T_1)$ ,  $\bar{t} = t / (c^2 / a)$ ,  $(\bar{x}, \bar{y}, \bar{h}) = (x, y, h) / c$ ,  $\bar{\tau}_q = \tau_q / (c^2 / a)$ ,  $\bar{\tau}_T = \tau_T / (c^2 / a)$ , are introduced, and thus the thermal governing equation is reduced to:

$$\nabla^2 T + \frac{\tau_T^\alpha}{\alpha!} \frac{\partial^\alpha}{\partial t^\alpha} \nabla^2 T = \frac{\partial T}{\partial t} + \frac{\tau_q^\alpha}{\alpha!} \frac{\partial^{1+\alpha} T}{\partial t^{1+\alpha}} + \frac{\tau_q^{2\alpha}}{(2\alpha)!} \frac{\partial^{1+2\alpha} T}{\partial t^{1+2\alpha}} \quad (4.4)$$

Here and after, the hats on the variables are neglected for simplicity. Besides, the dimensionless forms for the initial and boundary conditions of temperature field are:

$$\begin{aligned} T &= 0, \quad \frac{\partial T}{\partial t} = 0, \quad (t = 0) \\ T(x, -h) &= 1, \quad (t > 0, |x| < \infty) \\ T &= 0, \quad (y \rightarrow \infty) \\ \frac{\partial T}{\partial y} &= 0, \quad (y = 0, |x| \leq 1) \\ T(x, 0^+) &= T(x, 0^-), \quad (|x| > 1) \\ \frac{\partial T(x, 0^+)}{\partial y} &= \frac{\partial T(x, 0^-)}{\partial y}, \quad (|x| > 1) \end{aligned} \quad (4.5)$$

In this research, the viscoelastic relaxation of material will be focused on. Unlike the elastic materials, the viscoelastic stress-strain relationship is always time-dependent and highly depends on the history. The basic phenomenological mechanical models, such as the Maxwell and Kelvin models, are composed of two elements: a spring for elastic behavior and a damper for viscous behavior. More realistic mathematical models to represent the actual stress-strain response are the generalized Maxwell or Kelvin models. With the help of Boltzmann Superposition Principle and considering the rheological properties of the volume, the Hereditary Integral is employed to characterize the constitutive equations. Isotropic viscoelastic materials usually behave distinctly different in shear and dilatational deformation, so the constitutive equations of thermo-viscoelasticity are expressed separately. Assuming there is no strain history before time  $t=0$ , in order to take the history effects into account, the linear viscoelastic constitutive law is expressed in the form of convolution integral [52]:

$$\begin{aligned}
s_{ij} &= \int_0^t G_1(t-\tau) \frac{de_{ij}}{d\tau} d\tau \\
\sigma_{kk} &= \int_0^t G_2(t-\tau) \frac{d\varepsilon_{kk}}{d\tau} d\tau - 3 \int_0^t \varphi(t-\tau) \frac{dT}{d\tau} d\tau
\end{aligned} \tag{4.6}$$

with

$$s_{ij} = \sigma_{ij} - \frac{1}{3} \sigma_{kk} \delta_{ij}, \quad e_{ij} = \varepsilon_{ij} - \frac{1}{3} \varepsilon_{kk} \delta_{ij}$$

where  $G_1(t)$ ,  $G_2(t)$  are the shear and the bulk relaxation functions,  $\varphi(t)$  is the thermal relaxation function, and  $s_{ij}$ ,  $e_{ij}$  are deviatoric components of the stress and strain tensors. The Laplace transform is employed to convert these convolutions. Assume viscoelasticity can be well represented by the generalized Maxwell model in this research, the viscoelastic properties would be:

$$E(t) = E_0 f_1(t), \nu(t) = \nu_0 f_2(t), \lambda(t) = \lambda_0 f_3(t) \tag{4.7}$$

where  $E(t)$ ,  $\nu(t)$ ,  $\lambda(t)$  are Young's modulus, Poisson's ratio and thermal expansion coefficient, respectively,  $E_0, \nu_0, \lambda_0$  are the initial constants, and

$$f_1(t) = f_2(t) = f_3(t) = \frac{1}{E_0} \left( \sum_{i=1}^n E_i e^{-\frac{t}{t_i}} + E_\infty \right) \tag{4.8}$$

are the relaxation functions with no loading applied on the material before  $t = 0$ .  $E_i$  and  $t_i$  are the spring constants and the relaxation time of the  $i$ -th Maxwell element,  $E_\infty$  is the modulus when the time approach to infinity. Considering the following relationships [50] in the Laplace domain:

$$G_1^* = \frac{E^*}{1 + p\nu^*}, G_2^* = \frac{E^*}{1 - 2p\nu^*}, \varphi^* = pG_2^* \lambda^* \tag{4.9}$$

where  $p$  is the Laplace transform variable, the superscript “\*” denotes the variables in the Laplace domain, and thus Eq. (4.6) can be reduced to:

$$\begin{aligned}
\varepsilon_x^* &= \frac{\partial u^*}{\partial x} = \frac{1}{pE_0 f_1(p)} [\sigma_x^* - p\nu_0 f_2(p) \sigma_y^*] + p\alpha_0 f_3(p) T^* \\
\varepsilon_y^* &= \frac{\partial v^*}{\partial y} = \frac{1}{pE_0 f_1(p)} [\sigma_y^* - p\nu_0 f_2(p) \sigma_x^*] + p\alpha_0 f_3(p) T^* \\
\varepsilon_{xy}^* &= \frac{\partial u^*}{\partial y} + \frac{\partial v^*}{\partial x} = \frac{2(1 + p\nu_0 f_2(p))}{pE_0 f_1(p)} \sigma_{xy}^*
\end{aligned} \tag{4.10}$$

where  $f_i^*(p)$  are the Laplace transform of  $f_i(t)$  ( $i=1,2,3$ ). Then substituting the strains in Eq. (4.10) into the compatibility equation and introduce the Airy stress function, one can obtain the governing equation of the stress field:

$$\nabla^2 \nabla^2 U^* + E_0 \lambda_0 p^2 f_1^*(p) f_3^*(p) \nabla^2 T^* = 0 \tag{4.11}$$

where  $U^*$  is the Airy stress function in the Laplace domain. In addition to the previous dimensionless variables, some other dimensionless forms,  $\bar{\sigma}_{ij}^* = \sigma_{ij}^* / (E_0 \lambda_0 T_0)$ ,  $\bar{U}^* = U^* / (E_0 \lambda_0 T_0 c^2)$ ,  $(\bar{u}^*, \bar{v}^*) = (u^*, v^*) / (c \lambda_0 T_0)$ ,  $\bar{\varepsilon}_{ij}^* = \varepsilon_{ij}^* / (\lambda_0 T_0)$  are introduced as well. Similarly, dropping the hat of non-dimensional variables, we can simplify the governing equation as:

$$\nabla^2 \nabla^2 U^* + p^2 f_1^*(p) f_3^*(p) \nabla^2 T^* = 0 \tag{4.12}$$

The related boundary conditions of Eq. (4.12) can be expressed by:

$$\begin{aligned}
\sigma_{xy}(x, -h) &= \sigma_y(x, -h) = 0, \quad (|x| < \infty) \\
\sigma_{xy}(x, 0) &= \sigma_y(x, 0) = 0, \quad (|x| \leq 1) \\
\sigma_{xy}(x, 0^+) &= \sigma_{xy}(x, 0^-), \quad (|x| > 1) \\
\sigma_y(x, 0^+) &= \sigma_y(x, 0^-), \quad (|x| > 1) \\
u(x, 0^+) &= u(x, 0^-), \quad (|x| > 1) \\
v(x, 0^+) &= v(x, 0^-), \quad (|x| > 1)
\end{aligned} \tag{4.13}$$

### 4.3 Theoretical solutions

#### 4.3.1 Solutions of temperature field

The governing Eq. (4.4) is converted to the following form by Laplace transform to eliminate the time dependency,

$$\nabla^2 T \left(1 + \frac{\tau_T^\alpha}{\alpha!} p^\alpha\right) = \left(p + \frac{\tau_q^\alpha}{\alpha!} p^{\alpha+1} + \frac{\tau_q^{2\alpha}}{(2\alpha)!} p^{2\alpha+1}\right) T \quad (4.14)$$

Considering the boundary conditions of the temperature field, the solution of equation (4.14) can be obtained after Fourier transform,

$$\begin{aligned} T^*(x, y, p) &= \int_{-\infty}^{\infty} D(\xi, p) \exp(-my - ix\xi) d\xi + \frac{1}{p} \exp(-q(y+h)); \quad y > 0 \\ T^*(x, y, p) &= \int_{-\infty}^{\infty} \frac{-D(\xi, p)}{1 + \exp(-2mh)} \{ \exp(my) - \exp[-m(2h+y)] \} \exp(-ix\xi) d\xi \\ &\quad + \frac{1}{p} \exp(-q(y+h)); \quad y < 0 \end{aligned} \quad (4.15)$$

where  $m = \sqrt{R + \xi^2}$ ,  $q = \sqrt{R}$ , ( $R$  is shown in Appendix),  $\xi$  is the Fourier transform variable. The unknown coefficient  $D(\xi, p)$  can be determined by the mixed boundary conditions on crack faces. Introduce a temperature density function:

$$\phi^*(x, p) = \frac{\partial T^*(x, 0^+, p)}{\partial x} - \frac{\partial T^*(x, 0^-, p)}{\partial x} \quad (4.16)$$

From the boundary conditions, it is clear that:

$$\begin{aligned} \int_{-1}^1 \phi^*(x, p) dx &= 0 \\ \phi^*(x, p) &= 0, \quad (|x| > 1) \end{aligned} \quad (4.17)$$

Combining Eqs. (4.15) and (4.16), it is easy to find the relationship between the unknown coefficient and the temperature density function:

$$D(\xi, p) = \frac{i[1 + \exp(-2mh)]}{4\pi\xi} \int_{-1}^1 \phi^*(\tau, p) \exp(i\xi\tau) d\tau \quad (4.18)$$

Since no heat flux can pass across the crack, from the boundary condition on crack faces  $\partial T / \partial y = 0$ , ( $y = 0, |x| \leq 1$ ), one can obtain the following singular integral equation:

$$\int_{-1}^1 \phi^*(\tau, p) \left[ \frac{1}{\tau - x} + k^*(x, \tau, p) \right] d\tau = \frac{2\pi q}{p} \exp(-qh), \quad |x| \leq 1 \quad (4.19)$$

and the kernel function is:

$$k^*(x, \tau, p) = \int_0^\infty \left\{ 1 - \frac{m[1 + \exp(-2mh)]}{\xi} \right\} \sin[(x - \tau)\xi] d\xi \quad (4.20)$$

This singularity integral equation under the single-value condition (4.17) has the following form of the solution:

$$F^*(x, p) = \frac{\phi^*(x, p)}{\sqrt{1-x^2}}, \quad |x| \leq 1 \quad (4.21)$$

where  $F^*(x, p)$  is bounded and continuous on the interval  $[-1, 1]$ . To solve the integral equations (4.17) and (4.19), the numerical technique in [129] is employed to convert it into the following algebraic equations:

$$\sum_{k=1}^n \frac{1}{n} F^*(\tau_k, p) \left[ \frac{1}{\tau_k - x_r} + k^*(x_r, \tau_k, p) \right] = \frac{2\pi q}{p} \exp(-qh), \quad |x| \leq 1 \quad (4.22)$$

$$\sum_{k=1}^n \frac{\pi}{n} F^*(\tau_k, p) = 0 \quad (4.23)$$

where  $\tau_k = \cos \frac{(2k-1)\pi}{2n}$ ,  $k = 1, 2, \dots, n$ ;  $x_r = \cos \frac{r\pi}{n}$ ,  $r = 1, 2, \dots, n-1$ .

Once the algebraic equations are solved, the values of  $\phi^*(x, p)$  can be substituted into Eq. (4.18), and thus the temperature field expressed in Eq. (4.15) can be obtained after the numerical inversion of Laplace transform.

### 4.3.2 Intensity factors of temperature gradient

Proposed by Tzou [148], the temperature gradient around the macrocrack tip would be qualified to assess the energy bearing capacity of the solid media. The temperature gradient illustrates in which direction and how much the heat flows around the crack tip resulted from the abrupt change of the geometrical curvature. Therefore, the intensity factor of temperature gradient (IFTG) is introduced to quantify the dynamic thermal energy around the crack tips. From the expression of temperature field in Eq. (4.15), the temperature gradient is firstly obtained as:

$$\begin{aligned}\frac{\partial}{\partial y} T^*(x, y, p) &= -m \int_{-\infty}^{\infty} D(\xi, p) \exp(-my - ix\xi) d\xi - \frac{q}{p} \exp(-q(y+h)); \quad y > 0 \\ \frac{\partial}{\partial y} T^*(x, y, p) &= m \int_{-\infty}^{\infty} \frac{-D(\xi, p)}{1 + \exp(-2mh)} \{ \exp(my) + \exp[-m(2h+y)] \} \exp(-ix\xi) d\xi \\ &\quad - \frac{q}{p} \exp(-q(y+h)); \quad y < 0\end{aligned}\quad (4.24)$$

$$\begin{aligned}\frac{\partial}{\partial x} T^*(x, y, p) &= (-i\xi) \int_{-\infty}^{\infty} D(\xi, p) \exp(-my - ix\xi) d\xi \quad y > 0 \\ \frac{\partial}{\partial x} T^*(x, y, p) &= (-i\xi) \int_{-\infty}^{\infty} \frac{-D(\xi, p)}{1 + \exp(-2mh)} \{ \exp(my) - \exp[-m(2h+y)] \} \exp(-ix\xi) d\xi \\ &\quad y < 0\end{aligned}\quad (4.25)$$

Singularity of the temperature gradient can be examined from the asymptotic behaviors of the integrands in Eqs. (4.24) and (4.25) for the large values of the variable  $\xi$ , with the help from the procedure in [144] and using the asymptotic formula in [150],

$$\int_{-1}^1 \frac{F_j(x)}{\sqrt{1-x^2}} e^{ix\xi} dx = \sqrt{\frac{\pi}{2|\xi|}} \left\{ F_j(-1) \exp[-i(\xi - \frac{\pi\xi}{4|\xi|})] + F_j(1) \exp[i(\xi - \frac{\pi\xi}{4|\xi|})] + o\left(\frac{1}{|\xi|}\right) \right\} \quad (4.26)$$

$$\int_0^{\infty} x^{\mu-1} \exp(-sx) \{ \sin(\beta x), \cos(\beta x) \} dx = \frac{\Gamma(\mu)}{(s^2 + \beta^2)^{\mu/2}} \left\{ \sin[\mu \tan^{-1}(\frac{\beta}{s})], \cos[\mu \tan^{-1}(\frac{\beta}{s})] \right\}, \quad (4.27)$$

$(s > 0, \mu > 0)$

The singular temperature gradient could then be derived as:

$$\begin{aligned}
T_{,x}^*(r, \theta, p) &= \frac{F(1, p)}{2\sqrt{2r}} \sin\left(\frac{\theta}{2}\right) \\
T_{,x}^*(r, \theta, p) &= -\frac{F(1, p)}{2\sqrt{2r}} \cos\left(\frac{\theta}{2}\right) \\
T_{,r}^*(r, \theta, p) &= -\frac{F(1, p)}{2\sqrt{2r}} \sin\left(\frac{\theta}{2}\right)
\end{aligned} \tag{4.28}$$

Where the subscript “,  $j$ ” represents the gradient in the corresponding direction;  $(r, \theta)$  denotes the polar coordinates whose origin locates at the crack tip:

$$x = 1 + r \cos \theta, y = r \sin \theta \tag{4.29}$$

The intensity factors of temperature gradient in the Laplace domain can then be defined as:

$$K_T^*(p) = \lim_{r \rightarrow 0} 2\sqrt{r} T_{,r}^* |_{\theta=-\pi} = \frac{F(1, p)}{\sqrt{2}} \tag{4.30}$$

Obviously, the transient temperature gradient shows a  $\sqrt{r}$  singularity at the crack tips, which is the same as the stresses in linear elastic fracture mechanics. By employing the numerical inversion of Laplace transform, the IFTG in the time domain can be obtained.

### 4.3.3 Solutions of viscoelastic stresses field

In the present work, the uncoupled, thermo-viscoelasticity theory is employed, where only the temperature field will affect the stress field, but not vice versa. Once the temperature field in the Laplace domain is found by Eq. (4.15), the transient viscoelastic stresses can be acquired by solving the governing equation (4.12):

$$\nabla^2 \nabla^2 U^* = -p^2 f_1^*(p) f_3^*(p) \nabla^2 T^* \tag{4.31}$$

Fourier transform is employed to get the solution of Eq. (4.31):

$$\begin{aligned}
U^*(x, y, p) &= \int_{-\infty}^{\infty} (B_1 + B_2 y) \exp(-|\xi|y - ix\xi) d\xi - \int_{-\infty}^{\infty} C_1 \exp(-my - ix\xi) d\xi, \\
& \hspace{20em} y > 0 \\
U^*(x, y, p) &= \int_{-\infty}^{\infty} \{(A_1 + A_2 y) \exp(|\xi|y) + (A_3 + A_4 y) \exp(-|\xi|y)\} \exp(-ix\xi) d\xi \\
& - \int_{-\infty}^{\infty} \{C_{21} \exp(my) + C_{22} \exp(-my)\} \exp(-ix\xi) d\xi, \quad y < 0
\end{aligned} \tag{4.32}$$

where  $A_1, A_2, A_3, A_4, B_1, B_2$  is related to the boundary conditions in Eq. (4.13), and  $C_1, C_{21}, C_{22}$  will be determined by the obtained temperature field from Eq. (4.15), as shown in Appendix.

The existence of crack results in the discontinuity of not only the temperature field but also the displacement field and stress field. Considering the boundary conditions and the dimensionless variables, the jump of the displacement components in the Laplace domain at the line  $y=0$  can be obtained from Eq. (4.10), which is shown as:

$$\begin{aligned}
\frac{\partial[u^*]}{\partial x} &= \frac{1}{pf_1^*(p)} [\sigma_x^*] + pf_3^*(p) [T^*] \\
\frac{\partial^2[v^*]}{\partial x^2} &= -\frac{1}{pf_1^*(p)} \left[ \frac{\partial}{\partial y} \sigma_y^* \right]
\end{aligned} \tag{4.33}$$

where “[ ]” denotes the jump of a field variable across  $y=0$ . By employing the relationships  $\sigma_x^* = \partial^2 U^* / \partial y^2$ ,  $\sigma_y^* = \partial^2 U^* / \partial x^2$ ,  $\sigma_{xy}^* = -\partial^2 U^* / \partial x \partial y$ , the stress components  $\sigma_x^*, \sigma_y^*, \sigma_{xy}^*$  can be obtained. Substituting the stress components into Eq. (4.33), one can have:

$$\begin{aligned}
\frac{\partial[u^*]}{\partial x} &= \int_{-\infty}^{\infty} \frac{1}{pf_1(p)} \left\{ \frac{-2|\xi|(B_2 - A_4) + \xi^2(B_1 - A_3) + (-2|\xi|A_2 - \xi^2 A_1)}{m^2 C_{21} + m^2(C_{22} - C_1)} \right\} \exp(-ix\xi) d\xi \\
& + \int_{-\infty}^{\infty} pf_3(p) D(\xi) \frac{2}{1 + e^{-2mh}} \exp(-ix\xi) d\xi \\
\frac{\partial[v^*]}{\partial x} &= \int_{-\infty}^{\infty} \left(-\frac{i}{\xi}\right) \frac{1}{pf_1(p)} \left\{ \frac{-(\beta + |\xi|)[\xi^2(B_1 - A_3) - 2|\xi|(B_2 - A_4)] + \xi^2(B_2 - A_4)}{+(\beta - |\xi|)(2|\xi|A_2 + \xi^2 A_1) - \xi^2 A_2 + m^3 C_{21} - m^3(C_{22} - C_1)} \right\} \exp(-ix\xi) d\xi \\
& + \int_{-\infty}^{\infty} \left(-\frac{i}{\xi}\right) pf_3(p) D(\xi) \frac{2}{1 + e^{-2mh}} \exp(-ix\xi) d\xi
\end{aligned} \tag{4.34}$$

Defining two dislocation density functions as:

$$\psi_1^*(x, p) = \frac{\partial[u^*(x, p)]}{\partial x}, \quad \psi_2^*(x, p) = \frac{\partial[v^*(x, p)]}{\partial x} \quad (4.35)$$

Considering the mechanical boundary conditions on crack faces,  $\sigma_{xy}(x, 0) = \sigma_y(x, 0) = 0$ , ( $|x| \leq 1$ ), the following singular integral equations can be obtained:

$$\int_{-1}^1 \sum_{j=1}^2 \left[ \frac{\delta_{ij}}{\tau - x} + k_{ij}(x, \tau) \right] \psi_j^*(\tau, p) d\tau = 4\pi p f_3^*(p) W_i^*(x, p), \quad i=1, 2, \quad -1 \leq x \leq 1 \quad (4.36)$$

With

$$\int_{-1}^1 \psi_i^*(x, p) dx = 0, \quad i=1, 2 \quad (4.37)$$

where  $k_{ij}(x, \tau), W_i^*(x, p)$  are given in Appendix. Similar to the previous manipulation for temperature field, the singular integral equations subjected to Eq. (4.37) have the following form of solutions:

$$\psi_i^*(\tau, p) = \frac{F_i^*(\tau, p)}{\sqrt{1 - \tau^2}}, \quad (i=1, 2), \quad |\tau| \leq 1 \quad (4.38)$$

The Lobatto-Chebyshev method is employed to transform the above singular integral equations into the algebraic equations:

$$\begin{aligned} \sum_{i=1}^n A_i \left[ \frac{1}{\tau_i - x_k} + k_{11}(x_k, \tau_i) \right] F_1^*(\tau_i, p) + \sum_{i=1}^n A_i k_{12}(x_k, \tau_i) F_2^*(\tau_i, p) &= 4\pi p f_3^*(p) W_1^*(x_k, p) \\ \sum_{i=1}^n A_i F_1^*(\tau_i, p) &= 0 \\ \sum_{i=1}^n A_i k_{21}(x_k, \tau_i) F_1^*(\tau_i, p) + \sum_{i=1}^n A_i \left[ \frac{1}{\tau_i - x_k} + k_{22}(x_k, \tau_i) \right] F_2^*(\tau_i, p) &= 4\pi p f_3^*(p) W_2^*(x_k, p) \\ \sum_{i=1}^n A_i F_2^*(\tau_i, p) &= 0 \end{aligned} \quad (4.39)$$

where

$$\begin{aligned}
\tau_i &= \cos \frac{(i-1)\pi}{n-1}, \quad i = 1, 2, \dots, n; \\
x_k &= \cos \frac{(2k-1)\pi}{2(n-1)}, \quad k = 1, 2, \dots, n-1; \\
A_i &= \frac{\pi}{2(n-1)}, \quad i = 1, n; \quad A_i = \frac{\pi}{n-1}, \quad i = 2, 3, \dots, n-1.
\end{aligned} \tag{4.40}$$

The stress intensity factors (SIFs) in the Laplace domain are defined as:

$$\begin{aligned}
K_I^* &= -\frac{\pi}{4} F_2^*(1, p) \quad \text{mode I} \\
K_{II}^* &= -\frac{\pi}{4} F_1^*(1, p) \quad \text{mode II}
\end{aligned} \tag{4.41}$$

Again, the SIFs in the time domain can be obtained through numerical Laplace inversion of Eq. (4.41), and the results will be discussed in the following section.

#### 4.4 Numerical results and discussions

In the previous section, the theoretical solutions for both temperature distribution and SIFs in the Laplace domain have been acquired by transforming the PDE and applying boundary conditions to the singular integral equations. To obtain the corresponding results in the time domain, the numerical inversion of Laplace transform proposed by Miller and Guy [110] is employed in this research.

The dimensionless temperature (which is expressed as  $(T - T_1) / (T_0 - T_1)$ ) distributions are obtained firstly. The dimensionless temperatures along crack faces and the extension line are shown in Figure 4.2, where ‘‘UF’’ indicates the temperature of the upper crack face, while ‘‘LF’’ represents the temperature of the lower face. Since the crack faces are assumed to be completely insulated, temperature jumps can be observed in all curves. Different Non-Fourier heat conduction theories are employed and the predicted temperature distributions are compared with each other at four time instants  $t = 0.4, 0.8, 1.2, \infty$ , where the red lines ( $\tau_T = 0$ ) denotes the numerical results of conventional hyperbolic model, the blue lines give results of conventional DPL model, and the orange lines represent the results of fractional DPL model when the time fractional order  $\alpha = 0.8$ .

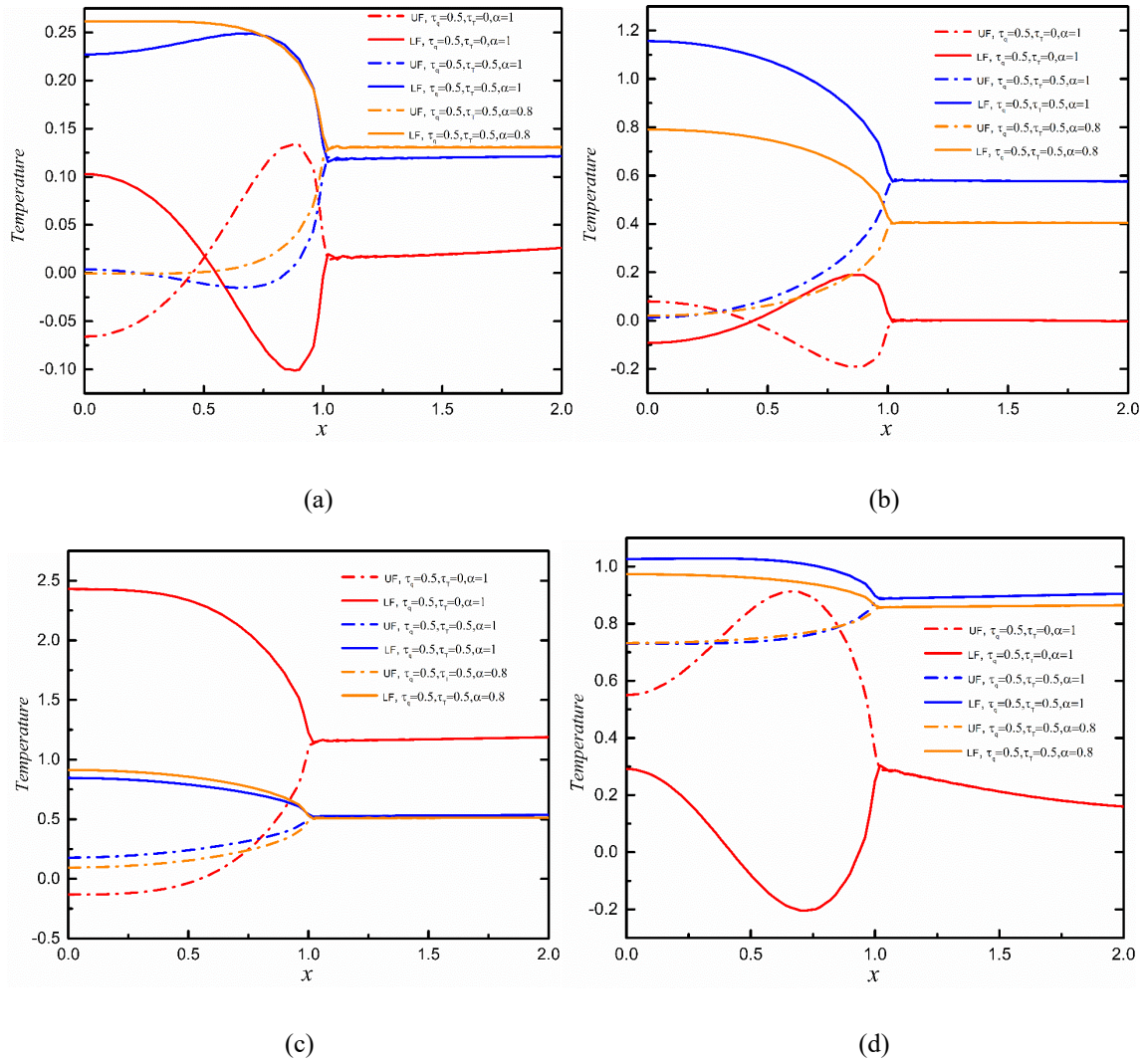


Figure 4.2 Non-dimensional temperature distributions on crack faces and the extension line based on different Non-Fourier heat conduction models at different time instants

(a)  $t=0.4$ ; (b)  $t=0.8$ ; (c)  $t=1.2$ ; (d)  $t=\infty$ .

It should be noted that since all temperatures are assumed to be  $T_1$  initially and a hot, thermal shock is applied at the free boundary, the dimensionless temperature (rise)  $(T - T_1)/(T_0 - T_1)$  should always be nonnegative. Any appearance of negative dimensionless temperature indicates the heat flow from cold areas to hot areas happened, which violates the second law of thermodynamics. Obviously, the conventional hyperbolic heat conduction model gives the least accurate results with negative dimensionless temperatures appearing at all four instants, although this model takes the finite speed of thermal wave into consideration. Another

unphysical phenomenon could be observed in Figure 4.2, where the temperature of the upper crack face can be higher than the lower crack face. The temperature of the lower crack face definitely should be higher due to the fact that the hot thermal shock is applied to the lower free boundary.

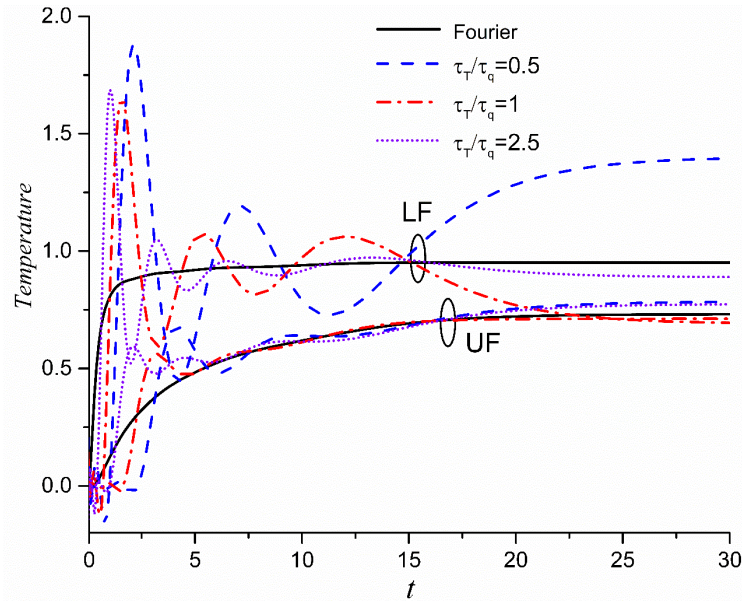


Figure 4.3 Non-dimensional temperature’s variation of the midpoints of crack faces under influence of the ratio between two thermal relaxation lags, when time fractional order  $\alpha = 1$ .

Compared to the hyperbolic model, both conventional DPL and fractional DPL models give much more realistic results. However, some differences can still be easily observed between them, especially for the temperature distribution at earlier stages. In Figure 4.2(a), conventional DPL model still gives some negative temperatures. Compared with the conventional DPL model, introducing time fractional order leads to nonnegative temperature (rise). Besides, the fractional model decreases the temperature jumps, as indicated by Figure 4.2 (b).

In order to figure out more clearly how the temperature varies with time, the temperatures of the midpoints of crack faces are plotted in Figure 4.3-4.5, where “UF” indicates the temperature of the midpoint of the upper crack face, while “LF” represents the temperature of the midpoint of the lower crack face. The solid lines labeled as “Fourier” in the figures is the temperature history calculated by the classical Fourier’s law, where two thermal lags  $\tau_T = \tau_q = 0$ . The Fourier’s law always indicates the temperature of both the upper and lower midpoints will increase gradually from zero to a steady state, whereas the DPL models bring significant wave-like oscillations.

Figure 4.3 illustrates the temperature history corresponding to the conventional DPL model when  $\alpha = 1$ . The temperature fluctuates even at the very early beginning and then increases to its peak value before decreasing to a steady state value with significant oscillations. Drastic oscillations and very high overshooting can be observed, and the peak point reaches almost twice of the temperature on the free surface. In addition, obvious negative temperature appears during the early stage of the temperature history, which takes a very long time to reach steady state value when  $\tau_T / \tau_q = 0.5$ . Compared to Fig. 4.3, the introduction of fractional calculus gives much better results. With the decrease of fractional order  $\alpha$  from 1 to 0.5, the wave-like oscillations are decreased, which results in the decrease of the peak point of the temperature history. This can be explained by the memory effects caused by the fractional calculus, i.e., the next state of the system depends on not only the current state but also the historical states. When  $\alpha$  decreases to 0.5, the wave-like oscillations almost disappear and the temperatures of the early stage are all positive. The “LF” curves always increase from zero to the peak point and then decrease to the steady state, where the peak point is only slightly higher than the applied temperature on the free surface. The “UF” curves will take a finite time to start increasing, then reach the steady state value smoothly. Both the steady state values of “LF” and “UF” curves are very close to the steady state value of Fourier’s law, which supports the necessity of introducing fractional calculus. In addition, the influence of the ratio between two thermal relaxation lags is investigated. Unlike the disturbing regularity in the conventional DPL results, the results of fractional DPL models (from Figure 4.4 & Figure 4.5) show that with the increase of the ratio of thermal lags  $\tau_T / \tau_q$ , the peak values of the temperature history are reduced and the values of steady states increase a little. Besides, the time instant corresponds to the peak point will be delayed with the decrease of the lag ratio.

In order to evaluate the effect of two thermal lags in the fractional DPL theory, the temperature distribution along  $x = 0$  at three time instants are plotted in Figure 4.6 with  $\alpha = 0.5$ . A clear temperature jump can be found at the crack midpoint corresponding to  $y = 0$ . The model reduces to fractional CV theory when  $\tau_T / \tau_q = 0$ . Significant difference in the results between fractional CV theory and fractional DPL model can be observed in all three figures. Compared with the moderate temperature change predicted by the fractional DPL model, the temperature changes dramatically along the  $y$ -axis in front of crack ( $y < 0$ ) when the thermal lag of heat flux

$\tau_T$  is not considered, while the temperature behind the crack ( $y > 0$ ) almost stays around zero, i.e. no heating happens across the crack at all three time instants, which raise the doubt on the accuracy of this model. A similar trend can be found for the temperatures at all three time instants behind the crack, i.e., the thermal penetration depth would be larger and the temperature level would be higher with the increase of the lag ratio  $\tau_T / \tau_q$ . This observation justifies the same conclusion “*The effect of microstructural interactions is absorbed in the phase lag of the temperature gradient  $\tau_T$* ” in [21]. However, compared with [21], the very sharp thermal wavefront which implies an infinite temperature gradient does not appear here due to the introduction of time fractional order derivative. The temperature in front of the crack shows quite different trends at different time instants, and the overshooting appears in Figure 4.6(b) will be weakened with the increase of the lag ratio  $\tau_T / \tau_q$ , which is consistent with the results in Figure 4.5.

The transient IFTGs can be obtained once the algebraic Eqs. (4.22-4.23) are solved numerically and the numerical inversion of Laplace transform is performed. Figure 4.7 illustrates the variation of IFTG with time for different heat conduction models. Characterizing the temperature gradient, IFTG has quite different behaviors based on different heat conduction models. The classical Fourier model indicates the IFTG will increase from zero to its peak value smoothly, and then decrease a little to its steady state. The CV model still leads to significant oscillations in IFTG fluctuating all the time within the considered time range. All DPL models, including the fractional ones, show the IFTGs vary similarly to the curve of the Fourier model. Besides, the steady state values of the DPL models coincide exactly with the Fourier’s result. With the decrease of fractional order  $\alpha$ , the peak values of IFTG decreases and the corresponding time is delayed, which indicates the fractional order weakens the temperature gradient as well.

The temperature field will eventually determine the thermal stresses and SIFs. The reasonable temperature history obtained from the fractional DPL theory would be beneficial to obtaining the accurate fracture behavior. For simplicity and better comparison, we assume  $n = 1$  in the relaxation function, which resulted in the standard linear viscoelastic Maxwell model [111]:

$$f_i(t) = \frac{E_\infty}{E_0} + \left(1 - \frac{E_\infty}{E_0}\right) e^{-\frac{t}{t_0}} \quad (4.42)$$

Figure 4.8 shows the dynamic SIFs between viscoelastic and elastic materials are significantly different without considering the Non-Fourier effect by letting  $\tau_T = \tau_q = 0$ . This is for better understanding the viscoelastic SIFs without the interference from the non-Fourier wave-like thermal behaviors. Besides, the parameters in the viscoelastic relaxation function are investigated to show their influence on the fracture response. For the elastic materials, both  $K_I$  and  $K_{II}$  increase gradually from zero to their steady state values, while both SIFs in viscoelastic materials will increase to their peak values and then drop dramatically. The peak points of SIFs in viscoelastic materials appear much earlier than elastic materials. The peak values of viscoelastic SIFs increase with increasing value of  $E_\infty / E_0$ , and can even be higher than the corresponding values in elastic materials, which should be acknowledged in designing the viscoelastic materials. The relaxation time  $t_0$  will not influence the peak values but the rate of decay, which is consistent with the physical meaning of the viscous element.

Figures 4.9-4.11 illustrates the effects of fractional order  $\alpha$  and the thermal lag ratio  $\tau_T / \tau_q$  on the SIFs in viscoelastic materials considering the non-Fourier effect. When  $\alpha = 1$ , the conventional DPL theory predicts the SIFs increase to their peak values and then decrease rapidly with significant fluctuations all the time within the time range considered, similar to the wave-like behaviors of temperature history in Figure 4.3. The peak values of both  $K_I$  and  $K_{II}$  increase with the decrease of the thermal lag ratio. The corresponding times of peak points of  $K_I$  and  $K_{II}$  are delayed with the decrease of lag ratio. The wave-like behaviors and fluctuations are weakened as the fractional order decreases, and completely disappear when  $\alpha = 0.5$ . Figure 4.11 shows quite sharp pulses at the early stage of the history of  $K_I$  and  $K_{II}$ , and their steady state values approach to each other under different ratios of thermal lags. Compared to the results in Figures 4.9-4.10, the time to reach peak points in  $K_I$  will not be significantly influenced by the thermal lag ratio, and the peak values of both  $K_I$  and  $K_{II}$  are obviously lower when  $\alpha = 0.5$ , which indicates the fractional order derivative weakens not only the thermal wave propagation but also the SIFs.

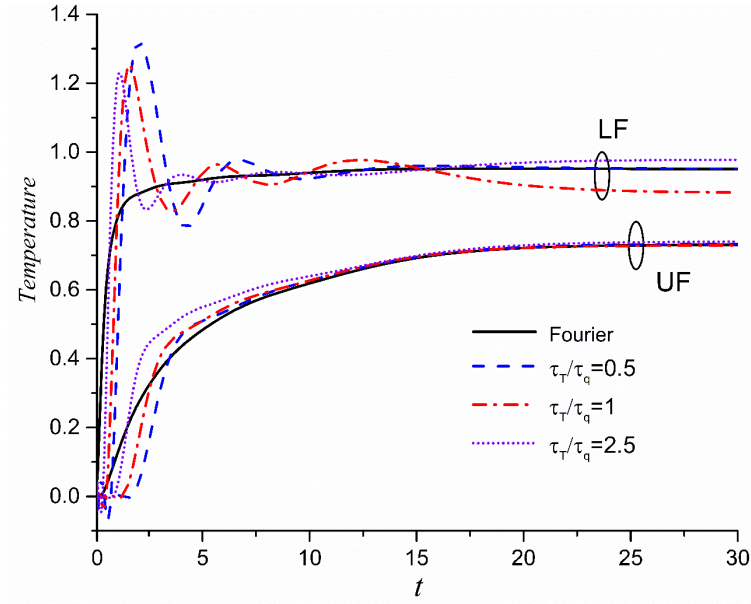


Figure 4.4 Non-dimensional temperature's variation of the midpoints of crack faces under influence of the ratio between two thermal relaxation lags, when time fractional order  $\alpha = 0.75$ .

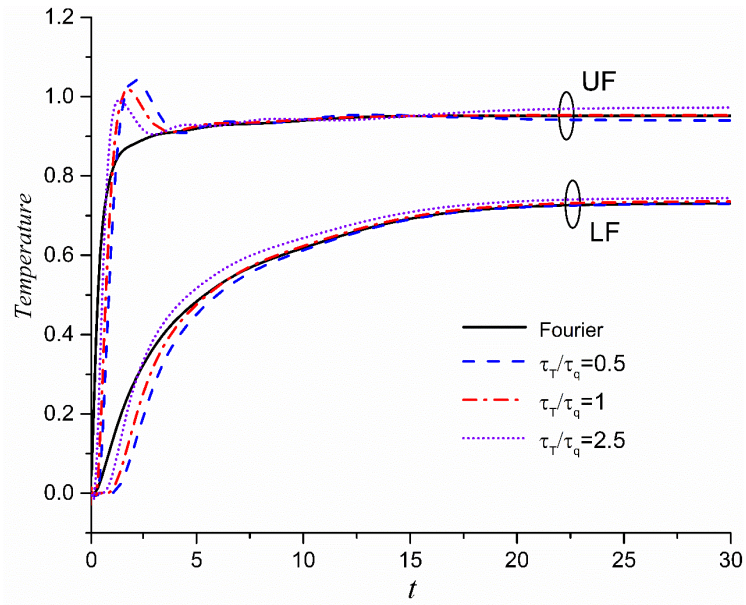
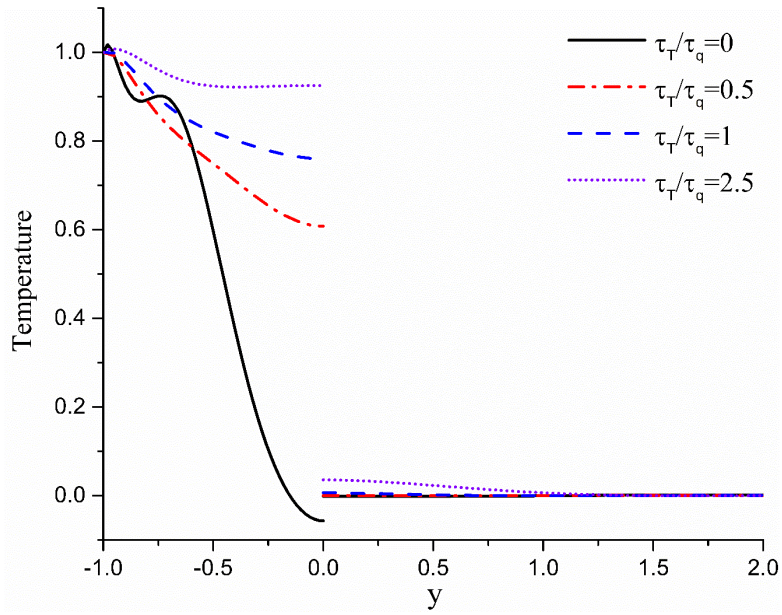
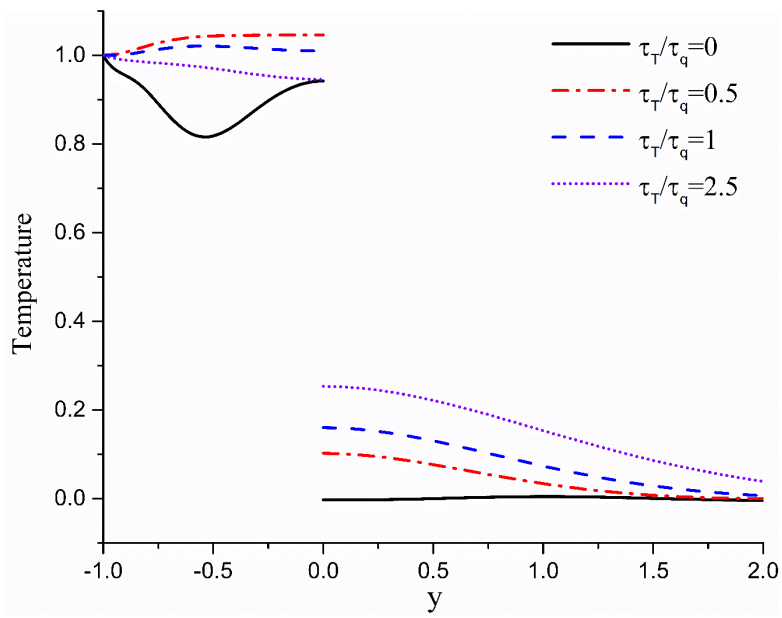


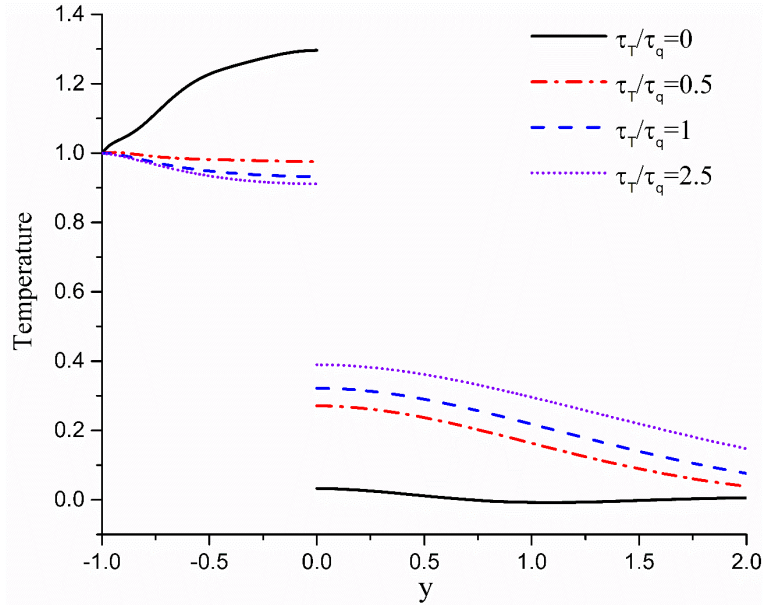
Figure 4.5 Non-dimensional temperature's variation of the midpoints of crack faces under influence of the ratio between two thermal relaxation lags, when time fractional order  $\alpha = 0.5$ .



(a)  $t=1$



(b)  $t=2$



(c)  $t=3$

Figure 4.6 The temperature distribution along  $x = 0$  at time instant (a)  $t=1$ ; (b)  $t=2$ ; (c)  $t=3$  under the influence of the ratio of thermal lags  $\tau_T/\tau_q$  in fractional DPL model when  $\alpha = 0.5$  .

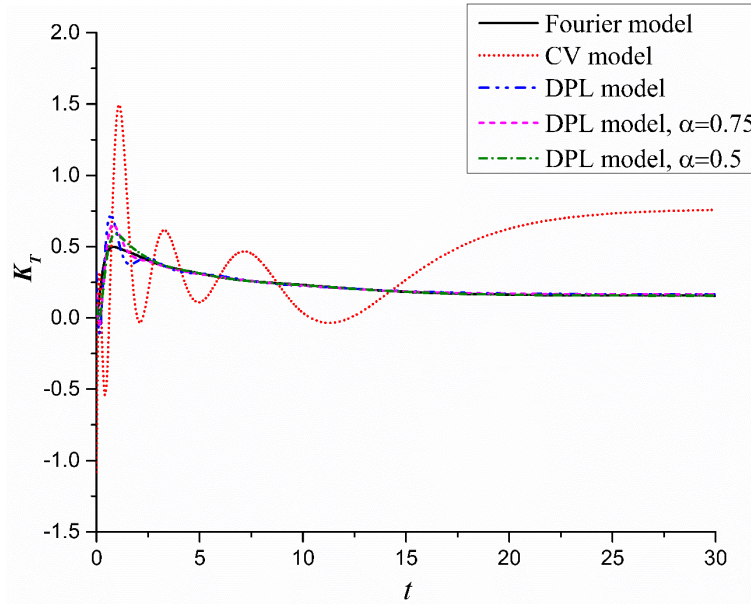


Figure 4.7 The dynamic IFTGs for different heat conduction models

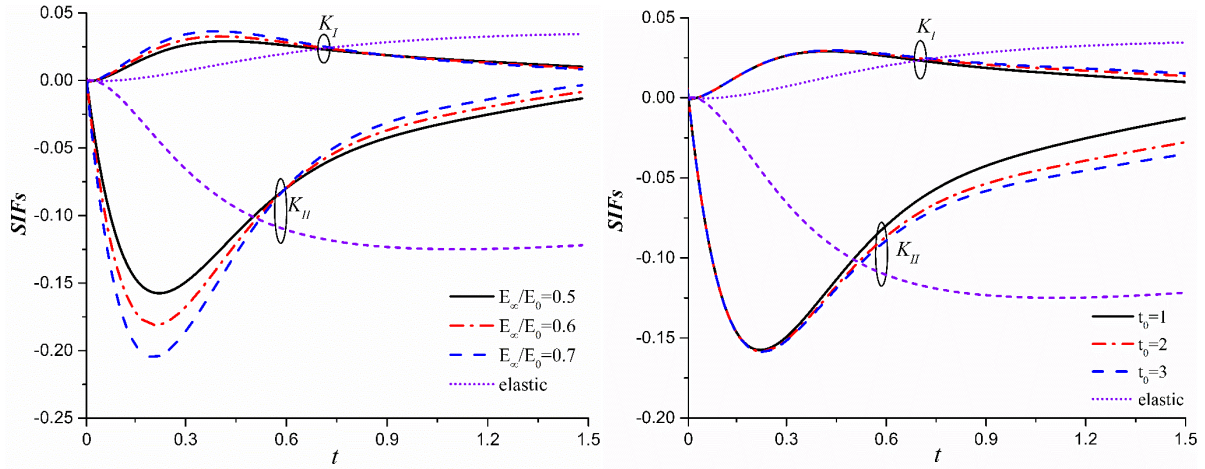


Figure 4.8 The parametric investigation of dynamic SIFs

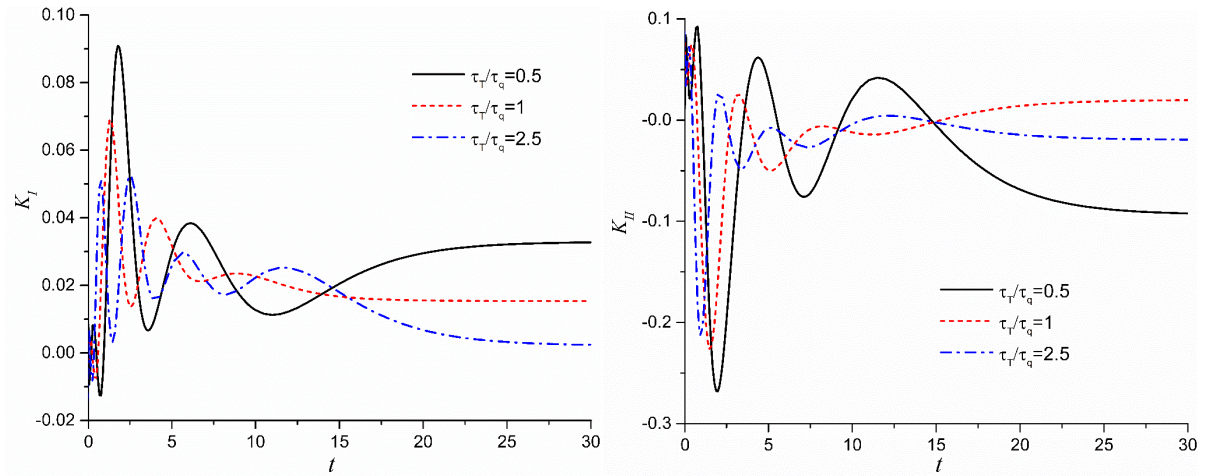


Figure 4.9 Transient SIFs under the influence of the ratio of two thermal lags  $\tau_T/\tau_q$ ,

when the fractional order  $\alpha=1$ .

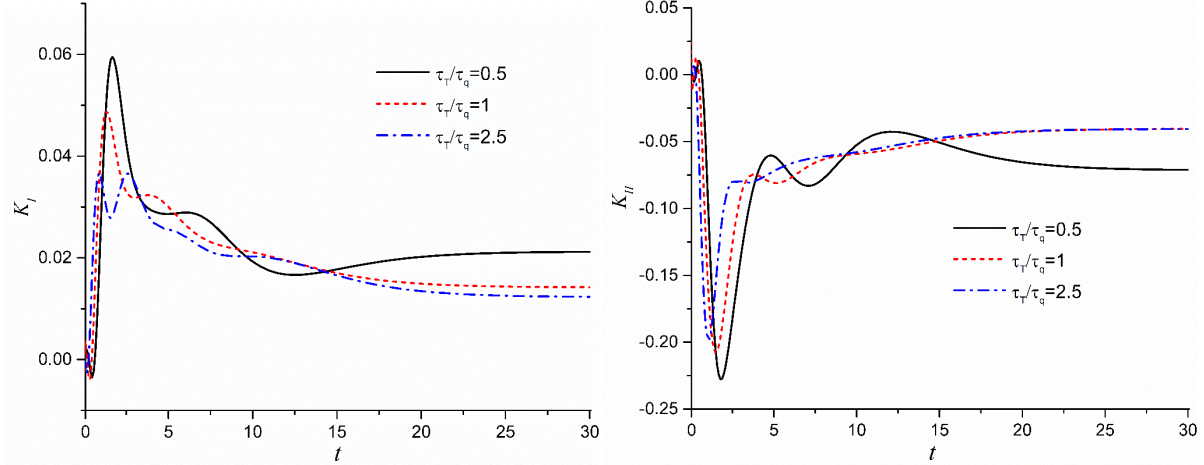


Figure 4.10 Transient SIFs under the influence of the ratio of two thermal lags  $\tau_T/\tau_q$ , when the fractional order  $\alpha = 0.75$ .

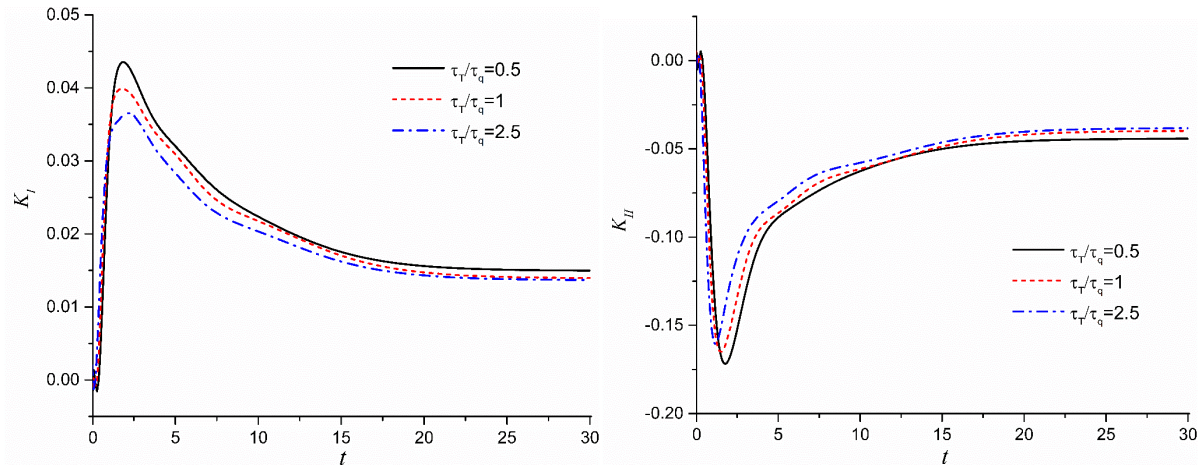


Figure 4.11 Transient SIFs under the influence of the ratio of two thermal lags  $\tau_T/\tau_q$ , when the fractional order  $\alpha = 0.5$ .

## 4.5 Conclusion

In this study, the crack problem under thermal shock is investigated within the framework of a more generalized, thermo-viscoelasticity by extending the fractional calculus to dual-phase-lag (DPL) heat conduction theory, and considering the viscoelastic relaxation phenomena at high

temperature. The time fractional order shows great potential to predict a more reasonable temperature field by weakening the thermal wave propagation, leading to the removal of the unphysical fracture behavior and weakened oscillations in temperature history. The thermal penetration depth would be larger and the temperature level would be higher behind the crack for a higher value of the lag ratio  $\tau_T/\tau_q$ , which is consistent with the prediction in [21]. However, the temperature level would be quite different in front of the crack. The SIFs show quite different behaviors between viscoelastic and elastic materials, as a series of the parametric study shows. The fractional DPL model predicts the viscoelastic SIFs with a very sharp pulse in the early stage of fracture response, which should be considered carefully in viscoelastic material design.

#### 4.6 Appendix

$$R = \frac{p + \frac{\tau_q^\alpha}{\alpha!} p^{1+\alpha} + \frac{\tau_q^{2\alpha}}{2\alpha!} p^{1+2\alpha}}{1 + \frac{\tau_T^\alpha}{\alpha!} p^\alpha}$$

$$C_1(\xi, p) = [m^2 - \xi^2]^{-2} D(\xi, p) p^3 f_1^*(p) f_3^*(p)$$

$$C_{21}(\xi, p) = [m^2 - \xi^2]^{-2} \frac{-D(\xi, p)}{1 + \exp(-2mh)} p^3 f_1^*(p) f_3^*(p)$$

$$C_{22}(\xi, p) = [m^2 - \xi^2]^{-2} \frac{D(\xi, p) \exp(-2mh)}{1 + \exp(-2mh)} p^3 f_1^*(p) f_3^*(p)$$

$$W_1^*(x, p) = 2 \int_0^\infty \xi w_1^*(\xi, p) \sin(x\xi) d\xi$$

$$W_2^*(x, p) = -2 \int_0^\infty \xi^2 w_2^*(\xi, p) \cos(x\xi) d\xi$$

$$w_1^*(\xi, p) = -\frac{2g_2 h_{11} + 2|\xi| h_{12} (s_2 g_1 - g_2)}{8|\xi| \xi^2} - g_3$$

$$w_2^*(\xi, p) = -\frac{2g_2 h_{21} + 2|\xi| h_{22} (s_2 g_1 - g_2)}{8|\xi| \xi^2} - g_4$$

$$k_{11}(x, \tau) = \int_0^{\infty} [1 - 4\xi f_{11}(\xi)] \sin[(x - \tau)\xi] d\xi$$

$$k_{22}(x, \tau) = \int_0^{\infty} [1 - 4\xi^2 f_{22}(\xi)] \sin[(x - \tau)\xi] d\xi$$

$$k_{12}(x, \tau) = \int_0^{\infty} -4\xi f_{12}(\xi) \cos[(x - \tau)\xi] d\xi$$

$$k_{21}(x, \tau) = \int_0^{\infty} -4\xi^2 f_{21}(\xi) \cos[(x - \tau)\xi] d\xi$$

$$h_{11}(\xi) = |\xi| + \exp(-2|\xi|h)(-|\xi| + 2h\xi^2)$$

$$h_{12}(\xi) = 1 - \exp(-2|\xi|h)(1 - 2h|\xi| + 2h^2\xi^2)$$

$$h_{21}(\xi) = 1 - \exp(-2|\xi|h)(1 + 2h|\xi|)$$

$$h_{22}(\xi) = 2|\xi|h^2 \exp(-2|\xi|h)$$

$$f_{11}(\xi) = h_{12}(4|\xi|)^{-1}$$

$$f_{12}(\xi) = (-2\xi h_{11} + 2\xi|\xi|h_{12})(-2|\xi|)^{-3}$$

$$f_{21}(\xi) = h_{22}(4|\xi|)^{-1}$$

$$f_{22}(\xi) = [-2\xi h_{21} + 2\xi|\xi|h_{22}](2|\xi|)^{-3}$$

$$g_1(\xi) = -\xi^2 f_3' - 2|\xi| f_4' + f_5'$$

$$g_2(\xi) = -2|\xi|\xi^2 f_3' - 3\xi^2 f_4' - f_6'$$

$$g_3(\xi) = \exp(-|\xi|h)[(1 - h|\xi|)f_2' - h\xi^2 f_1'] - mI_{21} + mI_{22}$$

$$g_4(\xi) = \exp(-|\xi|h)[(1 + h|\xi|)f_1' + hf_2'] - I_{21} - I_{22}$$

$$f_1'(\xi) = I_{21} \exp(-mh) + I_{22} \exp(mh)$$

$$f_2'(\xi) = mI_{21} \exp(-mh) - mI_{22} \exp(mh)$$

$$f_3'(\xi) = I_1 - I_{21} - I_{22}$$

$$f_4'(\xi) = -mI_{21} + m(I_{22} - I_1)$$

$$f_5'(\xi) = m^2 I_{21} + m^2 (I_{22} - I_1) + \frac{2}{1 + e^{-2mh}} D(\xi)$$

$$f_6'(\xi) = m^3 I_{21} - m^3 (I_{22} - I_1)$$

$$I_1(\xi, p) = \frac{1}{p^2 f_1^*(p) f_3^*(p)} C_1(\xi, p)$$

$$I_{21}(\xi, p) = \frac{1}{p^2 f_1^*(p) f_3^*(p)} C_{21}(\xi, p)$$

$$I_{22}(\xi, p) = \frac{1}{p^2 f_1^*(p) f_3^*(p)} C_{22}(\xi, p)$$

# Chapter 5: Nonlocal dual-phase-lag heat conduction and the associated nonlocal thermal-viscoelastic analysis

A modified extension of the nonlocal dual-phase-lag (DPL) theory is proposed to account for the heat conduction at nanoscale. Both the temporally and spatially nonlocal effects are considered in heat conduction, which are verified experimentally by the size-dependent thermal conductivity of silicon nanofilms and the transient temperature variation during the femtosecond laser heating of gold films. A generalized uncoupled nonlocal thermoviscoelasticity is hence proposed, which is applied to a one-dimensional analysis of a finite plate under sudden thermal shock. Non-dimensional numerical analyses are performed to illustrate the effects of both nonlocal heat conduction and nonlocal elasticity on thermal propagations and thermoviscoelastic responses.

## 5.1 Introduction

Initiated by Eringen et al. [65-66], the stress-strain relation is expressed in an integral form:

$$t_{ij}(X) = \int_{\Omega} \alpha(|X - X'|) \sigma_{ij}(X') d\Omega(X') \quad (5.1)$$

In which  $t_{ij}$  is the nonlocal stress,  $\sigma_{ij}$  is the classical local stress,  $\alpha(|X - X'|)$  is the kernel function characterizing the long-range interactions between molecules or atoms. Compared with the classical continuum, nonlocal theory indicates the stress of one spatial point does not depend uniquely only on the strain at that point, but also on the strains in a surrounding space, and thus building the connections between macroscopic mechanical behaviors with the microscopic, molecular or atomic interactions. In 1983, the equivalent, partial differential form of nonlocal theory was proposed by Eringen et al. [70] for some specific, physically admissible kernels expressed as:

$$(1 - (e_0 a)^2 \nabla^2) t_{ij} = \sigma_{ij} \quad (5.2)$$

where  $e_0$  is a constant depending on materials,  $a$  is an internal characteristic length, and  $\nabla^2$  is the Laplacian operator.

Nano-structural materials always work in various thermal environments. Heat conduction in solids has been treated as a diffusive process in many engineering problems, especially for those at macro temporal and spatial scales. The governing equation, namely Fourier's law, established on the macroscopic level, implying the speed of thermal propagation is infinite. However, it has been well recognized that Fourier's law breaks down for heat conduction at the nanoscale [46]. When the heat conduction enters nanoscale, the individual behaviors of thermal energy carriers (like phonons) and their interactions become pronounced, as the heat transport time is approaching their mean free time, or the length scale of nanomaterials is comparable with their mean free path. To address these concerns, several constitutive laws of non-Fourier heat conduction were proposed, such as the Cattaneo-Vernotte (CV) model [27-28], thermomass model [45], dual-phase-lag model [20], and the temperature wave theory based on the inertial entropy theory [151]. In particular, by introducing two thermal lags, the DPL model gives a simple and user-friendly macroscopic formulation of the heat transfer at microscopic levels, which enables engineering analyses with sufficient accuracy. The DPL model can be expressed as:

$$\mathbf{q}(\mathbf{x}, t + \tau_q) = -k \nabla T(\mathbf{x}, t + \tau_T) \quad (5.3)$$

where  $\tau_q$  and  $\tau_T$  are the thermal phase lags of heat flux vector and temperature gradient, respectively;  $k$  is the thermal conductivity,  $\nabla$  is the gradient operator and  $T$  is temperature. DPL model can capture the transient heat propagation behaviors accounting for the interactions of microscopic thermal carriers verified by experiment results [20,152]. Although the DPL model characterizes the temporally nonlocal behaviors, i.e., the thermal lagging, the nonlocal effect in space, a necessity for heat conduction at the nanoscale, is neglected. Experimental evidence showed the thermal conductivity of nano-structural materials, such as silicon nanofilm or nanowires, graphene sheets, is size-dependent, which is remarkably different from bulk materials [47]. However, the DPL model is unable to accommodate the size-dependency of thermal conductivity.

In this paper, aiming at taking the spatially nonlocal effect into consideration, the extension of nonlocal DPL model based on Tzou's work [50-51] is employed, and both the stationary and transient responses of the model will be verified by the experimental results. A generalized, uncoupled, nonlocal thermoviscoelasticity theory is proposed based on the nonlocal

DPL model and Eringen's nonlocal theory. The one-dimensional, numerical analysis of thermal response is performed for a plate with finite thickness under a sudden thermal shock.

## 5.2 Nonlocal DPL model

To incorporate the spatially nonlocal effect in heat conduction, different mathematical models have been proposed. Based on the linearized Boltzmann equation for the pure phonon field, the well-known Guyer-Krumhansl model was proposed in [43-44]. Considering the mass, pressure and inertial force of the phonon gas [45], the thermomass model can also characterize the nonlocal effect in heat transport. Stemming from the analogy with the integral form of the nonlocal elasticity, an integro-differential equation governing nonlocal effect was proposed by Xu [46-47]. Obviously, there is still no common agreement on the spatial nonlocality in heat conduction [48-49]. Parallel to these works, Tzou et. al. extended their DPL model by introducing a nonlocal length to accommodate the spatially nonlocal effect [20,50-51], shown as:

$$\mathbf{q}(\mathbf{x} + \boldsymbol{\xi}, t + \tau_q) = -k\nabla T(\mathbf{x}, t + \tau_T) \quad (5.4)$$

in which  $\boldsymbol{\xi}$  is the vector relating to the spatial nonlocality of the heat flux vector. The advantage of this theory is the macroscopic unification of both the temporally and spatially nonlocal effects in a simple form, especially for some engineering analyses without sufficient knowledge of the phonon dynamics. By Taylor series expansion to the first order of space dimension, and neglecting all terms involving time, the steady state form of this theory,

$$(1 + \boldsymbol{\xi} \cdot \nabla)\mathbf{q}(\mathbf{x}) = -k\nabla T(\mathbf{x}) \quad (5.5)$$

was verified by the experimental results of thin nanowires as it captured the linear dependence of the effective thermal conductivity on their radiuses [50]. In order to interpret the correlations to the thermomass model, the extension of the model with transient terms was given by including the least numbers of terms in Taylor series approximation [50-51]:

$$\mathbf{q}(\mathbf{x}, t) + \tau_q \frac{\partial \mathbf{q}(\mathbf{x}, t)}{\partial t} + (\boldsymbol{\xi} \cdot \nabla)\mathbf{q}(\mathbf{x}, t) = -k[\nabla T(\mathbf{x}, t) + \tau_T \frac{\partial \nabla T(\mathbf{x}, t)}{\partial t}] \quad (5.6)$$

In the above extension, the spatial derivative of heat flux  $(\boldsymbol{\xi} \cdot \nabla)\mathbf{q}(\mathbf{x}, t)$  represents the spatially nonlocal term. However, Eq. (5.6) is not the exact Taylor expansion of Eq. (5.4). Here, in order

to verify the transient response, the full extension of Eq. (5.4) to the first order of its Taylor expansion, is considered as:

$$(1 + \xi \cdot \nabla) [\mathbf{q}(\mathbf{x}, t) + \tau_q \frac{\partial \mathbf{q}(\mathbf{x}, t)}{\partial t}] = -k [\nabla T(\mathbf{x}, t) + \tau_r \frac{\partial \nabla T(\mathbf{x}, t)}{\partial t}] \quad (5.7)$$

Compared with Eq. (5.6), an additional mixed-derivative term  $\tau_q \cdot (\xi \cdot \nabla) \frac{\partial \mathbf{q}(\mathbf{x}, t)}{\partial t}$  in Eq. (5.7) will also contribute to the spatial nonlocality in heat conduction. It would be difficult to determine which extension is better to represent the transient response of spatial nonlocality based on pure, theoretical discussions. Therefore, validation of the new model will be performed based on experimental results. To this end, both the steady state and transient response based on the extension of nonlocal DPL model will be compared to the experimental results.

### 5.2.1 Effective thermal conductivity of nanofilms

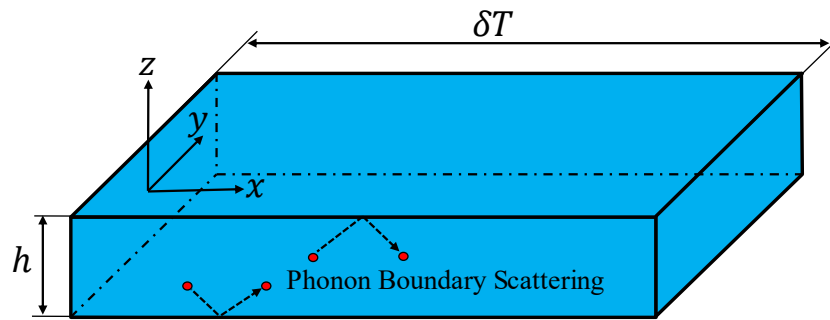


Figure 5.1 Schematic diagram of nanofilms

One obvious phenomenon that the Fourier's law breaks down is the size dependent thermal conductivity of nanostructures, where the mean free path of phonons is comparable with the characteristic lengths. The effective thermal conductivity (ETC) of silicon thin films or nanowires is reduced significantly from that of the corresponding bulk material as the size of nanostructure decreases, which has been demonstrated by many experiments [153-158]. For instance, Ju [157] experimentally showed that ETC of silicon layers at 20 nm can be dropped to around  $30 \text{ Wm}^{-1}\text{K}^{-1}$  compared to  $148 \text{ Wm}^{-1}\text{K}^{-1}$  of bulk material at room temperature. The low ETC raises the concern to remove the excessive heat in nanodevices. In order to figure out the mechanism behind this problem, different simplified mathematical models have been developed to predict the size

dependent ETC [159-162]. Tzou [50] developed a theoretical model based on the steady state form of nonlocal heat conduction and captured the linear dependence of ETC on the radius of nanowires. In this paper, we will re-examine the steady state form of nonlocal heat conduction model, i.e., Eq. (5.5), and compare the predicted ETC to the experimental results in silicon nanofilms.

Figure 5.1 illustrates a nanofilm that carries one-dimensional heat transport in the  $x$ -direction. Assume there is a constant temperature gradient applied in the  $x$ -direction and the size in  $x$  and  $y$  directions are large enough to omit the associated spatial nonlocalities. Therefore, the spatially nonlocal effect is uniquely decided by the nanoscale thickness  $h$  in the  $z$  direction and accompanying boundary scattering of phonons. Obviously, the nonlocal, characteristic length vector  $\xi$  will be different in the upper and lower half plane due to the fact the boundary scattering always occurred in different directions. Here, we assume the nonlocal length is decided by the mean free path of phonons [20], the nonlocal vector  $\xi$  would be  $-l_p \mathbf{e}_x$  in the upper half plane and  $l_p \mathbf{e}_x$  in the lower half plane, where  $l_p$  denotes the mean free path of phonons. Only the upper half plane will be considered here because of the symmetry. Considering ETC is pertinent to the steady state of heat transfer in nanostructural materials, the governing equation of the steady state heat transport in the  $x$  direction can be expressed as:

$$(1 - l_p \frac{\partial}{\partial z}) q_x = -k \frac{dT}{dx} \quad (5.8)$$

Introducing non-dimensional variables:

$$\bar{q} = \frac{q_x}{-k \cdot dT / dx}, \quad \bar{z} = \frac{z}{h}, \quad K_n = \frac{l_p}{h} \quad (5.9)$$

where  $K_n$  is the Knudsen number [161]. Then the partial differential equation (5.8) is reduced to:

$$(1 - K_n \frac{\partial}{\partial \bar{z}}) \bar{q} = 1 \quad (5.10)$$

The general solution can be obtained as:

$$\bar{q} = C \cdot \exp(\frac{1}{K_n} \bar{z}) + 1 \quad (5.11)$$

where  $C$  is a constant depending on the boundary conditions. To determine the heat flux distribution, the Matthiessen rule [161] is used to account for the wall condition. Here, the effective mean free path of phonons from [163] is adopted, such that

$$\bar{q}(\bar{z} = 0.5) = \frac{l_{p\text{-effective}}}{l_p} = \frac{1}{1 + K_n} \quad (5.12)$$

Then the heat flux profile is obtained as

$$\bar{q} = \frac{-K_n}{1 + K_n} \exp\left(\frac{1}{K_n}(\bar{z} - 0.5)\right) + 1 \quad (5.13)$$

and the ETC can be expressed as:

$$\begin{aligned} \frac{k_{eff}}{k} &= 2 \int_0^{0.5} \left\{ \frac{-K_n}{1 + K_n} \exp\left(\frac{1}{K_n}(\bar{z} - 0.5)\right) + 1 \right\} d\bar{z} \\ &= 1 - \frac{2K_n^2}{1 + K_n} \left[ 1 - \exp\left(-\frac{1}{2K_n}\right) \right] \end{aligned} \quad (5.14)$$

Although the governing equation would be  $(1 + l_p \cdot \partial / \partial z)q_x = -k \cdot dT / dx$  in the lower half plane, the accompanying boundary condition would also change to  $\bar{q}(\bar{z} = -0.5) = 1 / (1 + K_n)$ , and thus the same expression for Eq. (5.14) can be obtained. The ETC based on the nonlocal heat conduction model is compared with the experimental data [154-157] and the results based on simplified thermotical models [159-160]. In the calculation, the mean free path of phonons is selected as 220 nm [164] and the thermal conductivity of bulk material is  $148 \text{ Wm}^{-1}\text{K}^{-1}$  for silicon at room temperature. Figure 5.2 clearly shows that the results of the new model is in good agreement with the experimental data and outperforms the other two theoretical models for both the ballistic transport region ( $K_n \gg 1$ ) and diffusion region ( $K_n \ll 1$ ).

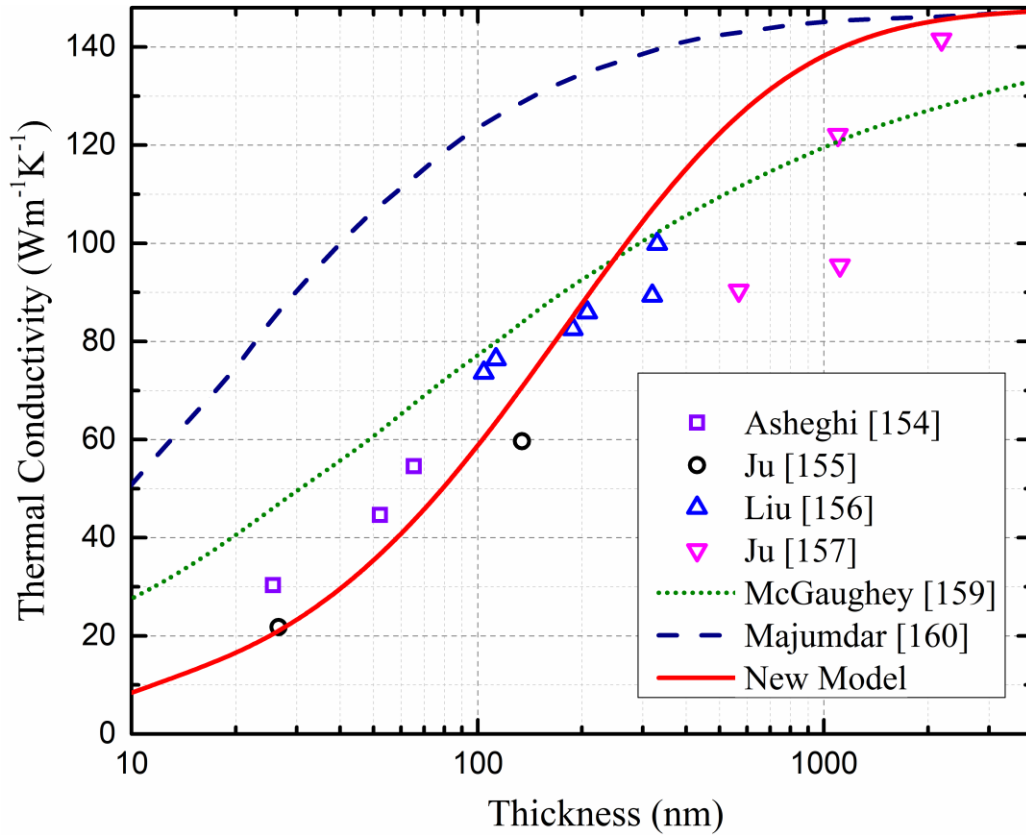


Figure 5.2 Comparison of thermal conductivity models and experimental data for nanofilms at room temperature

### 5.2.2 Femtosecond laser heating of gold films

The transient response of nonlocal DPL model will be examined here by the experiment of ultrafast laser heating. Ultrafast laser processing of nanomaterials has been a commonly-used method in nanotechnologies. Here, the experiment of ultrafast laser heating on thin gold films performed by Brorson [26] is selected for validation of the current nonlocal DPL model. The samples were heated by an intense laser beam, and the temperature of the surface was obtained by the probe beam measuring the reflectivity change of the sample surfaces. In this paper, three different mathematical models are selected for theoretical predictions of the one dimensional transient temperature variations [20, 50-51]:

$$\left\{ \begin{array}{l} q + \tau_q \frac{\partial q}{\partial t} = -k[\nabla T + \tau_r \frac{\partial \nabla T}{\partial t}], \quad DPL \\ q + \tau_q \frac{\partial q}{\partial t} + \xi \cdot \frac{\partial q}{\partial x} = -k[\nabla T + \tau_r \frac{\partial \nabla T}{\partial t}], \quad DPL - NL\_Tzou \\ (1 + \xi \frac{\partial}{\partial x})(q + \tau_q \frac{\partial q}{\partial t}) = -k[\nabla T + \tau_r \frac{\partial \nabla T}{\partial t}], \quad DPL - NL\_New \end{array} \right. \quad (5.15)$$

According to [20], the laser heating source can be expressed as:

$$S(x, t) = S_0 \cdot \exp\{-(x/\delta) - [a|(t - 2t_p)]/t_p\}, S_0 = 0.94[(1 - R)/t_p \delta]J \quad (5.16)$$

Consider the energy conservation in the presence of heat source,

$$-\frac{\partial q}{\partial x} + S = c_p \frac{\partial T}{\partial t} \quad (5.17)$$

The governing equation of the heat conduction in gold films controlled by the full extension of nonlocal DPL model would read as follows:

$$\frac{\partial^2 T}{\partial x^2} + \tau_r \frac{\partial^3 T}{\partial x^2 \partial t} + \frac{1}{k} \{S + \tau_q \frac{\partial S}{\partial t} + \xi \frac{\partial S}{\partial x} + \xi \cdot \tau_q \frac{\partial^2 S}{\partial x \partial t}\} = \frac{1}{\alpha} (\frac{\partial T}{\partial t} + \tau_q \frac{\partial^2 T}{\partial t^2}) + \frac{l}{\alpha} (\frac{\partial^2 T}{\partial x \partial t} + \tau_q \frac{\partial^3 T}{\partial x \partial t^2}) \quad (5.18)$$

while other two models in Eq. (5.15) can be treated in a similar manner. Assume the initial condition of gold films subjected to laser heating is stationary, then:

$$T(x, 0) = T_0, \frac{\partial T(x, 0)}{\partial t} = 0 \quad (5.19)$$

Usually, the processing time is too short, thus the heating loss from the front or back surface is negligible, then:

$$\frac{\partial T(0, t)}{\partial x} = \frac{\partial T(L, t)}{\partial x} = 0 \quad (5.20)$$

To continue the analysis, Eq. (5.18) is solved by Laplace transform:

$$T^*(x, p) = \int_0^{\infty} T(x, t) e^{-pt} dt \quad (5.21)$$

Hereafter,  $p$  is the Laplace transform variable and the superscript “\*” denotes the variables in the Laplace domain. The solution of Eq. (5.18) in the Laplace domain satisfying the initial conditions and the boundary conditions can be obtained as:

$$T^*(x, p) - T_0 = A_1 e^{r_1 x} + A_2 e^{r_2 x} + A_3 e^{-x/\delta} \quad (5.22)$$

where

$$\begin{aligned} r_{1,2} &= \frac{\frac{\xi}{\alpha}(p + p^2 \tau_q) \pm \sqrt{\frac{\xi^2}{\alpha^2}(p + p^2 \tau_q)^2 + \frac{4}{\alpha}(1 + p\tau_r)(p + p^2 \tau_q)}}{2(1 + p\tau_r)} \\ A_3 &= \frac{(\frac{\xi}{\delta} - 1) \frac{S_0}{k} [S_b(1 + p\tau_q) - \tau_q e^{-2a}]}{(1 + p\tau_q) / \delta^2 + \frac{\xi}{\alpha\delta}(p + p^2 \tau_q) - \frac{1}{\alpha}(p + p^2 \tau_q)} \\ A_2 &= \frac{A_3 e^{r_1 L} - A_3 e^{-L/\delta}}{\delta(r_2 e^{r_1 L} - r_1 e^{r_2 L})}, \quad A_1 = \frac{1/\delta \cdot A_3 - r_2 A_2}{r_1} \\ S_b &= t_p \left( \frac{e^{-2a} - e^{-2pt_p}}{pt_p - a} + \frac{e^{-2pt_p}}{pt_p + a} \right) \end{aligned} \quad (5.23)$$

To get the temperatures in the time domain, numerical inversion of Laplace transform [165] is performed. The normalized temperature,  $\Delta T / (\Delta T)_{\max}$  at the front surface is plotted against time as shown in Fig. 3. Obviously, the results of the new, nonlocal DPL model agree well with the experimental data. Moreover, the new model has a better performance than Tzou’s extension. This can be explained by the more accuracy brought by the added effect of the cross derivative  $\xi \tau_q \frac{\partial^2 q}{\partial x \partial t}$ . If we assume the nonlocal length is related to the relaxation time  $\tau_q$  by the finite speed  $c$  of the energy carriers, i.e.,  $\xi \sim c\tau_q$ , then  $\xi \tau_q \frac{\partial^2 q}{\partial x \partial t} \sim c\tau_q^2 \frac{\partial^2 q}{\partial x \partial t}$ , which appears as the second-order effect of  $\tau_q^2$  in the governing equation.

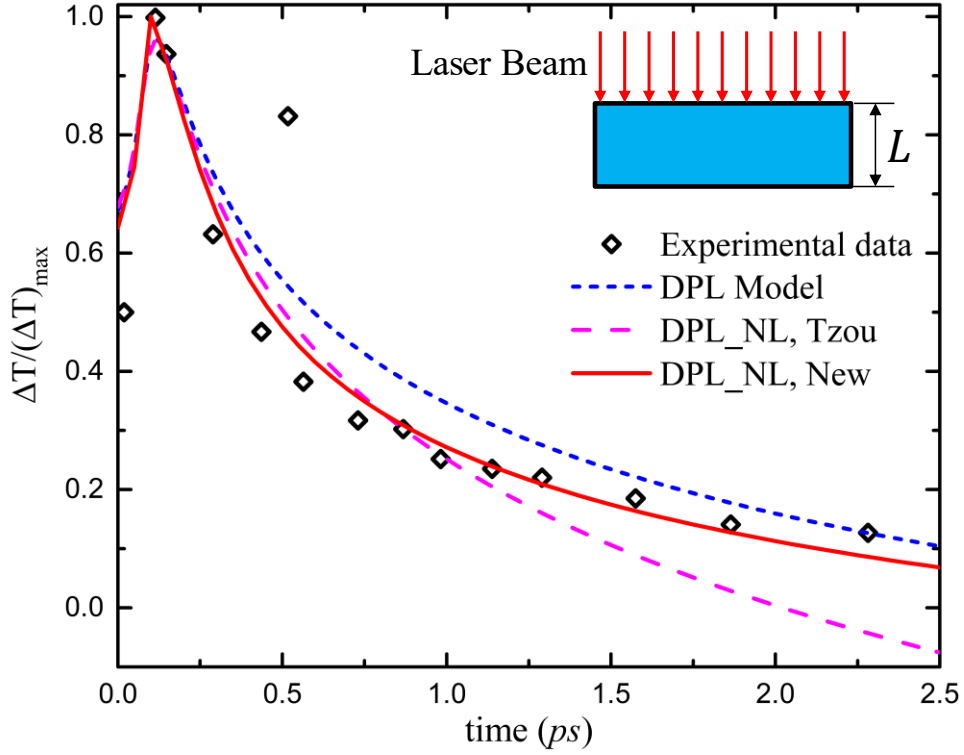


Figure 5.3 Normalized temperature change in the femtosecond heating of gold films (from Ref. [20] based on experimental data in [26]) and predictions from different theories,  $L = 200 \text{ nm}$ ,  $J = 13.4 \text{ Joule} / m_3$ ,  $\delta = 15.3 \text{ nm}$ ,  $t_p = 100 \text{ fs}$ ,  $a = 1.88$ ,  $\tau_T = 90 \text{ ps}$ ,  $\tau_q = 8.5 \text{ ps}$ ,  $R = 0.93$ ,  $\delta = 15.3 \text{ nm}$ ,  $\xi = 0.1L$ .

### 5.3 Generalized nonlocal thermoviscoelasticity

With the wider application of soft materials like polymer thin films, the viscoelastic relaxations of materials need to be considered in thermal stress analysis. In this section, a generalized, uncoupled nonlocal thermoviscoelasticity is formulated by taking into account both the previous nonlocal DPL heat conduction and Eringen's nonlocal theory. The influence of strain field on the temperature field is neglected for simplicity. The fundamental equations for thermoviscoelastic materials are expressed as follows.

The viscoelastic constitutive equations [166]:

$$\begin{aligned}
S_{ij} &= \int_0^t R(t-\tau) \frac{\partial e_{ij}}{\partial \tau} d\tau \\
\sigma &= \frac{\sigma_{kk}}{3} = \int_0^t R_v(t-\tau) \frac{\partial(e-3\alpha_T T)}{\partial \tau} d\tau
\end{aligned} \tag{5.24}$$

where  $\varepsilon_{ij} = \frac{1}{2}(u_{i,j} + u_{j,i})$ ,  $e_{ij} = \varepsilon_{ij} - \frac{e}{3}\delta_{ij}$ ,  $e = \varepsilon_{kk}$ ,  $S_{ij} = \sigma_{ij} - \frac{\sigma_{kk}}{3}\delta_{ij}$  and  $R(t), R_v(t)$  are the relaxation modules functions, shown as:

$$R(t) = 2\mu(1 - Af(t)), R_v(t) = K(1 - A_0f(t)) \tag{5.25}$$

where  $K = \lambda + 2\mu/3$  is the bulk modulus,  $f(t) = f_1(t) = e^{-\beta t} t^{\alpha-1}$  and  $\alpha, \beta, A, A_0$  are empirical constants.

With the help of Eq. (5.2), the nonlocal stresses are obtained as:

$$(1 - \zeta^2 \nabla^2) t_{ij} = \int_0^t R(t-\tau) \frac{\partial(\varepsilon_{ij} - \frac{e}{3}\delta_{ij})}{\partial \tau} d\tau + \delta_{ij} \int_0^t R_v(t-\tau) \frac{\partial(e - 3\alpha_T T)}{\partial \tau} d\tau \tag{5.26}$$

where  $\zeta = e_0 a$  is the nonlocal characteristic length.

The equation of motion:

$$(1 - \zeta^2 \nabla^2) \rho \frac{\partial^2 u_i}{\partial t^2} = \int_0^t R(t-\tau) \frac{\partial(\varepsilon_{ij,j} - \frac{e_j}{3}\delta_{ij})}{\partial \tau} d\tau + \delta_{ij} \int_0^t R_v(t-\tau) \frac{\partial(e_{,j} - 3\alpha_T T_{,j})}{\partial \tau} d\tau \tag{5.27}$$

The equation of heat conduction neglecting heating source and effects of deformation:

$$(1 + \xi \cdot \nabla)(1 + \tau_q \frac{\partial}{\partial t})(\rho c_e \frac{\partial T}{\partial t}) = -k[\nabla^2 T + \tau_r \frac{\partial \nabla^2 T}{\partial t}] \tag{5.28}$$

### 5.3.1 Formulation of the problem

Now consider a homogeneous isotropic viscoelastic plate with finite thickness  $L$  subject to a transient thermal shock on its left surface, which is initially quiescent. The whole plate is initially at room temperature  $T_r$ . At time  $t=0$ , a sudden thermal shock  $T_0 H(t)$  is applied on the left

surface while the right end is keep fixed, where  $H(t)$  is the Heaviside function. Assume the dimension in  $y$  and  $z$  directions are much larger than that in  $x$  direction and the spatial nonlocality is uniquely decided by the  $x$  direction. Obviously, all physical variables are only dependent on spatial coordinate  $x$  and time  $t$ . The displacement vector has the following form:

$$u_x = u(x, t), u_y = 0, u_z = 0 \quad (5.29)$$

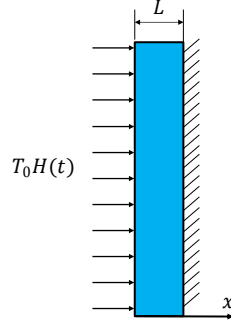


Figure 5.4 Schematic diagram of a viscoelastic plate under transient thermal shock

The initial conditions are:

$$u(x, 0) = \frac{\partial u(x, 0)}{\partial t} = 0, t_{ij}(x, 0) = \frac{\partial t_{ij}(x, 0)}{\partial t} = 0, \frac{\partial T(x, 0)}{\partial t} = 0 \quad (5.30)$$

The left surface is traction free and the temperature of the right end is assumed to keep unchanged, the boundary conditions are:

$$\begin{aligned} T(0, t) &= T_0 H(t), T(L, t) = T_r \\ u(L, t) &= 0, t_{xx}(0, t) = 0 \end{aligned} \quad (5.31)$$

The governing equations for this one-dimensional problem are:

$$(1 + \xi \frac{\partial}{\partial x})(1 + \tau_q \frac{\partial}{\partial t})(\rho c_e \frac{\partial T}{\partial t}) = -k[\frac{\partial^2 T}{\partial x^2} + \tau_T \frac{\partial}{\partial t} \frac{\partial^2 T}{\partial x^2}] \quad (5.32)$$

$$(1 - \zeta^2 \frac{\partial^2}{\partial x^2})\rho \frac{\partial^2 u}{\partial t^2} = \int_0^t \frac{2}{3} R(t - \tau) \frac{\partial}{\partial \tau} (\frac{\partial^2 u}{\partial x^2}) d\tau + \int_0^t R_v(t - \tau) \frac{\partial}{\partial \tau} (\frac{\partial^2 u}{\partial x^2} - 3\alpha_T \frac{\partial T}{\partial x}) d\tau \quad (5.33)$$

and the nonlocal stresses can be expressed as:

$$(1 - \zeta^2 \frac{\partial^2}{\partial x^2})t_{xx} = \int_0^t \frac{2}{3} R(t - \tau) \frac{\partial}{\partial \tau} \left( \frac{\partial u}{\partial x} \right) d\tau + \int_0^t R_v(t - \tau) \frac{\partial}{\partial \tau} \left( \frac{\partial u}{\partial x} - 3\alpha_T T \right) d\tau \quad (5.34)$$

$$(1 - \zeta^2 \frac{\partial^2}{\partial x^2})t_{yy} = (1 - \zeta^2 \frac{\partial^2}{\partial x^2})t_{zz} = \int_0^t -\frac{1}{3} R(t - \tau) \frac{\partial}{\partial \tau} \left( \frac{\partial u}{\partial x} \right) d\tau + \int_0^t R_v(t - \tau) \frac{\partial}{\partial \tau} \left( \frac{\partial u}{\partial x} - 3\alpha_T T \right) d\tau \quad (5.35)$$

Then introduce the following dimensionless variables:

$$\begin{aligned} (\bar{x}, \bar{u}, \bar{\xi}, \bar{\lambda}) &= c_0 \eta_0(x, u, \xi, \lambda), \quad (\bar{t}, \bar{\tau}_q, \bar{\tau}_T) = c_0^2 \eta_0(t, \tau_q, \tau_T), \\ \bar{R}_v &= \frac{R_v}{K}, \quad \bar{R} = \frac{2R}{3K}, \quad \bar{t}_{ij} = \frac{t_{ij}}{K}, \quad \bar{T} = \frac{3\alpha_T(T - T_r)}{T_0 - T_r} \end{aligned} \quad (5.36)$$

Equations (5.32)-(5.35) can then be reduced to the dimensionless forms (the overbar will be dropped here and after for convenience):

$$(1 + \xi \frac{\partial}{\partial x})(1 + \tau_q \frac{\partial}{\partial t}) \frac{\partial T}{\partial t} = \frac{\partial^2 T}{\partial x^2} + \tau_T \frac{\partial}{\partial t} \frac{\partial^2 T}{\partial x^2} \quad (5.37)$$

$$(1 - \zeta^2 \frac{\partial^2}{\partial x^2}) \frac{\partial^2 u}{\partial t^2} = \int_0^t R(t - \tau) \frac{\partial}{\partial \tau} \left( \frac{\partial^2 u}{\partial x^2} \right) d\tau + \int_0^t R_v(t - \tau) \frac{\partial}{\partial \tau} \left( \frac{\partial^2 u}{\partial x^2} - \frac{\partial T}{\partial x} \right) d\tau \quad (5.38)$$

$$(1 - \zeta^2 \frac{\partial^2}{\partial x^2})t_{xx} = \int_0^t R(t - \tau) \frac{\partial}{\partial \tau} \left( \frac{\partial u}{\partial x} \right) d\tau + \int_0^t R_v(t - \tau) \frac{\partial}{\partial \tau} \left( \frac{\partial u}{\partial x} - T \right) d\tau \quad (5.39)$$

$$(1 - \zeta^2 \frac{\partial^2}{\partial x^2})t_{yy} = (1 - \zeta^2 \frac{\partial^2}{\partial x^2})t_{zz} = \int_0^t -\frac{1}{2} R(t - \tau) \frac{\partial}{\partial \tau} \left( \frac{\partial u}{\partial x} \right) d\tau + \int_0^t R_v(t - \tau) \frac{\partial}{\partial \tau} \left( \frac{\partial u}{\partial x} - T \right) d\tau \quad (5.40)$$

where the relaxation moduli are reduced to:

$$R(t) = \frac{4\mu}{3K} [1 - Af(t)], \quad R_v(t) = 1 - A_0 f_1(t), \quad f(t) = f_1(t) = e^{-\beta t} t^{\alpha-1} \quad (5.41)$$

### 5.3.2 Analytical solutions by Laplace transform

Performing Laplace transform to both sides of Eqs. (5.37)-(5.41), one can get:

$$(1 + \xi \frac{\partial}{\partial x})(1 + \tau_q p) p T^* = (1 + \tau_T p) \frac{\partial^2 T^*}{\partial x^2} \quad (5.42)$$

$$(1 - \zeta^2 \frac{\partial^2}{\partial x^2}) p^2 u^* = (R^* + R_v^*) p \frac{\partial^2 u^*}{\partial x^2} + R_v^* p \frac{\partial T^*}{\partial x} \quad (5.43)$$

$$(1 - \zeta^2 \frac{\partial^2}{\partial x^2}) t_{xx}^* = [R^* + R_v^*] p \frac{\partial u^*}{\partial x} - R_v^* p T^* \quad (5.44)$$

$$(1 - \zeta^2 \frac{\partial^2}{\partial x^2}) t_{yy}^* = (1 - \zeta^2 \frac{\partial^2}{\partial x^2}) t_{zz}^* = (-\frac{1}{2} R^* + R_v^*) p \frac{\partial u^*}{\partial x} - R_v^* p T^* \quad (5.45)$$

$$R^* = \frac{4\mu}{3K} \left[ \frac{1}{p} - A \frac{\Gamma(\alpha)}{p(p + \beta)^\alpha} \right], \quad R_v^* = \frac{1}{p} - A_0 \frac{\Gamma(\alpha)}{p(p + \beta)^\alpha} \quad (5.46)$$

Since the effect of deformation on temperatures has been neglected, so the governing equation of temperature field can be solved directly using boundary conditions expressed in Eq. (5.31). The temperature field in the Laplace domain is expressed as:

$$T^*(p) = \sum_{i=1}^2 A_i e^{r_i x} \quad (5.47)$$

where

$$r_{1,2} = \frac{\xi p \pm \sqrt{\xi^2 p^2 + 4p(1 + \tau_T p) / (1 + \tau_q p)}}{2(1 + \tau_T p) / (1 + \tau_q p)} \quad (5.48)$$

$$A_1 = \frac{1}{p} + \frac{1}{p} \frac{e^{r_1 L}}{e^{r_2 L} - e^{r_1 L}}, \quad A_2 = -\frac{1}{p} \frac{e^{r_1 L}}{e^{r_2 L} - e^{r_1 L}}$$

Substituting Eq. (5.47) into Eq. (5.43), the general solution of displacement field can be obtained as:

$$u^*(p) = \sum_{i=1}^4 B_i e^{r_i x} \quad (5.49)$$

where

$$r_{3,4} = \pm \sqrt{\frac{p}{(R^* + R_v^*) + \zeta^2 p}} \quad (5.50)$$

$$B_1 = \frac{R_v^* r_1}{(R^* + R_v^*) r_1^2 + \zeta^2 p r_1^2 - p} A_1, \quad B_2 = \frac{R_v^* r_2}{(R^* + R_v^*) r_2^2 + \zeta^2 p r_2^2 - p} A_2$$

The two unknown coefficients  $B_3, B_4$  need to be determined by the related boundary conditions. Substitute solution Eq. (5.47) and (5.49) into Eq. (5.44), one can obtain:

$$(1 - \zeta^2 \frac{\partial^2}{\partial x^2}) t_{xx}^* = (R^* + R_v^*) p \sum_{i=1}^4 B_i r_i e^{r_i x} - R_v^* p \sum_{i=1}^2 A_i e^{r_i x} \quad (5.51)$$

The particular solution of the PDE (5.51) is:

$$t_{xx}^*(p) = \sum_{i=1}^4 C_i e^{r_i x} \quad (5.52)$$

where

$$\begin{aligned} C_1 &= \frac{(R^* + R_v^*) p B_1 r_1 - R_v^* p A_1}{1 - r_1^2 \zeta^2}, C_2 = \frac{(R^* + R_v^*) p B_2 r_2 - R_v^* p A_2}{1 - r_2^2 \zeta^2} \\ C_3 &= \frac{(R^* + R_v^*) p B_3 r_3}{1 - r_3^2 \zeta^2}, C_4 = \frac{(R^* + R_v^*) p B_4 r_4}{1 - r_4^2 \zeta^2} \end{aligned} \quad (5.53)$$

Applying the boundary conditions  $t_{xx}^*(0, p) = u^*(L, p) = 0$  to Eq. (5.52), we have:

$$\begin{aligned} B_1 e^{r_1 L} + B_2 e^{r_2 L} + B_3 e^{r_3 L} + B_4 e^{r_4 L} &= 0 \\ C_1 + C_2 + C_3 + C_4 &= 0 \end{aligned} \quad (5.54)$$

Solving the algebraic Eq. (5.54) to obtain the two unknown coefficients  $B_3, B_4$ , we can obtain the displacement field  $u^*(p)$  and nonlocal stresses  $t_{xx}^*(p)$ . Similarly, the other two nonlocal stresses can be obtained as:

$$t_{yy}^*(p) = t_{zz}^*(p) = \sum_{i=1}^4 D_i e^{r_i x} \quad (5.55)$$

where

$$\begin{aligned} D_1 &= \frac{(-\frac{1}{2} R^* + R_v^*) p B_1 r_1 - R_v^* p A_1}{1 - r_1^2 \zeta^2}, D_2 = \frac{(-\frac{1}{2} R^* + R_v^*) p B_2 r_2 - R_v^* p A_2}{1 - r_2^2 \zeta^2} \\ D_3 &= \frac{(-\frac{1}{2} R^* + R_v^*) p B_3 r_3}{1 - r_3^2 \zeta^2}, D_4 = \frac{(-\frac{1}{2} R^* + R_v^*) p B_4 r_4}{1 - r_4^2 \zeta^2} \end{aligned} \quad (5.56)$$

Until now, all analytical solutions have been obtained in the Laplace domain. To obtain the results in the time domain, a numerical inversion method [160] based on the fast Fourier transform is applied to the expressions of  $T^*$ ,  $u^*$ ,  $t_{xx}^*$ ,  $t_{yy}^*$ ,  $t_{zz}^*$  in the above equations.

## 5.4 Results and discussions

In this section, the main emphasis is on the effects of both nonlocal DPL heat conduction and nonlocal elasticity on the thermal and mechanical responses. A series of parametric investigations are performed. The viscoelastic, polymethyl methacrylate material is selected for numerical analysis with material parameters listed in Table 1 [56]. The non-dimensional finite thickness of the plate is assumed to be  $L=1$  and the two non-dimensional thermal lags are specified as  $\tau_q = 0.04$ ,  $\tau_T = 0.02$ .

The resulting temperature distributions along the thickness direction at  $t=0.05$  are shown in Figure 5.5 based on different non-Fourier heat conduction models. The C-V model predicts a temperature profile with high temperature gradient, which can be eliminated by the DPL models. The nonlocal DPL model always predicts a faster propagation of temperature than the conventional DPL model, and the propagation speed will increase with increasing nonlocal characteristic length  $\xi$  of heat conduction, which is consistent with the findings in [50-51].

Table 5.1 Material parameters of polymethyl methacrylate [56]

$\lambda = 453.7 \times 10^7 \text{ kg} / \text{ms}^2$	$\mu = 194 \times 10^7 \text{ kg} / \text{ms}^2$	$c_0 = 2200 \text{ m} / \text{s}$
$\rho = 1.2 \times 10^3 \text{ kg} / \text{m}^3$	$k = 0.55 \text{ W} / \text{mK}$	$E = 5.25 \times 10^9 \text{ N} / \text{m}^2$
$\alpha_T = 1.3 \times 10^{-4} \text{ K}^{-1}$	$c_E = 1.4 \times 10^3 \text{ J} / (\text{kgK})$	

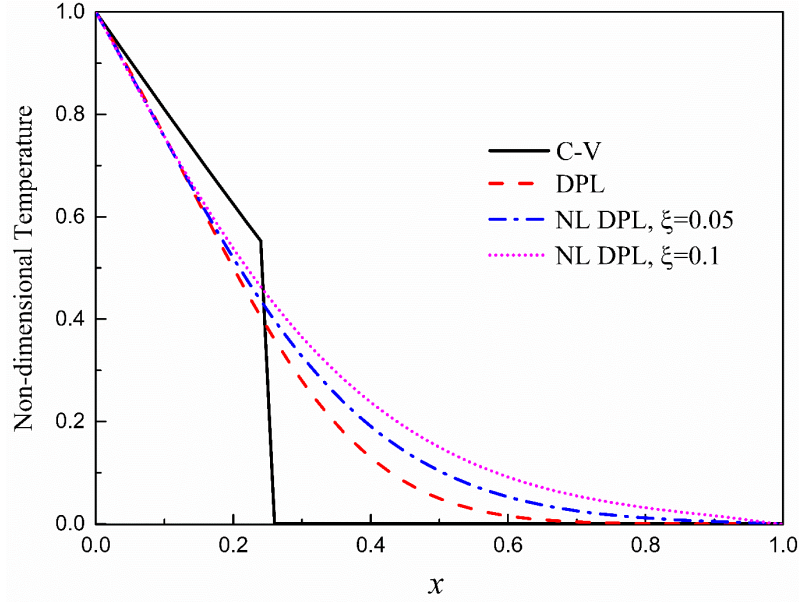


Figure 5.5 Temperature distributions along the thickness direction at  $t=0.05$ .

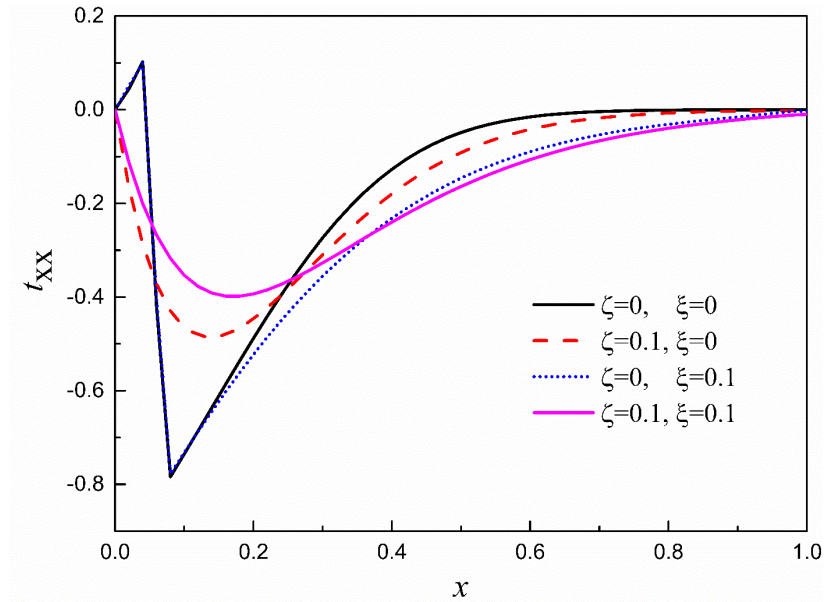


Figure 5.6 Distributions of the non-dimensional nonlocal stress  $t_{xx}$  along  $x$  coordinate at  $t=0.05$  under the influence of different combinations of nonlocal lengths

The transient mechanical response would be complicated by the transient, non-Fourier heat conduction, the relaxation properties resulted from viscosity of the material, and the nonlocal elasticity. In this research, we are interested in the transient, nonlocal stress distribution, which

directly relates to the safety of materials under a sudden thermal shock. As shown in Figure 5.6, the distributions of the non-dimensional nonlocal stress  $t_{xx}$  along  $x$  coordinate are plotted at  $t=0.05$  under different combinations of nonlocal lengths. The nonlocal length  $\zeta$  significantly affects the nonlocal stress distribution, and the introduction of nonlocal elasticity removes the sharp spatial jump of stress profiles. The nonlocal length  $\xi$  in heat conduction also influences stress distribution, although the effect is not as significant as the nonlocal length  $\zeta$ . Almost all stresses are negative, indicating the compress stresses are the dominant response at the early stage after a thermal shock is applied to the plate.

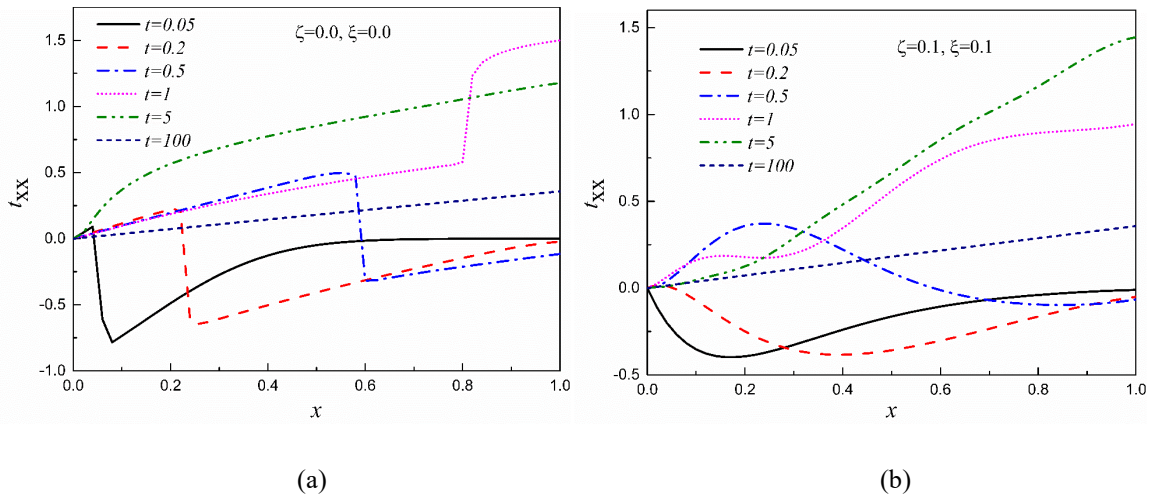


Figure 5.7 The evolutions of non-dimensional nonlocal stress  $t_{xx}$  profile for (a): without considering nonlocality (b) considering nonlocality

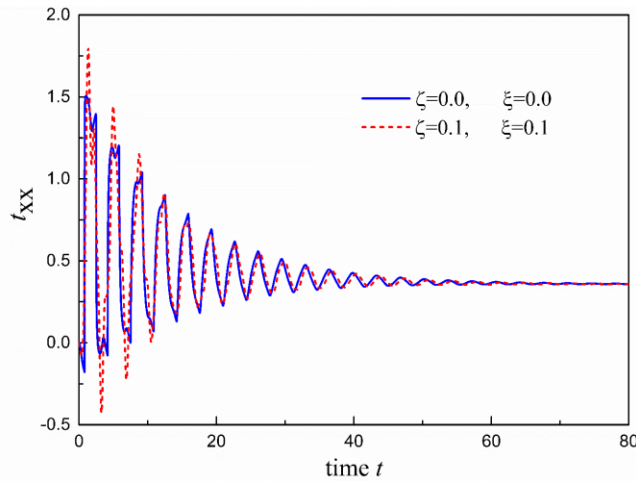


Figure 5.8 The time history of non-dimensional nonlocal stress  $t_{xx}$  at the right end ( $x=L$ )

In order to quantify the influence of the two nonlocal lengths on the mechanical response, the distributions of the non-dimensional, nonlocal stress  $t_{xx}$  at different instants are presented in Figure 5.7. A comparison is performed between classical local analysis and the nonlocal analysis. Nonlocal theories will remove the sharp jump in stress profiles at all time instants. When the time elapsed is long enough, the classical stress and the nonlocal stress profiles will coincide with each other, reducing to a linear distribution along the thickness direction. To illustrate the effect of nonlocal lengths on the dynamic stress, the time history of nonlocal stress  $t_{xx}$  at the right end of the plate is displayed in Figure 5.8. The stress starts from a compressive stress, increasing to the peak value of tensile stress before subsequent fluctuations about the steady state values. The peak values will decrease with time elapsed. Similar fluctuations can be found between two curves but the nonlocal analysis presents higher peak values, especially for  $t < 20$ . Therefore, the nonlocal analysis is essential to the safety of nanodevices. Both responses in the long term will converge to the steady state value, which verifies the results in Figure 5.7.

Figure 5.9 displays the distribution of  $t_{yy}$  (or  $t_{zz}$ ) at  $t=0.05$  predicted based on different combinations of nonlocal lengths. Similar effects of nonlocality on  $t_{xx}$  can be observed with these two stress components, where both nonlocal lengths will influence the stresses clearly, and the nonlocal length  $\zeta$  plays a more significant role. Besides, the nonlocal length  $\zeta$  will remove the sharp jump in the distribution of  $t_{yy}$ . The time history of  $t_{yy}$  shown in Figure 5.10 also displays a similar trend as that of  $t_{xx}$ , where the nonlocal analysis gives higher peak values of stresses. In addition, both the peak and steady state values of  $t_{yy}$  and  $t_{zz}$  are smaller than those of  $t_{xx}$ . The influence of nonlocality on the distribution of displacement and strain field is illustrated in Figure 5.11 and 5.12, respectively. It indicates the nonlocal length  $\zeta$  still plays a dominant role in the results. However, different from its effect on stresses, the nonlocal length  $\xi$  shows a negligible effect on the displacements and strains.

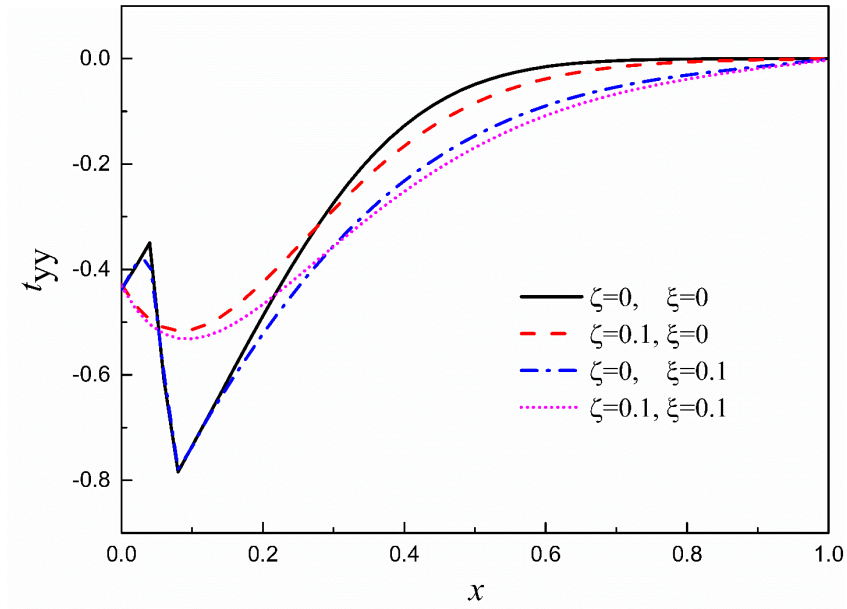


Figure 5.9 Distributions of the non-dimensional nonlocal stress  $t_{yy}$  along  $x$  coordinate at  $t=0.05$  under the influence of different combinations of nonlocal lengths.

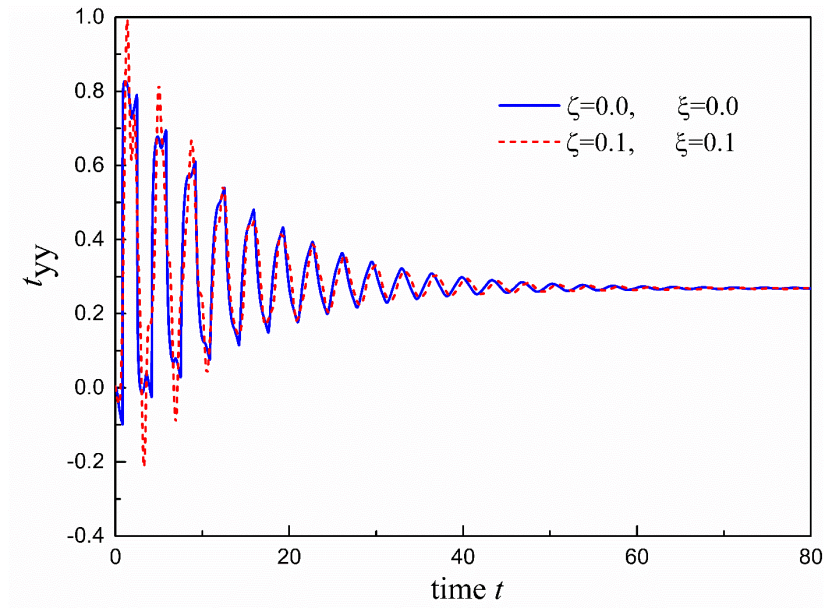


Figure 5.10 The time history of non-dimensional nonlocal stress  $t_{yy}$  at the right end ( $x=L$ )

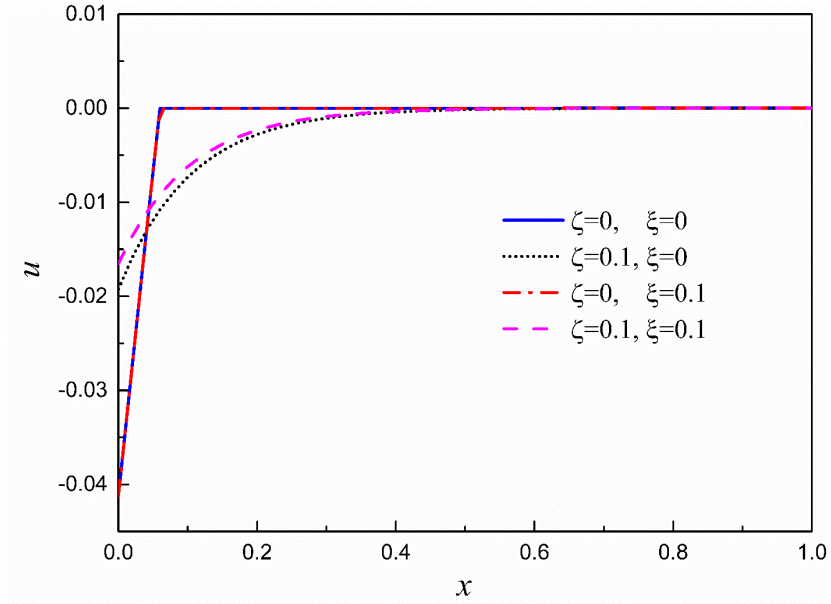


Figure 5.11 Distributions of the non-dimensional displacement  $u$  along  $x$  coordinate at  $t=0.05$  under the influence of different combinations of nonlocal lengths

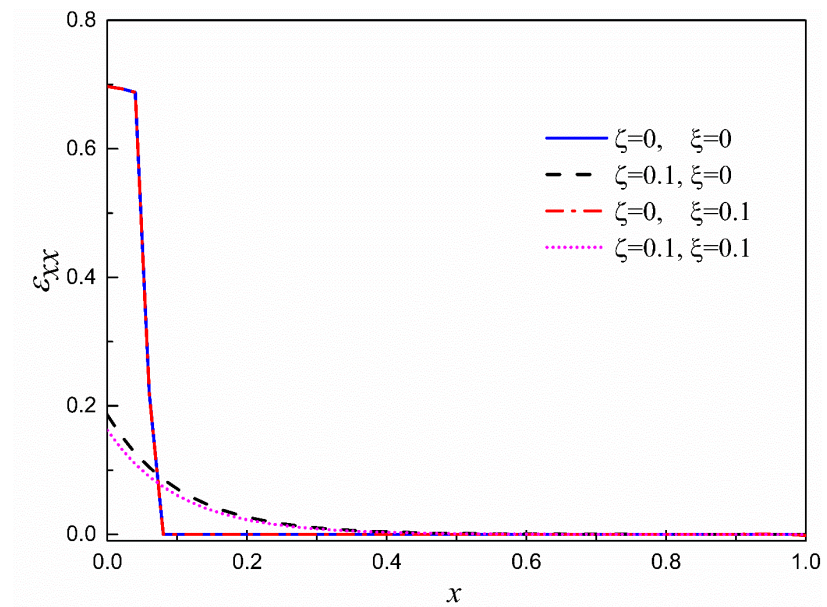


Figure 5.12 Distributions of the non-dimensional strain  $\epsilon_{xx}$  along  $x$  coordinate at  $t=0.05$  under the influence of different combinations of nonlocal lengths.

## 5.5 Conclusions

In this chapter, the full extension of nonlocal DPL model to the first order of the Taylor expansion is considered to account for the heat conduction at nanoscale, which is verified experimentally by the size-dependent thermal conductivity of silicon nanofilms and the femtosecond laser heating of gold films. The nonlocal DPL model is then employed in the generalized, nonlocal thermoviscoelasticity to investigate the transient, thermoviscoelastic response of nano-structural materials. Parametric studies are conducted considering both the nonlocal DPL model and Eringen's nonlocal theory to illustrate the effect of nonlocality on the transient response in a viscoelastic plate of finite thickness under a sudden thermal shock. The results show the nonlocal DPL model predicts a faster thermal propagation speed, and the nonlocal lengths can remove the spatial jump in mechanical responses. In addition, the nonlocal analysis predicts higher peak values of thermal stresses.

## **Chapter 6: Nonlocal fracture analysis of an interface crack between functionally graded coating and homogenous substrate under thermal loading**

In this chapter, the thermoelastic response of an interface crack between a functionally graded coating and the homogenous substrate under thermal loading is investigated using the nonlocal continuum theory to eliminate the stress singularities at the crack tips and address the size effects. The differential form of nonlocal theory is utilized to obtain the governing equations of the thermal stress field, whereas the integral form is employed for the boundary conditions. Finally, the mixed, boundary-value problems are reduced to two pairs of dual integral equations using Fourier transform. The Schmidt method is adopted to solve the dual integral equations numerically. The numerical results confirmed the finite values of thermal stresses at the crack tips, which enable us to establish a straightforward maximum stress-based criterion instead of the traditional, stress intensity factor- or energy-based fracture criterion. In addition, the location of maximum stresses is found to be slightly away from the crack tip, which is determined by the nonlocal characteristic length. Parametric studies are conducted to investigate the influence of nonhomogeneous properties on the thermal fracture behavior of the interface crack.

### **6.1 Introduction**

In high-temperature engineering applications such as jet engines, diesel engines and gas turbines, thermal barrier coatings (TBCs) are usually developed to provide high thermal resistance so as to protect the mechanical components [167-168]. The most commonly used material that makes up TBCs is ceramic yttria stabilized zirconia. However, the ceramic always possesses absolutely different thermal-mechanical properties than the metallic substrates (such as steel), which often results in high thermal stress concentration at the interface or even delamination and failure of the entire structure. In order to avoid the property mismatch leading poor interfacial bonding strength, functionally graded materials (FGMs) are introduced as TBCs which can effectively reduce thermal stresses and enhance the heat resistance. By mixing ceramic and metal alloys in various volume ratios, FGMs can achieve gradually variations of microstructure and

thermal-mechanical properties [169-170]. Other superior advantages of functionally graded coatings include improved wear resistance and bond strength, and elevated thermal fatigue life and fracture resistance. Very recently, with the rapid development of nanotechnology, FGMs have attracted considerable attention in developing ultra-small systems such as microelectromechanical system (MEMS) or nanoelectromechanical system (NEMS) [171].

Interfacial cracks in multiphase composites can be developed in the manufacturing process or under external loading. In designing the functionally graded thermal barrier coatings, a thorough understanding of the thermal fracture behavior of interface cracks is a necessity to assure the lifetime and reliability of the structure. Lee and Erdogan [172] considered the plane strain thermal stress problem for two interfacial, symmetric edge cracks between a homogenous substrate and a graded coating. Later, Jin investigated the effects of thermal property gradients on the edge cracking in an  $\text{Al}_2\text{O}_3/\text{Si}_3\text{N}_4$  graded coating bonded to a homogeneous substrate subject to a thermal shock [173]. Rangaraj and Kokini studied the thermal fracture behaviors in a functionally graded, yttria stabilized zirconia-NiCoCrAlY bonded thermal barrier coating using mean field micromechanical model to predict the effective thermoelastic and viscoplastic properties [174]. Yildirim et al. examined the three dimensional, semi-elliptical surface crack in a functionally graded coating subject to mode I mechanical or transient thermal loading [175]. The thermal fracture resistance of a functionally graded coating with an array of periodic edge cracks under thermal shock loading was studied by Jin and Feng [176]. Choi and Paulino analyzed a coupled, plane elasticity problem of crack/contact mechanics for a functionally graded coating/substrate system, where the rigid flat punch slides over the surface of the coated system with a crack [177].

Although there has been a lot of researches concerning the thermal fracture of interface cracks in FGMs coating/substrate systems, they were all based on stress intensity factor- or energy-based fracture criterion. These criteria always are always developed based on the stress field around the crack tip of  $r^{-1/2}$  singularity (where  $r$  is the distance from the crack tip). The singular stress field around the crack tip based on classical elasticity theory implies an infinite stress at the crack tip, which is problematic physically according to the observation of material rupture. The experimental study has shown the strain would be finite at the crack tips, and the maximum value is not exactly on the crack tip but locates on a short distance from the crack tip [178]. Another important issue associated with classical elasticity is the disability in accounting

for the size effect, which would be pronounced in the multiphase composites, nanostructured materials, or nano-sized devices like NEMS. Taking size effect into consideration, a recent research [179] has shown a higher fracture risk for a vertical surface crack in a homogeneous half plane than classical analysis. Both issues can be perfectly addressed using the modified, size-dependent continuum mechanics, such as nonlocal elasticity, strain gradient theory or couple stress theory. By means of nonlocal elasticity, Eringen has shown the finite stress at the crack tip in an isotropic, elastic plate subjected to uniform tension, shear, and anti-plane shear [72,77-78]. Alfantis [180] validated that adopting the strain gradient elasticity will remove the strain singularities in the results. Later, Zhou et. al. [80-82,181-182] employed the Schmidt method to investigate various crack problems under mechanical loadings based on nonlocal theory. However, till now, there exists no report of thermal fracture analysis that eliminates the stress singularity at the crack tip and takes the size effect into consideration. In order to develop a better understanding of the thermal fracture behavior in compositionally graded, thermal barrier coatings/substrate systems, the nonlocal continuum theory is utilized in this article.

Compared to classical continuum theory, the nonlocal theory no longer treats the stress at a point to be influenced uniquely by the strain at the same point. Instead, the nonlocal theory assumes the stress would be determined by the strains in a surrounding area, thus taking the size effect into consideration and building the connections between the classical continuum with the mechanics at the nanoscale. In this work, the nonlocal theory is employed to investigate the thermal fracture behavior of an interface crack between an FGM coating and a homogenous substrate. Fourier transform is employed to convert the governing partial differential equations (PDEs) into dual integral equations. Finally, the dual integral equations are solved by the Schmidt method numerically, and the finite, thermal stress fields around the crack tip are obtained.

## **6.2 Mathematical formulation of the problem**

A bimaterial composed of an FGM coating and a homogeneous substrate is considered as shown in Figure 6.1. The FGM coating for to the substrate except for an interface crack of length  $2c$ , which is partially, thermally insulated. Assume the crack is very small compared to the whole size of the biomaterial, both the FGM coating and the substrate are treated to be semi-infinite planes. For simplicity, a Cartesian coordinate system is established with its origin at the center of

the crack. A steady state, remote heat flux of intensity  $q_\infty$  is applied at infinity and the crack is free of traction. It is presumed the material properties vary exponentially in the  $y$ -direction. The Poisson's ratio  $\nu_p$  is a constant throughout the bimaterial for variation of Poisson's ratio is believed to have a negligible influence on the fracture behaviors [183]. The remaining thermo-mechanical properties are modeled as:

$$\mu = \mu_0 e^{\beta y}, \quad \kappa = \kappa_0 e^{\delta y}, \quad \alpha_T = \alpha_{T0} e^{\gamma y} \quad (6.1)$$

where  $\mu, \kappa, \alpha_T$  are the shear modulus, thermal conductivity and coefficient of linear expansion, respectively.  $\mu_0, \kappa_0, \alpha_{T0}$  correspond to the values of the homogeneous substrate and  $\beta, \delta, \gamma$  are the nonhomogeneity parameters.

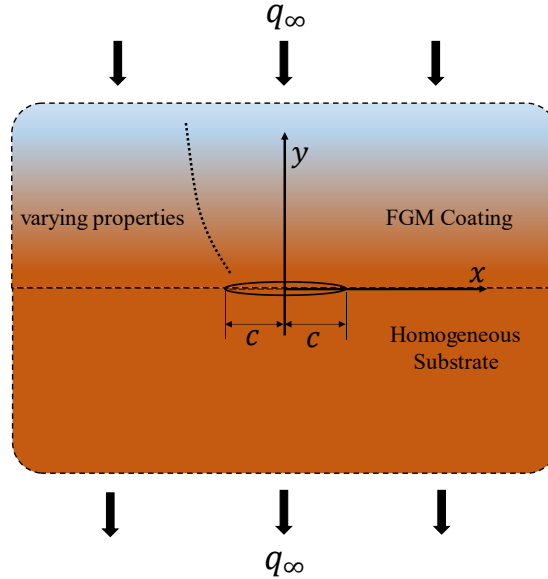


Figure 6.1 Geometry of the interface crack between FGM coating and homogeneous substrate

The governing equation of the heat conduction is:

$$\begin{aligned} \frac{\partial}{\partial x} \left( \kappa \frac{\partial T}{\partial x} \right) + \frac{\partial}{\partial y} \left( \kappa \frac{\partial T}{\partial y} \right) &= 0, & y > 0 \\ \frac{\partial^2 T}{\partial x^2} + \frac{\partial^2 T}{\partial y^2} &= 0, & y < 0 \end{aligned} \quad (6.2)$$

The corresponding thermal boundary conditions are:

$$\begin{aligned}
\kappa \frac{\partial T}{\partial y} &= q_\infty, & (y \rightarrow \pm\infty) \\
\kappa_0 \frac{\partial T}{\partial y} &= k^* q_\infty, & (y = 0, |x| \leq c) \\
T(x, 0^+) &= T(x, 0^-), & (|x| > c) \\
\frac{\partial T(x, 0^+)}{\partial y} &= \frac{\partial T(x, 0^-)}{\partial y}, & (|x| > c)
\end{aligned} \tag{6.3}$$

where  $0 \leq k^* \leq 1$  is the dimensionless variable of heat conductivity of the crack.  $k^* = 0$  and  $k^* = 1$  represent the complete insulation and perfect conduction of the crack, respectively. The plane elasticity equations based on the nonlocal elasticity theory, without considering body force are:

$$\frac{\partial t_{xx}}{\partial x} + \frac{\partial t_{xy}}{\partial y} = 0, \quad \frac{\partial t_{xy}}{\partial x} + \frac{\partial t_{yy}}{\partial y} = 0 \tag{6.4}$$

$$\varepsilon_{xx} = \frac{\partial u}{\partial x}, \quad \varepsilon_{yy} = \frac{\partial v}{\partial y}, \quad \varepsilon_{xy} = \frac{1}{2} \left( \frac{\partial u}{\partial y} + \frac{\partial v}{\partial x} \right) \tag{6.5}$$

$$\begin{aligned}
\sigma_{xx} &= \frac{\mu}{k-1} \left[ (k+1) \frac{\partial u}{\partial x} + (3-k) \frac{\partial v}{\partial y} - 4k_\alpha \alpha_T T \right] \\
\sigma_{yy} &= \frac{\mu}{k-1} \left[ (k+1) \frac{\partial v}{\partial y} + (3-k) \frac{\partial u}{\partial x} - 4k_\alpha \alpha_T T \right] \\
\sigma_{xy} &= \mu \left[ \frac{\partial u}{\partial y} + \frac{\partial v}{\partial x} \right]
\end{aligned} \tag{6.6}$$

where  $t_{ij}$  is the nonlocal stress,  $\sigma_{ij}$  is the classical local stress,  $\varepsilon_{ij}$  is the strain,  $k = 3 - 4\nu_p$ ,  $k_\alpha = 1$  are applied for the plane strain conditions and  $k = (3 - \nu_p) / (1 + \nu_p)$ ,  $k_\alpha = 1 + \nu_p$  are applied for the plane stress conditions. Different from the classical continuum, nonlocal theory assumes the stress at one point is determined by all the strains in the surrounding area, shown as:

$$t_{ij}(\mathbf{x}) = \int_V \alpha(|\mathbf{x} - \mathbf{x}'|) \sigma_{ij}(\mathbf{x}') dV(\mathbf{x}') \tag{6.7}$$

where  $\alpha(|\mathbf{x} - \mathbf{x}'|)$  is the kernel function of the distance between the point of interest and its neighboring point, characterizing the long-range interactions between molecules or atoms. In this study, a widely used kernel function by Eringen [77] and Zhou [80-82, 181-182] is adopted as:

$$\alpha(|\mathbf{x} - \mathbf{x}'|) = \frac{1}{\pi} \left(\frac{\eta}{a}\right)^2 \exp\left[-\left(\frac{\eta}{a}\right)^2 (\mathbf{x} - \mathbf{x}')(\mathbf{x} - \mathbf{x}')\right] \quad (6.8)$$

where  $\eta$  is a constant determined by experiments [181-182], and  $a$  is an internal, nonlocal characteristic length. In 1983, a more popular, equivalent, partial differential form of the nonlocal theory is proposed by Eringen et al. [70]:

$$(1 - (e_0 a)^2 \nabla^2) t_{ij} = \sigma_{ij} \quad (6.9)$$

where  $e_0$  is a constant depending on materials, and  $\nabla^2$  is the Laplacian operator. By means of the differential form, the equilibrium equation (6.4) would be equivalent to the following form, which is the result found in Eringen [77] and Zhou [181-182] after a detailed analysis of the stress conditions across the crack face, expressed as:

$$\frac{\partial \sigma_{xx}}{\partial x} + \frac{\partial \sigma_{xy}}{\partial y} = 0, \quad \frac{\partial \sigma_{xy}}{\partial x} + \frac{\partial \sigma_{yy}}{\partial y} = 0 \quad (6.10)$$

For concision, defining the following dimensionless variables,

$$\begin{aligned} T^* &= \frac{T}{q_\infty c / \kappa_0}, \quad (x, y, a)^* = \frac{(x, y, a)}{c}, \quad (\sigma_{ij}, t_{ij})^* = \frac{(\sigma_{ij}, t_{ij})}{\mu_0 \alpha_{T0} q_\infty c / \kappa_0}, \\ (u, v)^* &= \frac{(u, v)}{\alpha_{T0} q_\infty c^2 / \kappa_0}, \quad (\beta, \delta, \gamma)^* = (\beta, \delta, \gamma) \cdot c \end{aligned} \quad (6.11)$$

Considering the nonhomogeneity in FGM coating, then the Eq. (6.6) and Eq. (6.8) are simplified as:

$$\left\{ \begin{array}{l} \sigma_{xx} = \frac{e^{\beta y}}{k-1} \left[ (k+1) \frac{\partial u}{\partial x} + (3-k) \frac{\partial v}{\partial y} - 4k_\alpha e^{\gamma y} T \right] \\ \sigma_{yy} = \frac{e^{\beta y}}{k-1} \left[ (k+1) \frac{\partial v}{\partial y} + (3-k) \frac{\partial u}{\partial x} - 4k_\alpha e^{\gamma y} T \right] \\ \sigma_{xy} = e^{\beta y} \left[ \frac{\partial u}{\partial y} + \frac{\partial v}{\partial x} \right] \end{array} \right. \quad y > 0 \quad (6.12)$$

$$\begin{cases} \sigma_{xx} = \frac{1}{k-1} [(k+1) \frac{\partial u}{\partial x} + (3-k) \frac{\partial v}{\partial y} - 4k_\alpha T] \\ \sigma_{yy} = \frac{1}{k-1} [(k+1) \frac{\partial v}{\partial y} + (3-k) \frac{\partial u}{\partial x} - 4k_\alpha T] \\ \sigma_{xy} = \frac{\partial u}{\partial y} + \frac{\partial v}{\partial x} \end{cases} \quad y < 0 \quad (6.13)$$

$$\alpha(|x-x'|, |y-y'|) = \frac{1}{\pi} \left(\frac{\eta}{a}\right)^2 \exp\left\{-\left(\frac{\eta}{a}\right)^2 [(x-x')^2 + (y-y')^2]\right\} \quad (6.14)$$

Here and after, asterisk “\*” of the variables is neglected for simplicity. Substituting Eqs. (6.12-6.13) into Eq. (6.10), the dimensionless governing equations for the thermal stress field are expressed as:

$$\begin{aligned} (k+1) \frac{\partial^2 u}{\partial x^2} + (k-1) \frac{\partial^2 u}{\partial y^2} + 2 \frac{\partial^2 v}{\partial x \partial y} + \beta(k-1) \left( \frac{\partial u}{\partial y} + \frac{\partial v}{\partial x} \right) &= 4e^{\gamma y} \frac{\partial T}{\partial x} \\ (k-1) \frac{\partial^2 v}{\partial x^2} + (k+1) \frac{\partial^2 v}{\partial y^2} + 2 \frac{\partial^2 u}{\partial x \partial y} + \beta(3-k) \frac{\partial u}{\partial x} + \beta(k+1) \frac{\partial v}{\partial y} &= 4e^{\gamma y} [(\beta + \gamma)T + \frac{\partial T}{\partial y}] \end{aligned} \quad y > 0 \quad (6.15)$$

$$\begin{aligned} (k+1) \frac{\partial^2 u}{\partial x^2} + (k-1) \frac{\partial^2 u}{\partial y^2} + 2 \frac{\partial^2 v}{\partial x \partial y} &= 4 \frac{\partial T}{\partial x} \\ (k-1) \frac{\partial^2 v}{\partial x^2} + (k+1) \frac{\partial^2 v}{\partial y^2} + 2 \frac{\partial^2 u}{\partial x \partial y} &= 4 \frac{\partial T}{\partial y} \end{aligned} \quad y < 0 \quad (6.16)$$

The corresponding dimensionless thermal-mechanical boundary conditions are:

$$\begin{aligned} e^{\delta y} \frac{\partial T}{\partial y} &= 1, & (y \rightarrow +\infty) \\ \frac{\partial T}{\partial y} &= 1, & (y \rightarrow -\infty) \\ \frac{\partial T}{\partial y} &= k^*, & (y = 0, |x| \leq 1) \\ T(x, 0^+) &= T(x, 0^-), & (|x| > 1) \\ \frac{\partial T(x, 0^+)}{\partial y} &= \frac{\partial T(x, 0^-)}{\partial y}, & (|x| > 1) \end{aligned} \quad (6.17)$$

$$\begin{aligned}
t_{xy}(x, \infty) &= t_{yy}(x, \infty) = 0 \\
t_{xy}(x, 0) &= t_{yy}(x, 0) = 0, \quad (|x| \leq 1) \\
t_{xy}(x, 0^+) &= t_{xy}(x, 0^-), \quad (|x| > 1) \\
t_{yy}(x, 0^+) &= t_{yy}(x, 0^-), \quad (|x| > 1) \\
u(x, 0^+) &= u(x, 0^-), \quad (|x| > 1) \\
v(x, 0^+) &= v(x, 0^-), \quad (|x| > 1)
\end{aligned} \tag{6.18}$$

## 6.3 Solution procedures

### 6.3.1 Solutions of temperature field

Considering the nonhomogeneity in thermal conductivity, the governing equations of heat conduction become:

$$\begin{aligned}
\nabla^2 T + \delta \frac{\partial T}{\partial y} &= 0, \quad y > 0 \\
\nabla^2 T &= 0, \quad y < 0
\end{aligned} \tag{6.19}$$

Fourier transform is applied to transform the above PDEs to the following form:

$$\begin{aligned}
\frac{d^2 T}{dy^2} + \delta \frac{dT}{dy} + (-i\xi)^2 T &= 0, \quad y > 0 \\
\frac{d^2 T}{dy^2} + (-i\xi)^2 T &= 0, \quad y < 0
\end{aligned} \tag{6.20}$$

In which  $\xi$  is the Fourier transform variable. Considering the thermal boundary conditions, the solutions are obtained as:

$$\begin{aligned}
T(x, y) &= \int_{-\infty}^{\infty} C_1(\xi) \exp(m_1 y - ix\xi) d\xi + (1 - e^{-\delta y}) / \delta, \quad y > 0 \\
T(x, y) &= \int_{-\infty}^{\infty} C_2(\xi) \exp(m_2 y - ix\xi) d\xi + y, \quad y < 0
\end{aligned} \tag{6.21}$$

where  $m_1 = \frac{-\delta - \sqrt{\delta^2 + 4\xi^2}}{2}$ ,  $m_2 = |\xi|$ ,  $C_2(\xi) = \frac{m_1}{m_2} C_1(\xi)$ . In order to determine the unknown term

$C_1(\xi)$ , introduce a temperature jump density function:

$$\phi(x) = \frac{\partial T(x, 0^+)}{\partial x} - \frac{\partial T(x, 0^-)}{\partial x} \quad (6.22)$$

With the help of thermal boundary conditions on the crack ( $y = 0$ ) and its extension along  $x$ -axis, we have:

$$\int_{-1}^1 \phi(x) dx = 0 \quad (6.23)$$

$$\phi(x) = 0, \quad (|x| > 1) \quad (6.24)$$

Substituting Eq. (6.21) into Eq. (6.22), after performing inverse Fourier transform, we have:

$$C_1(\xi) = \frac{im_2}{2\pi\xi(m_2 - m_1)} \int_{-1}^1 \phi(\tau) \exp(i\xi\tau) d\tau \quad (6.25)$$

Finally, the partially thermal insulation of the interface crack leads to the following singular integral equation:

$$\int_{-1}^1 \phi(\tau) \left[ \frac{1}{\tau - x} + K(x, \tau) \right] d\tau = 2\pi(k^* - 1), \quad |x| \leq 1 \quad (6.26)$$

where the kernel function is:

$$K(x, \tau) = \int_0^\infty \left( 1 + \frac{2m_1 m_2}{\xi(m_2 - m_1)} \right) \sin[\xi(x - \tau)] d\xi \quad (6.27)$$

The Lobatto–Chebyshev numerical integral technique is employed to convert the integral equations (6.23) and (6.26) to the following algebraic equations:

$$\sum_{k=1}^n \frac{1}{n} F(\tau_k) \left[ \frac{1}{\tau_k - x_r} + K(x_r, \tau_k) \right] = 2\pi(k^* - 1), \quad |x| \leq 1 \quad (6.28)$$

$$\sum_{k=1}^n \frac{\pi}{n} F(\tau_k) = 0 \quad (6.29)$$

where  $\tau_k = \cos \frac{(2k-1)\pi}{2n}$ ,  $k=1, 2, \dots, n$ ;  $x_r = \cos \frac{r\pi}{n}$ ,  $r=1, 2, \dots, n-1$ ;  $F(x) = \frac{\phi(x)}{\sqrt{1-x^2}}$ .

Once the above algebraic equations are solved, the temperature field can be obtained numerically by incorporating Eq. (6.21) and (6.25) and evaluating the infinite integrals.

### 6.3.2 Solutions of the thermal stress field

Employing Fourier transform, the governing PDE (6.15-6.16) is converted to:

$$\begin{aligned} (k-1) \frac{d^2 u}{dy^2} - 2i\xi \frac{dv}{dy} + \beta(k-1) \frac{du}{dy} - (k+1)\xi^2 u - \beta(k-1)i\xi v &= -4e^{\gamma y} (i\xi)T \\ (k+1) \frac{d^2 v}{dy^2} - 2i\xi \frac{du}{dy} + \beta(k+1) \frac{dv}{dy} - \beta(3-k)i\xi u - (k-1)\xi^2 v &= 4e^{\gamma y} [(\beta + \gamma)T + \frac{\partial T}{\partial y}] \end{aligned} \quad y > 0 \quad (6.30)$$

$$\begin{aligned} (k-1) \frac{d^2 u}{dy^2} - 2i\xi \frac{dv}{dy} - (k+1)\xi^2 u &= -4i\xi T \\ (k+1) \frac{d^2 v}{dy^2} - 2i\xi \frac{du}{dy} - (k-1)\xi^2 v &= 4 \frac{\partial T}{\partial y} \end{aligned} \quad y < 0 \quad (6.31)$$

The general solution of above PDEs subjecting to the regular condition at infinity shows as:

$$\begin{cases} u(x, y) = \int_{-\infty}^{\infty} \left[ \sum_{i=1}^2 A_i(\xi) e^{\lambda_i y} + \omega_1(\xi) e^{(\gamma+m_1)y} \right] e^{-ix\xi} d\xi \\ v(x, y) = \int_{-\infty}^{\infty} \left[ \sum_{i=1}^2 B_i(\xi) A_i(\xi) e^{\lambda_i y} + \omega_2(\xi) e^{(\gamma+m_1)y} \right] e^{-ix\xi} d\xi \end{cases} \quad y > 0 \quad (6.32)$$

$$\begin{cases} u(x, y) = \int_{-\infty}^{\infty} \left[ (A_3(\xi) + A_4(\xi)y) e^{m_2 y} + \omega_3(\xi) e^{m_2 y} \right] e^{-ix\xi} d\xi \\ v(x, y) = \int_{-\infty}^{\infty} \left[ (B_3(\xi) + B_4(\xi)y) e^{m_2 y} + \omega_4(\xi) e^{m_2 y} \right] e^{-ix\xi} d\xi \end{cases} \quad y < 0 \quad (6.33)$$

where  $A_i(\xi)$ ,  $B_i(\xi)$ ,  $\omega_i(\xi)$  ( $i=1, 2, 3, 4$ ) are unknown functions to be determined, and  $\lambda_i$  ( $i=1, 2$ ) are the two negative roots of the characteristic equation. Substituting Eq. (6.32) into (6.30), we have:

$$\lambda^4 + 2\beta\lambda^3 + (\beta^2 - 2\xi^2)\lambda^2 - 2\beta\xi^2\lambda + (\xi^4 + \xi^2\beta^2\frac{3-k}{1+k}) = 0 \quad (6.34)$$

$$\lambda_1 = \frac{1}{2} \left( -\beta - \sqrt{\beta^2 + 4\xi^2 + 4i\xi\beta\sqrt{\frac{3-k}{k+1}}} \right), \lambda_2 = \frac{1}{2} \left( -\beta - \sqrt{\beta^2 + 4\xi^2 - 4i\xi\beta\sqrt{\frac{3-k}{k+1}}} \right) \quad (6.35)$$

And

$$B_i(\xi) = \frac{(k-1)\lambda_i^2 + \beta(k-1)\lambda_i - \xi^2(k+1)}{i\xi[2\lambda_i + \beta(k-1)]}, \quad i=1,2 \quad (6.36)$$

Substitute Eq. (6.33) into Eq. (6.31), the following characteristic equation is obtained:

$$\lambda^4 - 2\xi^2\lambda^2 + \xi^4 = 0 \quad (6.37)$$

whose dual roots are  $\pm|\xi|$ . Considering the regular condition at infinity, the positive dual root  $m_2 = |\xi|$  is selected here. In addition, there is:

$$\begin{aligned} B_3(\xi) &= \frac{i|\xi|}{\xi} A_3(\xi) + \frac{k}{i\xi} A_4(\xi) \\ B_4(\xi) &= \frac{i|\xi|}{\xi} A_4(\xi) \end{aligned} \quad (6.38)$$

In which  $\omega_i(\xi)$  can be determined by the particular  $(\xi)$  solution accompanied by the temperature field as shown in Eq. (6.21), expressed as:

$$\begin{aligned} \omega_1(\xi) &= \frac{4(a_2\beta + a_2n_1 + ia_4\xi)}{a_2a_3 - a_1a_4} C_1(\xi) \\ \omega_2(\xi) &= -\frac{4(a_1\beta + a_1n_1 + ia_3\xi)}{a_2a_3 - a_1a_4} C_1(\xi) \\ \omega_3(\xi) &= \frac{2i}{\xi} C_2(\xi) \\ \omega_4(\xi) &= 0 \end{aligned} \quad (6.39)$$

where  $n_1 = \gamma + m_1$  and  $a_i(\xi)$  ( $i=1,2,3,4$ ) are shown in the Appendix. With the help of the constitutive equations, the local thermal stresses can be obtained as:

$$\begin{aligned}\sigma_{yy} &= \frac{e^{\beta y}}{k-1} \int_{-\infty}^{\infty} \left( \sum_{i=1}^2 g_i A_i e^{\lambda_i y} + h_1 e^{n_1 y} \right) e^{-ix\xi} d\xi \\ \sigma_{xy} &= e^{\beta y} \int_{-\infty}^{\infty} \left( \sum_{i=1}^2 q_i A_i e^{\lambda_i y} + h_2 e^{n_1 y} \right) e^{-ix\xi} d\xi\end{aligned}\quad y > 0 \quad (6.40)$$

$$\begin{aligned}\sigma_{yy} &= \frac{e^{m_2 y}}{k-1} \int_{-\infty}^{\infty} (g_{11} A_3 + g_{12} A_4 + g_{13} + g_{11} A_4 y) e^{-ix\xi} d\xi \\ \sigma_{xy} &= e^{m_2 y} \int_{-\infty}^{\infty} (g_{21} A_3 + g_{22} A_4 + g_{23} + g_{21} A_4 y) e^{-ix\xi} d\xi\end{aligned}\quad y < 0 \quad (6.41)$$

where  $q_i, g_i, g_{ij}$  are shown in the Appendix. Thus far,  $A_i(\xi)$  ( $i=1,2,3,4$ ) are the unknown functions, which can be determined from the mechanical boundary conditions. To solve the present problem, the jumps of displacements across the crack surfaces are introduced as the function of coordinate  $x$ :

$$\begin{aligned}f_1(x) &= u(x, 0^+) - u(x, 0^-) \\ f_2(x) &= v(x, 0^+) - v(x, 0^-)\end{aligned}\quad (6.42)$$

Applying the Fourier transform to the above equations and using the boundary conditions, one can have:

$$\begin{pmatrix} 1 & 1 & -1 & 0 \\ B_1 & B_2 & -\tau_1 & -\tau_2 \\ g_1 & g_2 & -g_{11} & -g_{12} \\ q_1 & q_2 & -g_{21} & -g_{22} \end{pmatrix} \begin{pmatrix} A_1 \\ A_2 \\ A_3 \\ A_4 \end{pmatrix} = \begin{pmatrix} f_1 + G_1 \\ f_2 + G_2 \\ G_3 \\ G_4 \end{pmatrix}\quad (6.43)$$

where the unknown terms  $\tau_1, \tau_2, G_1, G_2, G_3, G_4$  are shown in the Appendix. From the integral form of nonlocal stresses Eq. (6.14), we have:

$$\begin{aligned}t_{yy}(x, y) &= \int_0^{\infty} \left[ \int_{-\infty}^{\infty} \alpha(|x-x'|, |y-y'|) \sigma_{yy}(x', y') dy' \right] + \int_{-\infty}^0 \left[ \int_{-\infty}^{\infty} \alpha(|x-x'|, |y-y'|) \sigma_{yy}(x', y') dy' \right] \\ t_{xy}(x, y) &= \int_0^{\infty} \left[ \int_{-\infty}^{\infty} \alpha(|x-x'|, |y-y'|) \sigma_{xy}(x', y') dy' \right] + \int_{-\infty}^0 \left[ \int_{-\infty}^{\infty} \alpha(|x-x'|, |y-y'|) \sigma_{xy}(x', y') dy' \right]\end{aligned}\quad (6.44)$$

Using the following relations [77]:

$$\int_{-\infty}^{\infty} \exp(-px'^2) \begin{Bmatrix} \sin[\xi(x+x')] \\ \cos[\xi(x+x')] \end{Bmatrix} dx' = \sqrt{\frac{\pi}{p}} \exp(-\xi^2/4p) \begin{Bmatrix} \sin(\xi x) \\ \cos(\xi x) \end{Bmatrix} \quad (6.45)$$

$$\int_0^{\infty} \exp(-py'^2 - \gamma y') dy' = \frac{1}{2} \sqrt{\frac{\pi}{p}} \exp(\gamma^2/4p) [1 - \Phi(\gamma/2\sqrt{p})] \quad (6.46)$$

In which  $\Phi(z)$  is the error function, defined as:

$$\Phi(z) = \frac{2}{\sqrt{\pi}} \int_0^z \exp(-t^2) dt \quad (6.47)$$

Then the nonlocal stress components can then be derived as:

$$\begin{aligned} t_{yy} &= \frac{1}{k-1} \int_{-\infty}^{\infty} \left( \sum_{i=1}^2 g_i A_i d_i + h_1 e_1 + (g_{11} A_3 + g_{12} A_4 + g_{13}) N_1 + g_{11} A_4 N_2 \right) e^{-ix\xi} d\xi \\ t_{xy} &= \int_{-\infty}^{\infty} \left( \sum_{i=1}^2 q_i A_i d_i + h_2 e_1 + (g_{21} A_3 + g_{22} A_4 + g_{23}) N_1 + g_{21} A_4 N_2 \right) e^{-ix\xi} d\xi \end{aligned} \quad (6.48)$$

where

$$\begin{aligned} e_1(\xi, y) &= \frac{1}{2} e^{\frac{(n_1+\beta)^2}{4p}} e^{(n_1+\beta)y} [1 - \Phi(\frac{-n_1 - \beta - 2py}{2\sqrt{p}})] e^{-\frac{\xi^2}{4p}} \\ d_i(\xi, y) &= \frac{1}{2} e^{\frac{(\lambda_i+\beta)^2}{4p}} e^{(\lambda_i+\beta)y} [1 - \Phi(\frac{-\lambda_i - \beta - 2py}{2\sqrt{p}})] e^{-\frac{\xi^2}{4p}} \quad (i=1,2) \\ N_1 &= \frac{1}{2} e^{m_2 y} [1 - \Phi(\frac{m_2 + 2py}{2\sqrt{p}})] \\ N_2 &= \frac{m_2 + 2py}{4p} e^{m_2 y} [1 - \Phi(\frac{m_2 + 2py}{2\sqrt{p}})] - e^{-py^2} \frac{1}{2p} \sqrt{\frac{p}{\pi}} e^{-\xi^2/4p} \\ p &= \left(\frac{\eta}{a}\right)^2 \end{aligned}$$

Until now, the only unknown functions are  $f_1(\xi), f_2(\xi)$ . Substituting the nonlocal stresses into the remaining boundary conditions on crack faces, “ $t_{xy}(x, 0) = t_{yy}(x, 0) = 0, (|x| \leq 1)$ ”, then the problem finally is reduced to two pairs of dual integral equations:

$$\int_{-\infty}^{\infty} (Q_1(\xi)f_1(\xi) + Q_2(\xi)f_2(\xi)) e^{-ix\xi} d\xi = - \int_{-\infty}^{\infty} Q_3(\xi)e^{-ix\xi} d\xi, \quad |x| < 1$$

$$\int_{-\infty}^{\infty} (Q_4(\xi)f_1(\xi) + Q_5(\xi)f_2(\xi)) e^{-ix\xi} d\xi = - \int_{-\infty}^{\infty} Q_6(\xi)e^{-ix\xi} d\xi, \quad |x| < 1$$
(6.49)

$$\int_{-\infty}^{\infty} f_1(\xi)e^{-i\xi x} d\xi = 0, \quad |x| > 1$$

$$\int_{-\infty}^{\infty} f_2(\xi)e^{-i\xi x} d\xi = 0, \quad |x| > 1$$
(6.50)

where

$$\begin{aligned} Q_1(\xi) &= g_1 d_{10} s_{11} + g_2 d_{20} s_{21} + g_{11} N_{10} s_{31} + (g_{12} N_{10} + g_{11} N_{20}) s_{41} \\ Q_2(\xi) &= g_1 d_{10} s_{12} + g_2 d_{20} s_{22} + g_{11} N_{10} s_{32} + (g_{12} N_{10} + g_{11} N_{20}) s_{42} \\ Q_3(\xi) &= g_{13} N_{10} + h_1 e_{10} + g_1 d_{10} s_{13} + g_2 d_{20} s_{23} + g_{11} N_{10} s_{33} + (g_{12} N_{10} + g_{11} N_{20}) s_{43} \\ Q_4(\xi) &= q_1 d_{10} s_{11} + q_2 d_{20} s_{21} + g_{21} N_{10} s_{31} + (g_{22} N_{10} + g_{21} N_{20}) s_{41} \\ Q_5(\xi) &= q_1 d_{10} s_{12} + q_2 d_{20} s_{22} + g_{21} N_{10} s_{32} + (g_{22} N_{10} + g_{21} N_{20}) s_{42} \\ Q_6(\xi) &= g_{23} N_{10} + h_2 e_{10} + q_1 d_{10} s_{13} + q_2 d_{20} s_{23} + g_{21} N_{10} s_{33} + (g_{22} N_{10} + g_{21} N_{20}) s_{43} \end{aligned}$$
(6.51)

where  $d_{10} = d_1(\xi, y = 0)$ ,  $d_{20} = d_2(\xi, y = 0)$ ,  $e_{10} = e_1(\xi, y = 0)$  and the remaining  $s_{ij}$  are shown in the Appendix. The unknown two functions  $f_1(\xi)$ ,  $f_2(\xi)$  can be obtained after solving the above two pairs of dual integral equations. However, as discussed by Eringen [72], for this kind of problem, the dual integral equations cannot be transformed to a Fredholm integral equation of the second kind. In this paper, the Schmidt method [181-182] is employed to solve the integral equations. The jumps of displacements are expressed by a series of Jacobi polynomials:

$$\begin{aligned} f_1(x) &= \sum_{i=0}^{\infty} a_n P_n^{(\frac{1}{2}, \frac{1}{2})}(x) \cdot (1-x^2)^{\frac{1}{2}}, \quad |x| < 1 \\ f_1(x) &= 0, \quad |x| > 1 \\ f_2(x) &= \sum_{i=0}^{\infty} b_n P_n^{(\frac{1}{2}, \frac{1}{2})}(x) \cdot (1-x^2)^{\frac{1}{2}}, \quad |x| < 1 \\ f_2(x) &= 0, \quad |x| > 1 \end{aligned}$$
(6.52)

where  $a_n, b_n$  are unknown coefficients and  $P_n^{(\frac{1}{2})}(x)$  is the Jacobian polynomial. By Fourier transform, there are:

$$f_1(\xi) = \sum_{i=0}^{\infty} a_n M_n J_{n+1}(\xi) / \xi, \quad f_2(\xi) = \sum_{i=0}^{\infty} b_n M_n J_{n+1}(\xi) / \xi$$

$$M_n = \frac{i^n}{\sqrt{\pi}} \frac{\Gamma(n+1+\frac{1}{2})}{n!} \quad (6.53)$$

where  $J_n(\xi), \Gamma(n)$  are the Bessel and Gamma functions, respectively. Substitution above equations into Eq. (6.49-6.50), we find that Eq. (6.50) is automatically satisfied. while Eq. (6.49) gives:

$$\sum_{n=0}^{\infty} a_n E_n(x) + \sum_{n=0}^{\infty} b_n F_n(x) = U(x), \quad |x| < 1 \quad (6.54)$$

$$\sum_{n=0}^{\infty} a_n G_n(x) + \sum_{n=0}^{\infty} b_n H_n(x) = V(x), \quad |x| < 1 \quad (6.55)$$

where

$$E_n(x) = M_n \int_{-\infty}^{\infty} \left( \frac{Q_1(\xi)}{\xi} J_{n+1}(\xi) \right) e^{-ix\xi} d\xi, \quad F_n(x) = M_n \int_{-\infty}^{\infty} \left( \frac{Q_2(\xi)}{\xi} J_{n+1}(\xi) \right) e^{-ix\xi} d\xi$$

$$G_n(x) = M_n \int_{-\infty}^{\infty} \left( \frac{Q_4(\xi)}{\xi} J_{n+1}(\xi) \right) e^{-ix\xi} d\xi, \quad H_n(x) = M_n \int_{-\infty}^{\infty} \left( \frac{Q_5(\xi)}{\xi} J_{n+1}(\xi) \right) e^{-ix\xi} d\xi$$

$$U(x) = - \int_{-\infty}^{\infty} Q_3(\xi) e^{-ix\xi} d\xi, \quad V(x) = - \int_{-\infty}^{\infty} Q_6(\xi) e^{-ix\xi} d\xi$$

For a large  $\xi$ , the integrands in the above equations would decrease to zero, so the infinite integrations can be evaluated directly. Then the coefficients  $a_n, b_n$  can be determined by the Schmidt method. Introducing a set of orthogonal functions satisfying,

$$\int_{-1}^1 P_m(x) P_n(x) dx = N_n \delta_{nm}, \quad N_n = \int_{-1}^1 P_n^2(x) dx \quad (6.56)$$

which can be constructed from  $G_n(x)$  by:

$$P_n(x) = \sum_{i=0}^n \frac{M_{in}}{M_{nn}} G_i(x) \quad (6.57)$$

where  $M_{in}$  is the cofactor of the element  $d_{in}$  of the following determinant:

$$D_n = \begin{vmatrix} d_{00}, d_{01}, d_{02}, \dots, d_{0n} \\ d_{10}, d_{11}, d_{12}, \dots, d_{1n} \\ d_{20}, d_{21}, d_{22}, \dots, d_{2n} \\ \dots \\ \dots \\ \dots \\ d_{n1}, d_{n2}, d_{n3}, \dots, d_{nn} \end{vmatrix}, \quad d_{in} = \int_{-1}^1 G_i(x) G_n(x) dx \quad (6.58)$$

Then the Eq. (6.55) can be rewritten as:

$$\sum_{n=0}^{\infty} a_n G_n(x) = \sum_{n=0}^{\infty} c_n P_n(x) = V(x) - \sum_{n=0}^{\infty} b_n H_n(x) \quad (6.59)$$

where

$$a_n = \sum_{i=n}^{\infty} r_{ni} b_i + \delta_n \quad (6.60)$$

$$r_{ni} = -\sum_{j=n}^{\infty} \frac{M_{nj}}{N_j M_{jj-1}} \int_{-1}^1 H_i(x) P_j(x) dx, \quad \delta_n = \sum_{j=n}^{\infty} \frac{M_{nj}}{N_j M_{jj-1}} \int_{-1}^1 V(x) P_j(x) dx \quad (6.61)$$

Substituting the above equations into Eq. (6.49) yields:

$$\sum_{n=0}^{\infty} b_n Y_n(x) = W(x) \quad (6.62)$$

where

$$Y_n(x) = F_n(x) + \sum_{i=0}^{\infty} r_{in} E_i(x), \quad W(x) = U(x) - \sum_{i=0}^{\infty} \delta_i E_i(x) \quad (6.63)$$

Finally, the coefficients  $b_n$  can be determined as

$$b_n = \sum_{j=n}^{\infty} q_j \frac{L_{nj}}{L_{jj}} \quad (6.64)$$

where

$$q_j = \frac{1}{K_j} \int_{-1}^1 W(x) Q_j(x) dx, \quad Q_j(x) = \sum_{i=0}^{\infty} \frac{L_{ij}}{L_{jj}} Y_i(x), \quad K_j = \int_{-1}^1 Q_j^2(x) dx \quad (6.65)$$

and  $L_{ij}$  is the cofactor of the element  $e_{in}$  of the following determinant:

$$DD_n = \begin{vmatrix} e_{00}, e_{01}, e_{02}, \dots, e_{0n} \\ e_{10}, e_{11}, e_{12}, \dots, e_{1n} \\ e_{20}, e_{21}, e_{22}, \dots, e_{2n} \\ \dots \\ \dots \\ \dots \\ e_{n1}, e_{n2}, e_{n3}, \dots, e_{nn} \end{vmatrix}, \quad e_{ij} = \int_{-1}^1 Y_i(x) Y_j(x) dx \quad (6.66)$$

## 6.4 Numerical results and discussions

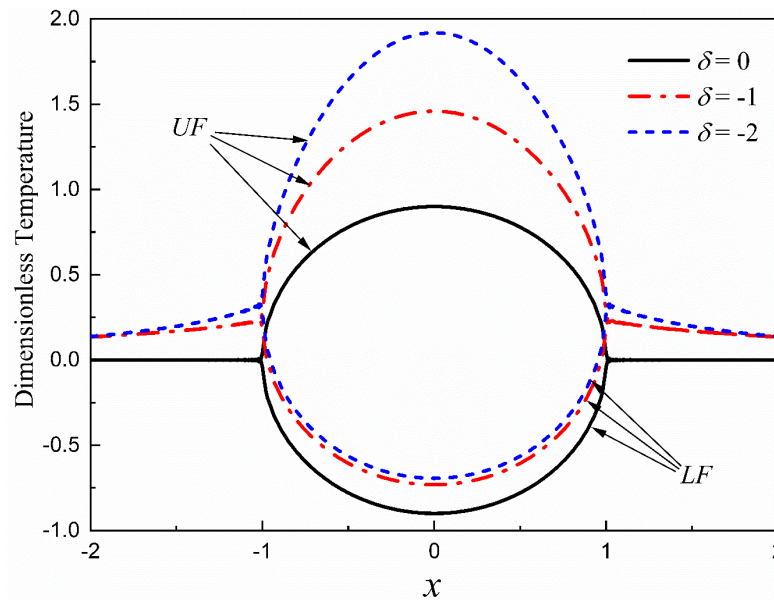


Figure 6.2 Dimensionless temperature distributions on crack faces and the extension line with the variation of nonhomogeneous parameter in thermal conductivity when  $k^*=0.1$ .

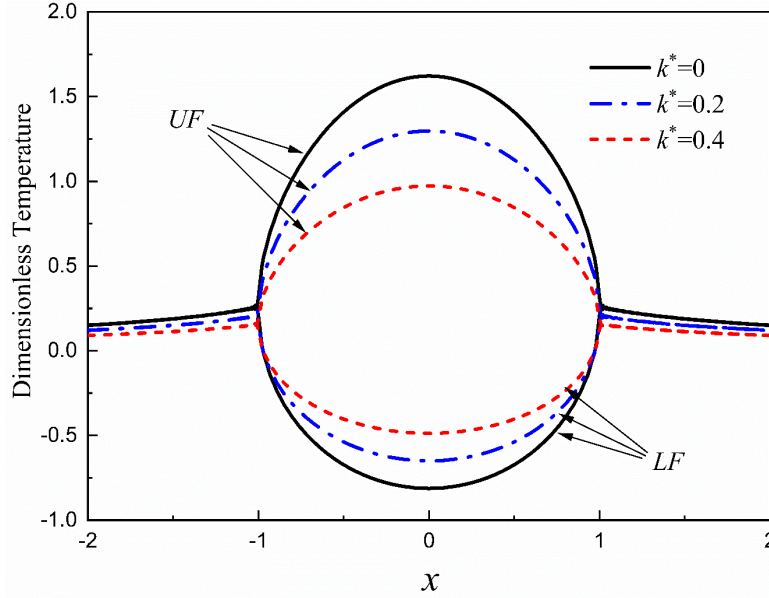


Figure 6.3 Dimensionless temperature distributions on crack faces and the extension line varied with partially insulations parameter when  $\delta = -1$ .

Serving as thermal barrier coatings, FGMs always are exposed the side of heat resistive ceramic to high temperature environment while another side of metallic materials is connected to the homogenous substrate so as to avoid the properties mismatch. Usually, material properties such as Young's modulus, thermal expansion coefficient and thermal conductivity of ceramics are lower than those of the metallic phase in FGMs, for example, Rene-41/Zirconia functionally graded composites [184]. Therefore, the nonhomogeneous parameters  $\beta, \delta, \gamma$  are selected as negative values in this article. The following numerical results are calculated for plane strain condition and Poisson's ratio is set to be 0.33. Due to the introduction of dimensionless variables, the crack locates between the interval  $[-1, 1]$ .

The temperature distributions are calculated using Eqs. (6.28) and (6.29) and displayed in Figures 6.2 and 6.3. Figure 6.2 shows the effect of nonhomogeneous parameter of thermal conductivity  $\delta$  on the temperature distributions along the crack line ( $y=0$ ), while Figure 6.3 gives out the influence of the partially insulating parameters  $k^*$ , where "UF" denotes the temperature on the upper crack face and "LF" refers to the lower crack face. The temperatures on the crack extension line (out of the interval  $[-1, 1]$ ) are continuous, satisfying the boundary conditions in Eq.

(6.17). Obviously, the temperature jump across the crack increases with increasing  $\delta$ . With the increase of the partially insulating parameters  $k^*$ , the temperature jumps decrease reasonably.

After solving the two pairs of dual integral equations, the coefficients  $a_n, b_n$  are known and the displacement jumps can thus be expressed by a series of the Jacobian polynomials. In fracture mechanics, the stresses along the crack line play a dominant role in determining the crack propagation. The thermal stresses can be obtained numerically by:

$$t_{yy} = \frac{1}{k-1} \left( \sum_{n=0}^{\infty} a_n E_n(x) + \sum_{n=0}^{\infty} b_n F_n(x) - U(x) \right) \quad (6.67)$$

$$t_{xy} = \sum_{n=0}^{\infty} a_n G_n(x) + \sum_{n=0}^{\infty} b_n H_n(x) - V(x) \quad (6.68)$$

Figures 6.4 and 6.5 illustrate the thermal stresses distribution along the crack extension line for two groups of arbitrarily selected parameters  $\chi, \beta, \delta, \gamma, k^*$  to examine the Schmidt method, where  $\chi = a / 2\eta c$  is the term from Eq. (6.8), whose values are found from reference [181-182]. The results show this numerical method performs effectively as the stresses between the interval  $[-1, 1]$  are very close to zero except minor numerical fluctuations, which is satisfying the boundary conditions on the crack faces. The existence of  $t_{xy}$  and  $t_{yy}$  confirm this interface crack problem between FGMs coating and homogenous substrate is equivalent to a mixed-mode fracture problem. The most valuable finding is that both thermal stresses  $t_{xy}$  and  $t_{yy}$  are finite values at the crack tips  $(-1, 0)$  and  $(1, 0)$ , which eliminates the stresses singularities in the classical, local analysis. Yielded from this nonlocal solution, the finite values of thermal stress around the crack tip allow us to build a more straightforward fracture criterion built on maximum stresses in assessing the risk of thermal fracture. For example, a fracture criterion can be built for the material stating that rupture will not occur before the maximum value of von Mises stress around the crack tip reaches the value of cohesive stress that holds the atomic bonds of lattice [181-182]. By substituting the displacement jumps into Eq. (6.48), Figure 6.6 displays the whole thermal stresses field distributions around the crack tip  $(1, 0)$ , where the parameters are the same as those used in Figure 5. Clearly, the peak values do not occur exactly at the crack tip but slightly away from it, which has been thoroughly

illustrated by Eringen. Due to the nonhomogeneous, graded properties in the  $y$  direction, the distribution of  $t_{yy}$  is not symmetric about the  $x$ -axis anymore.

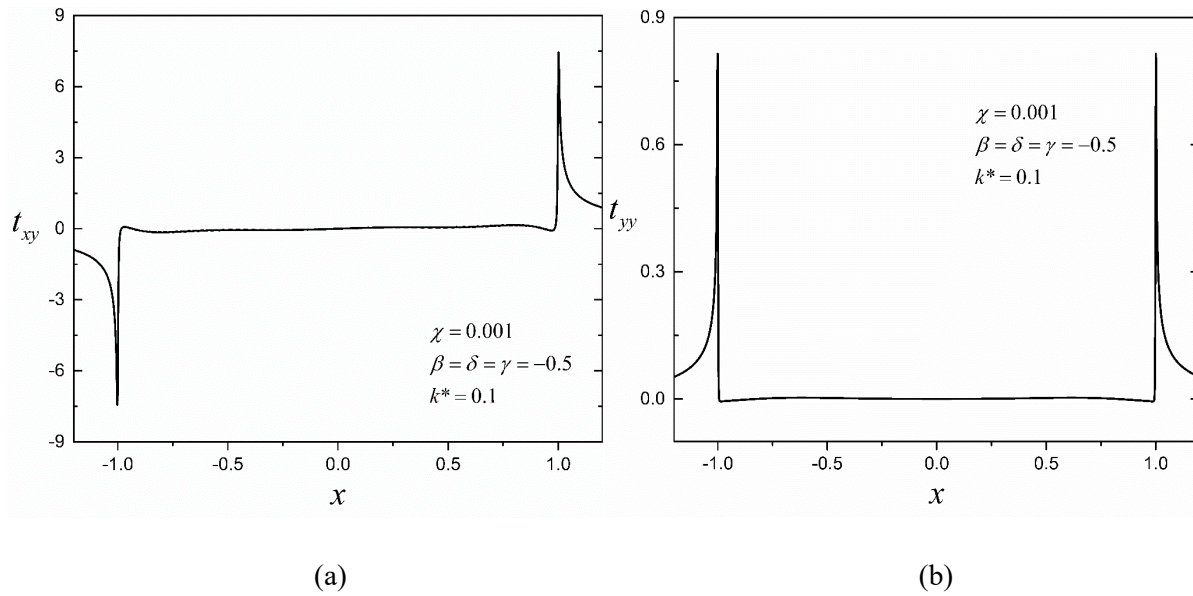


Figure 6.4 Dimensionless stresses: (a)  $t_{xy}$  (b)  $t_{yy}$  along crack faces and the extension line when  $\chi = 0.001$ ,  $\beta = \delta = \gamma = -0.5$ ,  $k^* = 0.1$ .

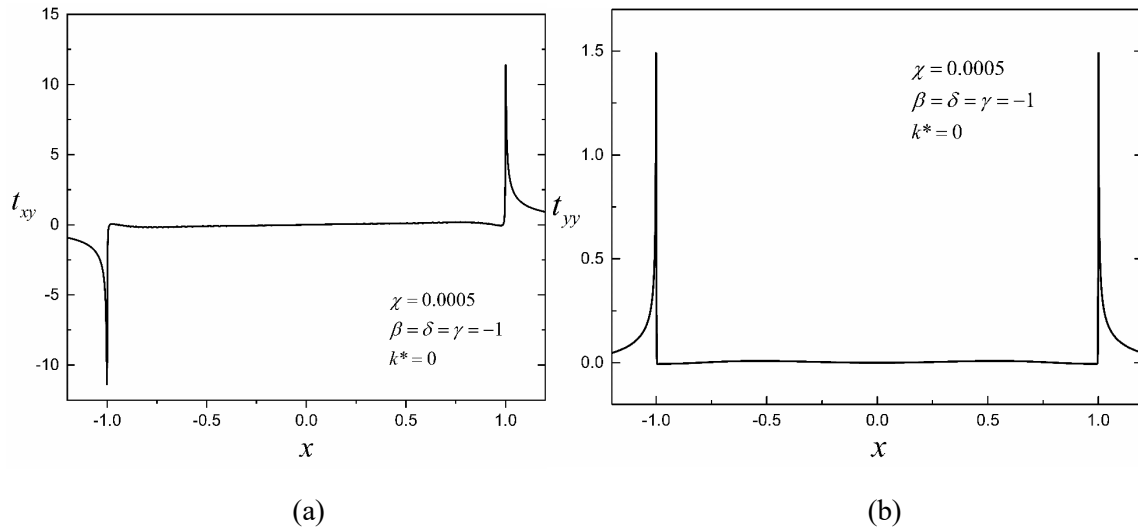


Figure 6.5 Dimensionless stresses: (a)  $t_{xy}$  (b)  $t_{yy}$  along crack faces and the extension line when  $\chi = 0.0005$ ,  $\beta = \delta = \gamma = -1$ ,  $k^* = 0$ .

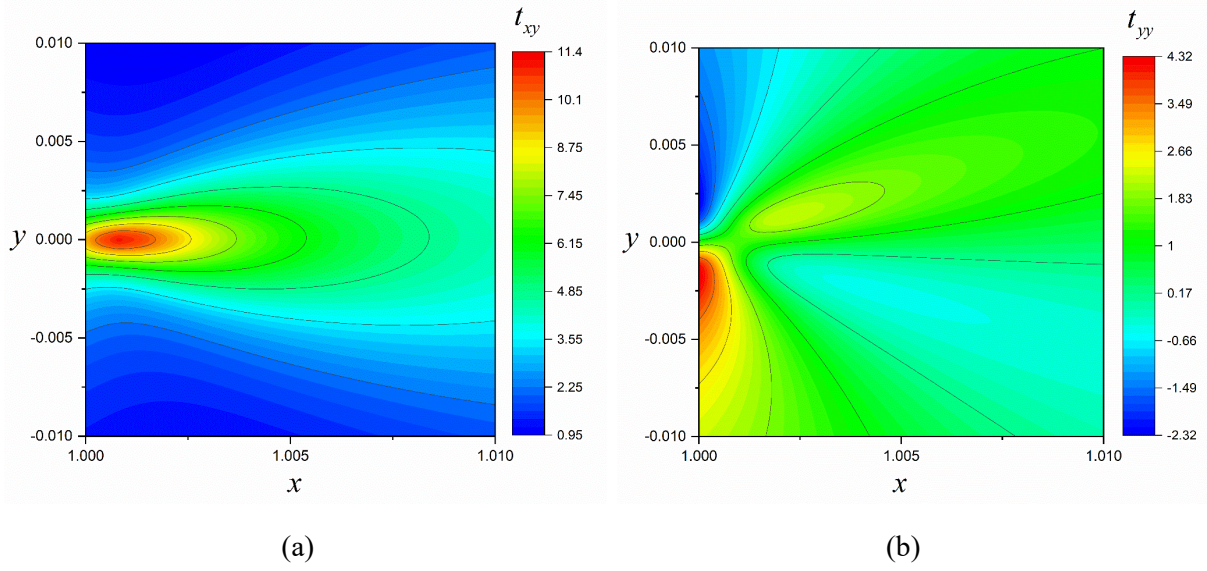


Figure 6.6 Dimensionless thermal stress distributions: (a)  $t_{xy}$  (b)  $t_{yy}$  around the crack tip (1,0) when  $\chi = 0.0005, \beta = \delta = \gamma = -1, k^* = 0$ .

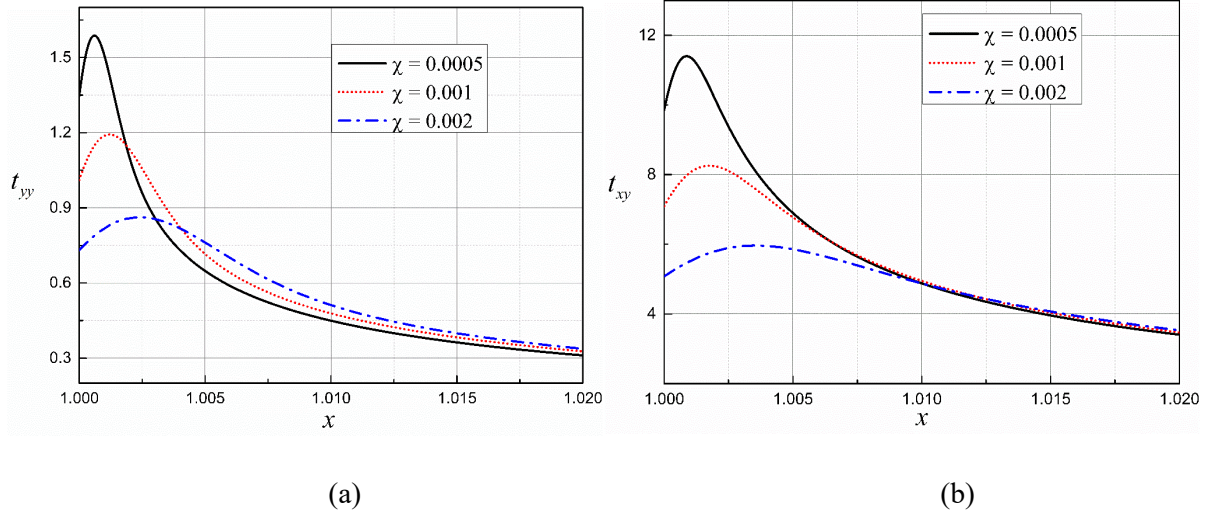


Figure 6.7 Dimensionless stress distributions (a)  $t_{xy}$  (b)  $t_{yy}$  along the crack line varied with nonlocal characteristic length

For a better understanding of the thermal fracture behavior concerning the size effect in the interface crack problem, how the material properties influence the peak values and the corresponding locations of thermal stress will be of vital importance. Figure 6.7 presents the stress distribution along the crack extension line influenced by the nonlocal characteristic length. The results show the nonlocal characteristic length plays a dominant role in determining the thermal stress field in the vicinity of the crack tip. With a decreasing nonlocal length, both the finite stress

on the crack tip and the peak values will increase, and the location of peak value moves towards the crack tip. When the characteristic length is reduced to zero, the results will reduce to the local results, where the peak value will be infinite and locates exactly on the crack tip. The nonlocal results reveal the finite thermal stress around the interface crack, and indicate the fracture risk would be much higher in systems with a smaller characteristic length, which should be the main concern in designing composite structures especially those adopted in NEMS with extremely small characteristic length. Figure 6.8 shows the influence of partially insulating parameter  $k^*$  on the thermal stresses. Obviously, with a higher ability to transfer heat across the crack, there will be less fracture risk, and moreover, this parameter has no influence on the locations of peak stress. Figures 6.9-6.11 give the effect of nonhomogeneity parameters  $\beta, \delta, \gamma$  on the thermomechanical

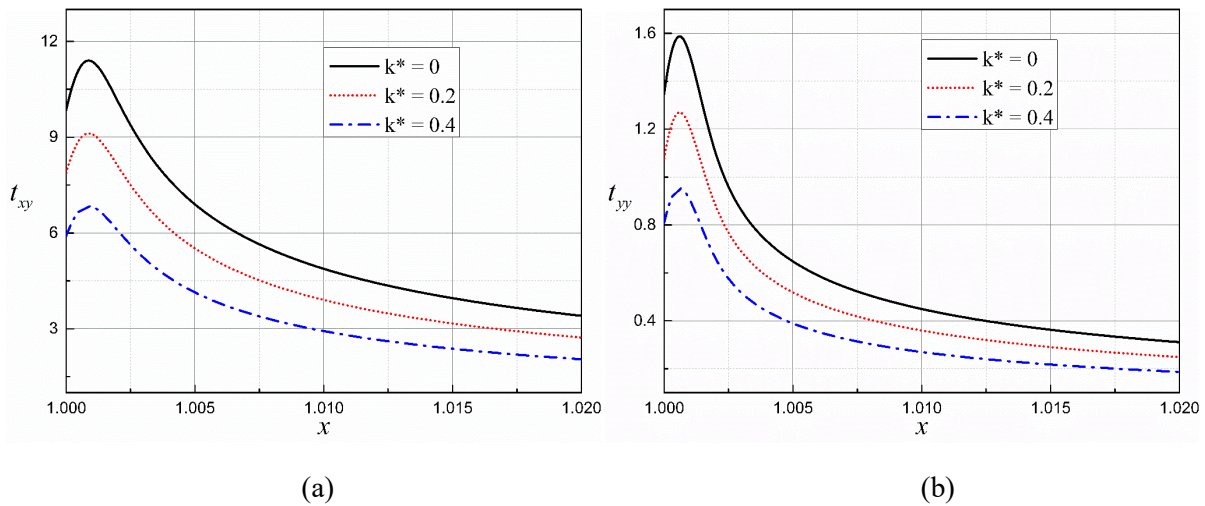


Figure 6.8 Dimensionless stress distributions (a)  $t_{xy}$  (b)  $t_{yy}$  along the crack line varied with partially insulations parameter

response. Basically the nonhomogeneity parameters will influence the thermal stress level significantly, such as the value at the crack tip and the peak values. However, their influence on the location of the peak value of stress is negligible. An interesting phenomenon is that the shear stresses are always much higher than the normal stresses, which means the in-plane shear is more likely to happen than tensile failure for the current problem. Detailed comparisons are conducted to demonstrate the relationships between peak values of thermal stress and the nonhomogeneity parameters, as shown in Figures 6.12-6.14. A higher value of  $\beta$  leads to a higher value of  $t_{xy}$  but

lower value of  $t_{yy}$ . With the increase of  $\delta$ , the peak value of  $t_{xy}$  increases but the peak value of  $t_{yy}$  decreases.  $\gamma$  exhibits a minor influence on the peak values of  $t_{yy}$ , but an increase of it will result in a significant increase of  $t_{xy}$ .

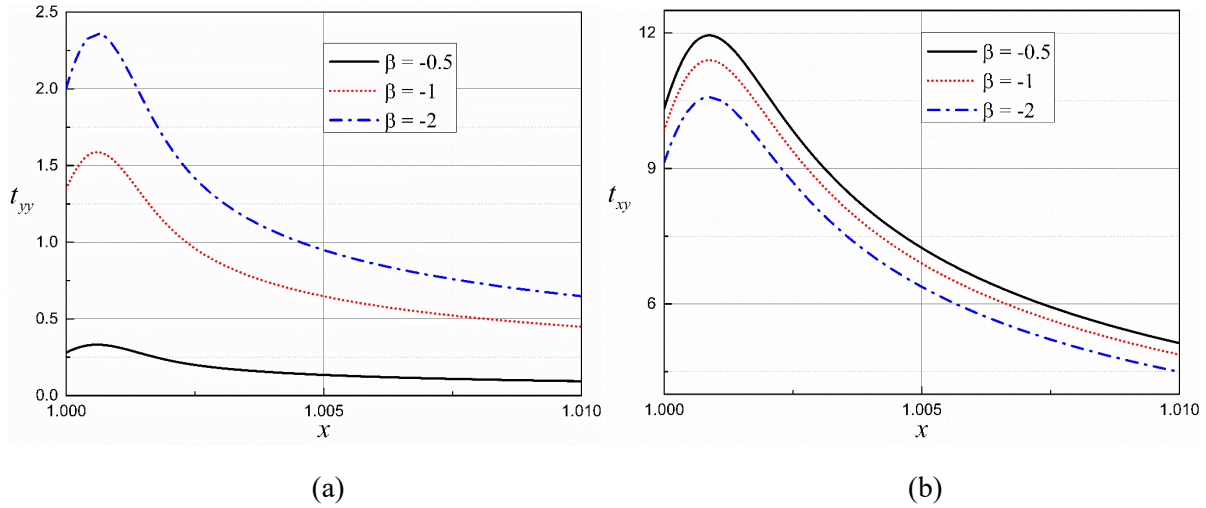


Figure 6.9 Dimensionless stress distributions (a)  $t_{xy}$  (b)  $t_{yy}$  along the crack line for different values of  $\beta$ .

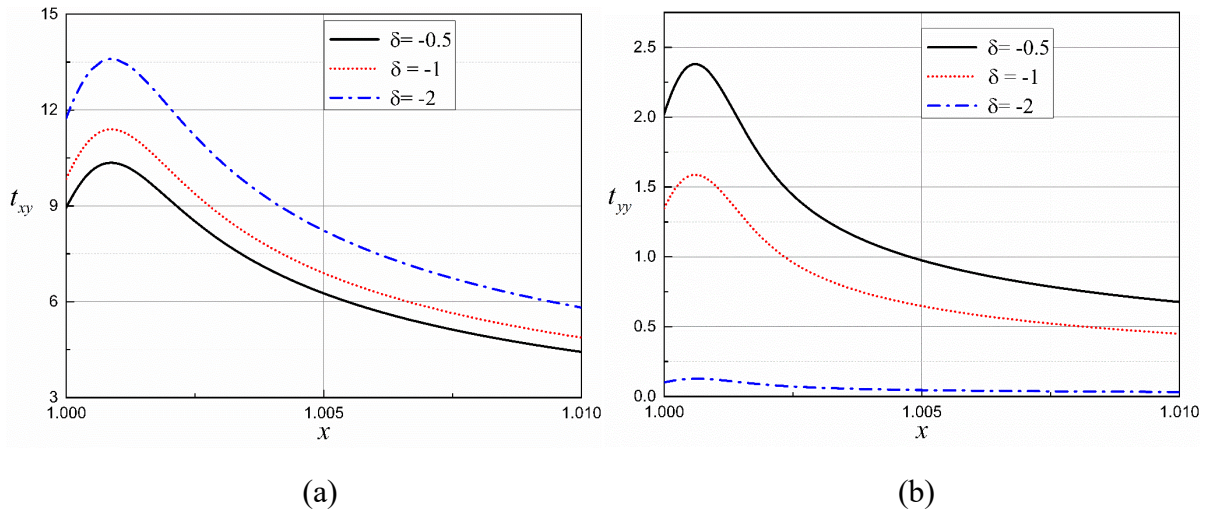


Figure 6.10 Dimensionless stress distributions (a)  $t_{xy}$  (b)  $t_{yy}$  along the crack line for different values of  $\delta$ .

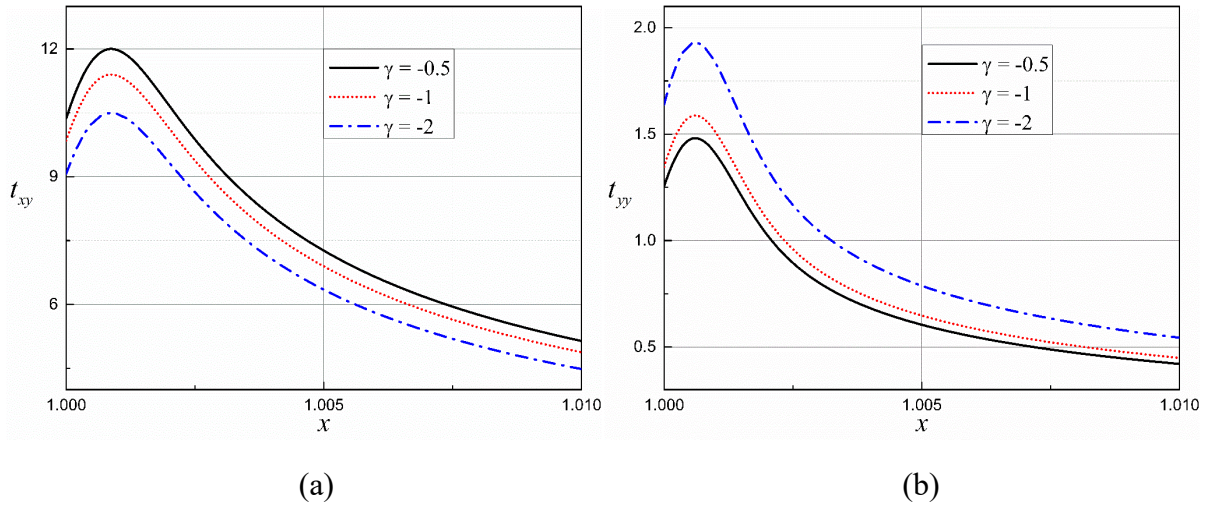


Figure 6.11 Dimensionless stress distributions (a)  $t_{xy}$  (b)  $t_{yy}$  along the crack line

for different values of  $\gamma$

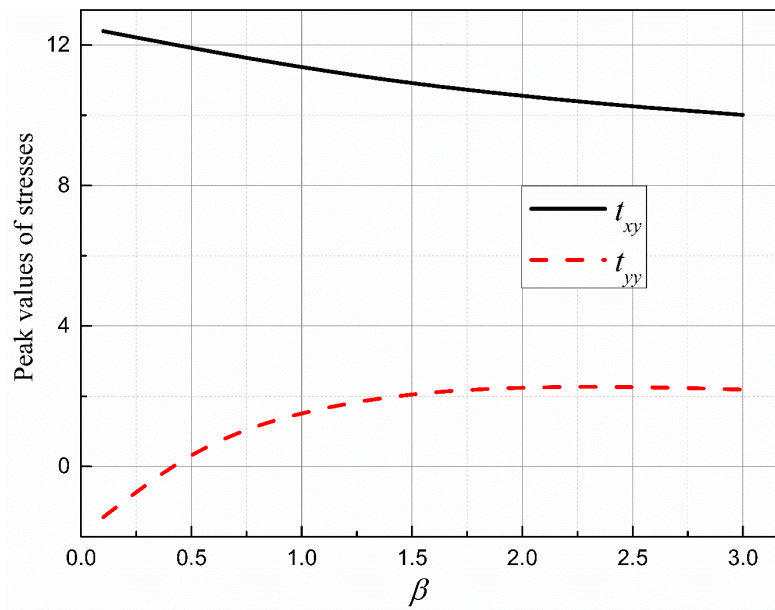


Figure 6.12 Peak values of the stresses along the crack line with the variation of  $\beta$ .

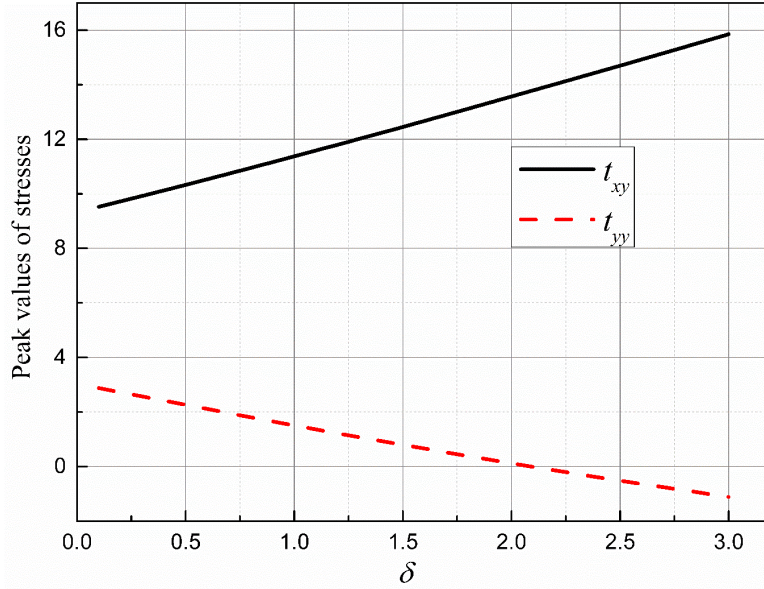


Figure 6.13 Peak values of the stresses along the crack line with the variation of  $\delta$ .

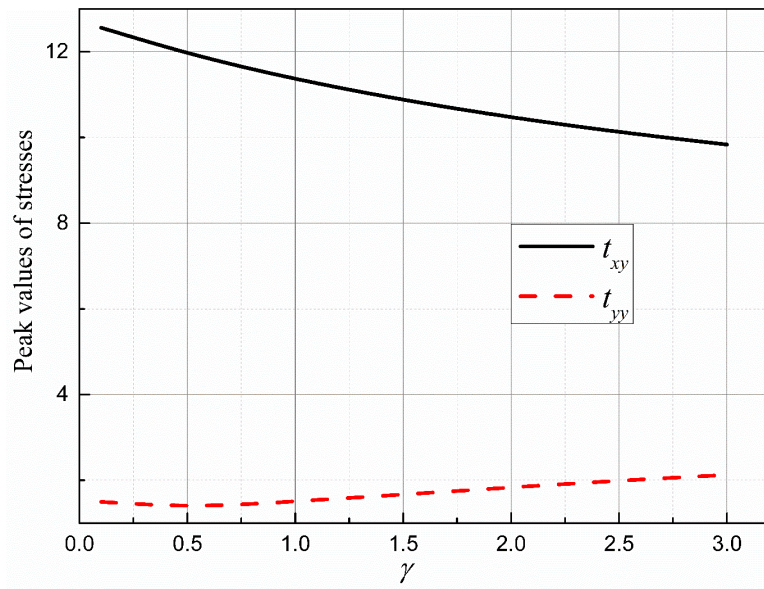


Figure 6.14 Peak values of the stresses along the crack line with the variation of  $\gamma$ .

## 6.5 Conclusions

In conclusion, the interface crack problem between a functionally graded coating and the homogenous substrate subject to remote heat flux is solved by nonlocal theory. The size effect is considered to remove the stress singularities at the crack tips. By utilizing the Fourier transform and the Schmidt method, the problem is solved numerically and finite stress distribution around

crack tips can then be displayed. Results show the nonlocal characteristic length is vitally important in eliminating the unreasonable infinite stresses at the crack tip yielded from the classical continuum analysis, and moreover, it determines the peak values and their locations. Parametric studies are conducted to investigate the influence of nonhomogeneous properties on the thermal fracture behavior of the interface crack.

## 6.6 Appendix

$$a_1(\xi) = (k-1)n_1^2 + \beta(k-1)n_1 - (k+1)\xi^2$$

$$a_2(\xi) = -2i\xi n_1 - i\xi\beta(k-1)$$

$$a_3(\xi) = -2i\xi n_1 - i\xi\beta(3-k)$$

$$a_4(\xi) = (k+1)n_1^2 + \beta(k+1)n_1 - (k-1)\xi^2$$

$$g_i = (k+1)\lambda_i B_i - i\xi(3-k), \quad (i=1,2)$$

$$q_i = \lambda_i - i\xi B_i, \quad (i=1,2)$$

$$h_1 = (k+1)n_1\omega_2 - i\xi(3-k)\omega_1 - 4k_\alpha C_1$$

$$h_2 = n_1\omega_1 - i\xi\omega_2$$

$$\tau_1 = i|\xi|/\xi, \tau_2 = -ik/\xi$$

$$g_{11} = (2k-2)i\xi, g_{12} = (k+1)(\tau_1 + m_2\tau_2),$$

$$g_{13} = -i\xi(3-k)w_3 - 4k_\alpha C_2$$

$$g_{21} = m_2 - i\xi\tau_1, g_{12} = 1 - i\xi\tau_2,$$

$$g_{13} = m_2 w_3.$$

$$G_1 = w_3 - w_1; G_2 = -w_2; G_3 = g_{13} - h_1; G_4 = g_{23} - h_2;$$

$$s_{11} = \frac{D_{11}}{D}, s_{12} = \frac{D_{21}}{D}, s_{21} = \frac{D_{12}}{D}, s_{22} = \frac{D_{22}}{D}$$

$$s_{31} = \frac{D_{13}}{D}, s_{32} = \frac{D_{23}}{D}, s_{41} = \frac{D_{14}}{D}, s_{42} = \frac{D_{24}}{D}$$

$$s_{13} = \frac{D_{11}}{D}G_1 + \frac{D_{21}}{D}G_2 + \frac{D_{31}}{D}G_3 + \frac{D_{41}}{D}G_4$$

$$s_{23} = \frac{D_{12}}{D}G_1 + \frac{D_{22}}{D}G_2 + \frac{D_{32}}{D}G_3 + \frac{D_{42}}{D}G_4$$

$$s_{33} = \frac{D_{13}}{D}G_1 + \frac{D_{23}}{D}G_2 + \frac{D_{33}}{D}G_3 + \frac{D_{43}}{D}G_4$$

$$s_{43} = \frac{D_{14}}{D}G_1 + \frac{D_{24}}{D}G_2 + \frac{D_{34}}{D}G_3 + \frac{D_{44}}{D}G_4$$

where  $D$  is determinant of the matrix in Eq. (36) and  $D_{ij}$  is the cofactor.

# Chapter 7: Conclusions and Future Perspectives

## 7.1 Conclusions

In order to overcome the drawbacks of classical thermoelasticity in thermal stress analysis of materials with time-dependent mechanical behavior or heterogeneity in microstructure under extreme thermal loading, non-classical thermomechanical analysis has been conducted for a series of non-classical, thermomechanical problems in this thesis. Nonlocal theory is combined with non-Fourier heat conduction theories to provide a comprehensive theoretical framework for the thermal stress analysis of advanced materials under extreme thermal loading. Through this work, major conclusions are summarized as follows.

- (1) Significant discrepancies of transient stresses intensity factors exist between functionally graded elastic and viscoelastic materials. Fracture occurs at a much earlier stage in viscoelastic FGMs under thermal shock than the elastic ones based on the predicted stress intensity factors. An increase in the gradient of thermal conductivity in viscoelastic FGMs can lower the thermal stresses and fracture risk.
- (2) Within the framework of the hyperbolic heat conduction model, the significant temperature overshooting and much higher transient SIFs are observed in FGMs. Designing structural components using the hyperbolic heat conduction model would be more viable and conservative.
- (3) By extending the fractional calculus to the DPL model, the time-fractional order model predicts a more reasonable temperature field by weakening the thermal wave propagation, leading to the removal of the unphysical fracture behavior and weakened oscillations in temperature history. The thermal penetration depth is larger and the temperature level is higher behind the crack but lower in front of the crack for a higher value of the lag ratio,  $\tau_T / \tau_q$ , between the phase lag of temperature gradient and heat flux.
- (4) The full extension of the nonlocal DPL model to the first order of the Taylor expansion is considered to account for the heat conduction at the nanoscale, which is verified

experimentally by the size-dependent thermal conductivity of silicon nanofilms [154-162] and the femtosecond laser heating of gold films [26]. The nonlocal DPL model predicts a faster thermal propagation speed, and the nonlocal characteristic length can remove the spatial jump in mechanical response. In addition, the nonlocal analysis predicts higher peak values of thermal stresses in viscoelastic media than the traditional DPL results.

- (5) Nonlocal theory is adopted to solve the interfacial crack problem under thermal loading for the first time. Consideration of the size effect can remove the stress singularities at the crack tips. Nonlocal characteristic length is vitally important in determining the peak values of thermal stresses and their locations in the vicinity of crack tips.

There exist some limitations of this thesis because of the theoretical nature of the work. The mathematical modelling cannot solve the problems with complex geometries, which may be common in engineering applications. As to chapter 6, although Schmidt method gives accurate thermal stresses, it takes much more computation time than the method employed in solving the singular integral equation. In order to build the transient thermoelastic fracture model based on nonlocal theory, it is necessary to develop a more efficient method.

## **7.2 Future Perspectives**

For the investigations of thermoelastic analysis in cracked media, due to the fact that crack would always disturb both the thermal fields and stress fields, the pure mathematical models cannot solve the problems with complex geometry. With many devices are downsized to micro- and nanoscale as well as increasing applications of soft materials, the coupled problem of non-Fourier heat conduction, nonlocal effect and time-dependent rheological process would be strongly nonlinear. Besides, some material properties, such as thermal conductivity, are temperature-dependent, which further increases the mathematical difficulty in theoretical modeling. Combination of theoretical work with some numerical simulations would be the focus of future work. In particular, the emerging peridynamics which considers the nonlocal effect and models the continuous body by discrete particles, would be very promising in dealing with small-sized, thermoelastic analysis and fracture mechanics involving large deformations and multiphase composites.

## References

1. Manson, S.S., 1953. *Behavior of materials under conditions of thermal stress* (Vol. 2933). National Advisory Committee for Aeronautics.
2. Praveen, G.N. and Reddy, J.N., 1998. Nonlinear transient thermoelastic analysis of functionally graded ceramic-metal plates. *International journal of solids and structures*, 35(33), pp.4457-4476.
3. Kingery, W.D., 1955. Factors affecting thermal stress resistance of ceramic materials. *Journal of the American Ceramic Society*, 38(1), pp.3-15.
4. Noda, N. and Jin, Z.H., 1993. Steady thermal stresses in an infinite nonhomogeneous elastic solid containing a crack. *Journal of Thermal stresses*, 16(2), pp.181-196.
5. Jin, Z.H. and Noda, N., 1993. An internal crack parallel to the boundary of a nonhomogeneous half plane under thermal loading. *International Journal of Engineering Science*, 31(5), pp.793-806.
6. Jin, Z.H. and Noda, N., 1994. Transient thermal stress intensity factors for a crack in a semi-infinite plate of a functionally gradient material. *International journal of solids and structures*, 31(2), pp.203-218.
7. Noda, N. and Jin, Z.H., 1993. Thermal stress intensity factors for a crack in a strip of a functionally gradient material. *International Journal of Solids and Structures*, 30(8), pp.1039-1056.
8. Jin, Z.H. and Noda, N., 1994. Edge crack in a nonhomogeneous half plane under thermal loading. *Journal of thermal stresses*, 17(4), pp.591-599.
9. Noda, N., Yasuhiro, M. and Hiroshi, N., 1990. Coupled thermoplastic problem of an infinite solid containing a penny-shaped crack. *International journal of engineering science*, 28(4), pp.347-353.
10. Nied, H.F. and Erdogan, F., 1983. Transient thermal stress problem for a circumferentially cracked hollow cylinder. *Journal of Thermal Stresses*, 6(1), pp.1-14.
11. Nabavi, S.M. and Ghajar, R., 2010. Analysis of thermal stress intensity factors for cracked cylinders using weight function method. *International Journal of Engineering Science*, 48(12), pp.1811-1823.
12. Wang, B.L., Han, J.C. and Du, S.Y., 2000. Crack problems for functionally graded materials under transient thermal loading. *Journal of thermal stresses*, 23(2), pp.143-168.
13. Bao, G. and Wang, L., 1995. Multiple cracking in functionally graded ceramic/metal coatings. *International Journal of Solids and Structures*, 32(19), pp.2853-2871.
14. Ueda, S., 2003. Thermally induced fracture of a piezoelectric laminate with a crack normal to interfaces. *Journal of Thermal Stresses*, 26(4), pp.311-331.
15. Ueda, S., 2006. Thermal stress intensity factors for a normal crack in a piezoelectric material strip. *Journal of Thermal Stresses*, 29(12), pp.1107-1125.
16. Ueda, S., 2007. Thermal intensity factors for a parallel crack in a functionally graded piezoelectric strip. *Journal of Thermal Stresses*, 30(4), pp.321-342.
17. Ueda, S., 2007. Effects of crack surface conductance on intensity factors for a functionally graded piezoelectric material under thermal load. *Journal of Thermal Stresses*, 30(7), pp.731-752.

18. Ueda, S., 2006. Transient response of a cracked piezoelectric strip under thermoelectric loading. *Journal of Thermal Stresses*, 29(10), pp.973-994.
19. Ueda, S., 2006. The crack problem in piezoelectric strip under thermoelectric loading. *Journal of Thermal Stresses*, 29(4), pp.295-316.
20. Tzou, D.Y., 2014. *Macro-to microscale heat transfer: the lagging behavior*. John Wiley & Sons.
21. Tzou, D.Y., 1995. The generalized lagging response in small-scale and high-rate heating. *International Journal of Heat and Mass Transfer*, 38(17), pp.3231-3240.
22. Tzou, D.Y., 1995. Experimental support for the lagging behavior in heat propagation. *Journal of Thermophysics and Heat Transfer*, 9(4), pp.686-693.
23. Joseph, D.D. and Preziosi, L., 1989. Heat waves. *Reviews of Modern Physics*, 61(1), p.41.
24. Peshkov, V.P., 1960. Second sound in helium II. *Sov. Phys. JETP*, 11, p.580.
25. Narayanamurti, V. and Dynes, R.C., 1972. Observation of second sound in bismuth. *Physical Review Letters*, 28(22), p.1461.
26. Brorson, S.D., Fujimoto, J.G. and Ippen, E.P., 1987. Femtosecond electronic heat-transport dynamics in thin gold films. *Physical Review Letters*, 59(17), p.1962.
27. Cattaneo, C., 1958. A form of heat-conduction equations which eliminates the paradox of instantaneous propagation. *Comptes Rendus*, 247, p.431.
28. Vernotte, P., 1961. Some possible complications in the phenomena of thermal conduction. *Compte Rendus*, 252(1), pp.2190-2191.
29. Ezzat, M.A. and El-Karamany, A.S., 2012. Fractional thermoelectric viscoelastic materials. *Journal of applied polymer science*, 124(3), pp.2187-2199.
30. Tarasov, V.E. and Aifantis, E.C., 2019. On fractional and fractal formulations of gradient linear and nonlinear elasticity. *Acta Mechanica*, 230(6), pp.2043-2070.
31. Cajić, M., Lazarević, M., Karličić, D., Sun, H. and Liu, X., 2018. Fractional-order model for the vibration of a nanobeam influenced by an axial magnetic field and attached nanoparticles. *Acta Mechanica*, 229(12), pp.4791-4815.
32. Atanackovic, T.M. and Pilipovic, S., 2018. On a constitutive equation of heat conduction with fractional derivatives of complex order. *Acta Mechanica*, 229(3), pp.1111-1121.
33. Mainardi, F., 1996. Fractional relaxation-oscillation and fractional diffusion-wave phenomena. *Chaos, Solitons & Fractals*, 7(9), pp.1461-1477.
34. Povstenko, Y.Z., 2004. Fractional heat conduction equation and associated thermal stress. *Journal of Thermal Stresses*, 28(1), pp.83-102.
35. Sherief, H.H., El-Sayed, A.M.A. and El-Latif, A.A., 2010. Fractional order theory of thermoelasticity. *International Journal of Solids and structures*, 47(2), pp.269-275.
36. Ezzat, M.A. and El Karamany, A.S., 2011. Theory of fractional order in electro-thermoelasticity. *European Journal of Mechanics-A/Solids*, 30(4), pp.491-500.

37. Ezzat, M.A., 2011. Thermoelectric MHD with modified Fourier's law. *International journal of thermal sciences*, 50(4), pp.449-455.
38. Akbarzadeh, A.H., Cui, Y. and Chen, Z.T., 2017. Thermal wave: from nonlocal continuum to molecular dynamics. *RSC advances*, 7(22), pp.13623-13636.
39. Caponetto, R., Sapuppo, F., Tomasello, V., Maione, G. and Lino, P., 2016. Fractional-order identification and control of heating processes with non-continuous materials. *Entropy*, 18(11), p.398.
40. Ezzat, M.A., El-Karamany, A.S. and Ezzat, S.M., 2012. Two-temperature theory in magneto-thermoelasticity with fractional order dual-phase-lag heat transfer. *Nuclear Engineering and Design*, 252, pp.267-277.
41. Huan-Ying, X. and Xiao-Yun, J., 2015. Time fractional dual-phase-lag heat conduction equation. *Chinese Physics B*, 24(3), p.034401.
42. Wu, Q., Volinsky, A.A., Qiao, L. and Su, Y., 2015. Surface effects on static bending of nanowires based on non-local elasticity theory. *Progress in Natural Science: Materials International*, 25(5), pp.520-524.
43. Guyer, R.A. and Krumhansl, J.A., 1966. Solution of the linearized phonon Boltzmann equation. *Physical Review*, 148(2), p.766.
44. Guyer, R.A. and Krumhansl, J.A., 1966. Thermal conductivity, second sound, and phonon hydrodynamic phenomena in nonmetallic crystals. *Physical Review*, 148(2), p.778.
45. Cao, B.Y. and Guo, Z.Y., 2007. Equation of motion of a phonon gas and non-Fourier heat conduction. *Journal of Applied Physics*, 102(5), p.053503.
46. Xu, M., 2018. A non-local constitutive model for nano-scale heat conduction. *International Journal of Thermal Sciences*, 134, pp.594-600.
47. Xu, M., 2019. Nonlocal heat conduction in suspended graphene. *Physics Letters A*, 383(36), p.126017.
48. Yu, Y.J., Tian, X.G. and Xiong, Q.L., 2016. Nonlocal thermoelasticity based on nonlocal heat conduction and nonlocal elasticity. *European Journal of Mechanics-A/Solids*, 60, pp.238-253.
49. Yu, Y.J., Li, C.L., Xue, Z.N. and Tian, X.G., 2016. The dilemma of hyperbolic heat conduction and its settlement by incorporating spatially nonlocal effect at nanoscale. *Physics Letters A*, 380(1-2), pp.255-261.
50. Tzou, D.Y., 2011. Nonlocal behavior in phonon transport. *International Journal of Heat and Mass Transfer*, 54(1-3), pp.475-481.
51. Tzou, D.Y. and Guo, Z.Y., 2010. Nonlocal behavior in thermal lagging. *International Journal of Thermal Sciences*, 49(7), pp.1133-1137.
52. Christensen, R., 2012. *Theory of viscoelasticity: an introduction*. Elsevier.
53. Cheng, Z.Q., Meguid, S.A. and Zhong, Z., 2010. Thermo-mechanical behavior of a viscoelastic FGMs coating containing an interface crack. *International journal of fracture*, 164(1), pp.15-29.
54. Ezzat, M.A., El-Karamany, A.S. and El-Bary, A.A., 2014. Generalized thermo-viscoelasticity with memory-dependent derivatives. *International Journal of Mechanical Sciences*, 89, pp.470-475.
55. Ezzat, M.A., El-Karamany, A.S. and El-Bary, A.A., 2015. Thermo-viscoelastic materials with fractional relaxation operators. *Applied Mathematical Modelling*, 39(23-24), pp.7499-7512.

56. Li, C., Guo, H., Tian, X. and He, T., 2019. Generalized thermoviscoelastic analysis with fractional order strain in a thick viscoelastic plate of infinite extent. *Journal of Thermal Stresses*, 42(8), pp.1051-1070.
57. Ezzat, M.A. and El-Bary, A.A., 2017. On thermo-viscoelastic infinitely long hollow cylinder with variable thermal conductivity. *Microsystem Technologies*, 23(8), pp.3263-3270.
58. Odegard, G.M., Gates, T.S., Nicholson, L.M. and Wise, K.E., 2002. Equivalent-continuum modeling of nanostructured materials. *Composites Science and Technology*, 62(14), pp.1869-1880.
59. Wang, L. and Hu, H., 2005. Flexural wave propagation in single-walled carbon nanotubes. *Physical Review B*, 71(19), p.195412.
60. Kambali, P.N., Nikhil, V.S. and Pandey, A.K., 2017. Surface and nonlocal effects on response of linear and nonlinear NEMS devices. *Applied Mathematical Modelling*, 43, pp.252-267.
61. Yu, Y.J., Xue, Z.N., Li, C.L. and Tian, X.G., 2016. Buckling of nanobeams under nonuniform temperature based on nonlocal thermoelasticity. *Composite Structures*, 146, pp.108-113.
62. Li, X.F., Zhang, H. and Lee, K.Y., 2014. Dependence of Young' s modulus of nanowires on surface effect. *International Journal of Mechanical Sciences*, 81, pp.120-125.
63. Peddieson, J., Buchanan, G.R. and McNitt, R.P., 2003. Application of nonlocal continuum models to nanotechnology. *International Journal of Engineering Science*, 41(3-5), pp.305-312.
64. Aria, A.I. and Biglari, H., 2018. Computational vibration and buckling analysis of microtubule bundles based on nonlocal strain gradient theory. *Applied Mathematics and Computation*, 321, pp.313-332.
65. Eringen, A.C., 1972. Nonlocal polar elastic continua. *International journal of engineering science*, 10(1), pp.1-16.
66. Eringen, A.C. and Edelen, D.G.B., 1972. On nonlocal elasticity. *International Journal of Engineering Science*, 10(3), pp.233-248.
67. Hutchinson, J.W. and Fleck, N., 1997. Strain gradient plasticity. *Advances in applied mechanics*, 33, pp.295-361.
68. Lam, D.C., Yang, F., Chong, A.C.M., Wang, J. and Tong, P., 2003. Experiments and theory in strain gradient elasticity. *Journal of the Mechanics and Physics of Solids*, 51(8), pp.1477-1508.
69. Toupin, R.A., Elastic Materials with Couple-Stresses, *Arch. Ration. Mech. Anal.*, vol. 11, pp. 385–414, 1962.
70. Eringen, A.C., 1983. On differential equations of nonlocal elasticity and solutions of screw dislocation and surface waves. *Journal of applied physics*, 54(9), pp.4703-4710.
71. Li, C., Lai, S.K. and Yang, X., 2019. On the nano-structural dependence of nonlocal dynamics and its relationship to the upper limit of nonlocal scale parameter. *Applied Mathematical Modelling*, 69, pp.127-141.
72. Eringen, A.C., Spziale, C.G. and Kim, B.S., 1977. Crack-tip problem in non-local elasticity. *Journal of the Mechanics and Physics of Solids*, 25(5), pp.339-355.
73. Zhang, Y., Zhang, L.W., Liew, K.M. and Yu, J.L., 2015. Transient analysis of single-layered graphene sheet using the kp-Ritz method and nonlocal elasticity theory. *Applied Mathematics and Computation*, 258, pp.489-501.

74. Xue, Z.N., Yu, Y.J. and Tian, X.G., 2017. Effects of two-temperature parameter and thermal nonlocal parameter on transient responses of a half-space subjected to ramp-type heating. *Waves in Random and Complex Media*, 27(3), pp.440-457.
75. Chang, T.P., 2013. Axial vibration of non-uniform and non-homogeneous nanorods based on nonlocal elasticity theory. *Applied Mathematics and Computation*, 219(10), pp.4933-4941.
76. Eltaher, M.A., Mahmoud, F.F., Assie, A.E. and Meletis, E.I., 2013. Coupling effects of nonlocal and surface energy on vibration analysis of nanobeams. *Applied Mathematics and Computation*, 224, pp.760-774.
77. Eringen, A.C., 1978. Line crack subject to shear. *International Journal of Fracture*, 14(4), pp.367-379.
78. Eringen, A.C., 1979. Line crack subject to antiplane shear. *Engineering Fracture Mechanics*, 12(2), pp.211-219.
79. Zhou, Z.G., Han, J.C. and Du, S.Y., 1999. Investigation of a Griffith crack subject to anti-plane shear by using the non-local theory. *International Journal of Solids and Structures*, 36(26), pp.3891-3901.
80. Zhou, Z.G., Liang, J. and Wu, L.Z., 2006. The nonlocal theory solution of a mode-I crack in functionally graded materials subjected to harmonic stress waves. *Journal of Mechanics of Materials and Structures*, 1(3), pp.447-470.
81. Zhou, Z.G. and Wang, B., 1999. Investigation of a Griffith crack subject to uniform tension using the non-local theory by a new method. *Applied Mathematics and Mechanics*, 20(10), pp.1099-1107.
82. Zhou, Z.G. and Wang, B., 2005. Investigation of the interaction of two collinear cracks in anisotropic elasticity materials by means of the nonlocal theory. *International journal of engineering science*, 43(13-14), pp.1107-1120.
83. Zhou, Z.G. and Wang, B., 2006. Nonlocal theory solution of two collinear cracks in the functionally graded materials. *International journal of solids and structures*, 43(5), pp.887-898.
84. Liu, H.T., Zhou, Z.G. and Pan, S.D., 2015. Non-local theory solution for a 3D rectangular permeable crack in piezoelectric composite materials. *Composite Structures*, 119, pp.513-527.
85. Liu, H.T., Qie, Y.H. and Zhou, Z.G., 2017. Investigation of non-local theory solution to a three-dimensional rectangular permeable crack in magneto-electro-elastic materials. *International Journal of Mechanical Sciences*, 134, pp.460-478.
86. Jamia, N., El-Borgi, S., Rekik, M. and Usman, S., 2014. Investigation of the behavior of a mixed-mode crack in a functionally graded magneto–electro-elastic material by use of the non-local theory. *Theoretical and Applied Fracture Mechanics*, 74, pp.126-142.
87. Jamia, N., El-Borgi, S. and Usman, S., 2016. Non-local behavior of two collinear mixed-mode limited-permeable cracks in a functionally graded piezoelectric medium. *Applied Mathematical Modelling*, 40(11-12), pp.5988-6005.
88. Hoffman, A.S., 2012. Hydrogels for biomedical applications. *Advanced drug delivery reviews*, 64, pp.18-23.
89. Suo, Z., 2010. Theory of dielectric elastomers. *Acta Mechanica Solida Sinica*, 23(6), pp.549-578.

90. Choi, H.J., Lee, K.Y. and Jin, T.E., 1998. Collinear cracks in a layered half-plane with a graded nonhomogeneous interfacial zone—Part I: Mechanical response. *International journal of fracture*, 94(2), pp.103-122.
91. Erdogan, F. and Wu, B.H., 1997. The surface crack problem for a plate with functionally graded properties. *Journal of applied Mechanics*, 64, pp.449-456.
92. Gu, P. and Asaro, R.J., 1997. Cracks in functionally graded materials. *International journal of solids and structures*, 34(1), pp.1-17.
93. Gu, P. and Asaro, R.J., 1997. Crack deflection in functionally graded materials. *International Journal of Solids and Structures*, 34(24), pp.3085-3098.
94. Jin, Z.H. and Batra, R.C., 1996. Some basic fracture mechanics concepts in functionally graded materials. *Journal of the Mechanics and Physics of Solids*, 44(8), pp.1221-1235.
95. Jin, Z.H. and Batra, R.C., 1996. Stress intensity relaxation at the tip of an edge crack in a functionally graded material subjected to a thermal shock. *Journal of Thermal Stresses*, 19(4), pp.317-339.
96. Noda, N. and Jin, Z.H., 1995. Crack-tip singularity fields in nonhomogeneous body under thermal stress fields. *JSME international journal. Ser. A, Mechanics and material engineering*, 38(3), pp.364-369.
97. Guo, L.C. and Noda, N., 2007. Modeling method for a crack problem of functionally graded materials with arbitrary properties—piecewise-exponential model. *International Journal of Solids and Structures*, 44(21), pp.6768-6790.
98. Wang, B.L., Mai, Y.W. and Noda, N., 2002. Fracture mechanics analysis model for functionally graded materials with arbitrarily distributed properties. *International Journal of Fracture*, 116(2), pp.161-177.
99. Alex, R. and Schovanec, L., 1996. An anti-plane crack in a nonhomogeneous viscoelastic body. *Engineering fracture mechanics*, 55(5), pp.727-735.
100. Herrmann, J.M. and Schovanec, L., 1990. Quasi-static mode III fracture in a nonhomogeneous viscoelastic body. *Acta mechanica*, 85(3-4), pp.235-249.
101. Herrmann, J.M. and Schovanec, L., 1994. Dynamic steady-state mode III fracture in a nonhomogeneous viscoelastic body. *Acta mechanica*, 106(1-2), pp.41-54.
102. Schovanec, L. and Walton, J.R., 1987. The quasi-static propagation of a plane strain crack in a power-law inhomogeneous linearly viscoelastic body. *Acta mechanica*, 67(1-4), pp.61-77.
103. Schovanec, L. and Walton, J.R., 1987. The energy release rate for a quasi-static mode I crack in a nonhomogeneous linearly viscoelastic body. *Engineering fracture mechanics*, 28(4), pp.445-454.
104. Paulino, G.H. and Jin, Z.H., 2001. Correspondence principle in viscoelastic functionally graded materials. *J. Appl. Mech.*, 68(1), pp.129-132.
105. Paulino, G.H. and Jin, Z.H., 2001. Viscoelastic functionally graded materials subjected to antiplane shear fracture. *J. Appl. Mech.*, 68(2), pp.284-293.
106. Paulino, G.H. and Jin, Z.H., 2001. A crack in a viscoelastic functionally graded material layer embedded between two dissimilar homogeneous viscoelastic layers—antiplane shear analysis. *International journal of fracture*, 111(3), pp.283-303.

107. Jin, Z.H. and Paulino, G.H., 2002. A viscoelastic functionally graded strip containing a crack subjected to in-plane loading. *Engineering Fracture Mechanics*, 69(14-16), pp.1769-1790.
108. Wang, Z.H., Zhang, L. and Guo, L.C., 2014. A viscoelastic fracture mechanics model for a functionally graded materials strip with general mechanical properties. *European Journal of Mechanics-A/Solids*, 44, pp.75-81.
109. Chen, Z.T. and Hu, K.Q., 2012. Thermo-elastic analysis of a cracked half-plane under a thermal shock impact using the hyperbolic heat conduction theory. *Journal of Thermal Stresses*, 35(4), pp.342-362.
110. Miller, M.K. and Guy, Jr, W.T., 1966. Numerical inversion of the Laplace transform by use of Jacobi polynomials. *SIAM Journal on Numerical Analysis*, 3(4), pp.624-635.
111. Sladek, J., Sladek, V., Zhang, C. and Schanz, M., 2006. Meshless local Petrov-Galerkin method for continuously nonhomogeneous linear viscoelastic solids. *Computational Mechanics*, 37(3), pp.279-289.
112. El-Borgi, S., Erdogan, F. and Hidri, L., 2004. A partially insulated embedded crack in an infinite functionally graded medium under thermo-mechanical loading. *International Journal of Engineering Science*, 42(3-4), pp.371-393.
113. Tamuzs, V., Petrova, V. and Romalis, N., 1996. Plane problem of macro-microcrack interaction taking account of crack closure. *Engineering fracture mechanics*, 55(6), pp.957-967.
114. Petrova, V. and Schmauder, S., 2015. Crack closure effects in thermal fracture of functionally graded/homogeneous bimaterials with systems of cracks. *ZAMM-Journal of Applied Mathematics and Mechanics/Zeitschrift für Angewandte Mathematik und Mechanik*, 95(10), pp.1027-1036.
115. Babaei, M.H. and Chen, Z.T., 2008. Hyperbolic heat conduction in a functionally graded hollow sphere. *International Journal of Thermophysics*, 29(4), pp.1457-1469.
116. Zhou, Y., Li, X. and Yu, D., 2010. A partially insulated interface crack between a graded orthotropic coating and a homogeneous orthotropic substrate under heat flux supply. *International journal of solids and structures*, 47(6), pp.768-778.
117. Maurer, M.J. and Thompson, H.A., 1973. Non-Fourier effects at high heat flux. *Journal of heat transfer*, 95(2), pp.284-286.
118. Chen, Z.T. and Hu, K.Q., 2014. Thermoelastic analysis of a cracked substrate bonded to a coating using the hyperbolic heat conduction theory. *Journal of Thermal Stresses*, 37(3), pp.270-291.
119. Hu, K. and Chen, Z., 2012. Thermoelastic analysis of a partially insulated crack in a strip under thermal impact loading using the hyperbolic heat conduction theory. *International Journal of Engineering Science*, 51, pp.144-160.
120. Chang, D.M. and Wang, B.L., 2012. Transient thermal fracture and crack growth behavior in brittle media based on non-Fourier heat conduction. *Engineering Fracture Mechanics*, 94, pp.29-36.
121. Wang, B.L. and Li, J.E., 2013. Thermal shock resistance of solids associated with hyperbolic heat conduction theory. *Proceedings of the Royal Society A: Mathematical, Physical and Engineering Sciences*, 469(2153), p.20120754.

122. Fu, J., Chen, Z., Qian, L. and Hu, K., 2014. Transient thermoelastic analysis of a solid cylinder containing a circumferential crack using the C–V heat conduction model. *Journal of Thermal Stresses*, 37(11), pp.1324-1345.
123. Wang, B.L., 2013. Transient thermal cracking associated with non-classical heat conduction in cylindrical coordinate system. *Acta Mechanica Sinica*, 29(2), pp.211-218.
124. Zhang, X.Y. and Li, X.F., 2017. Transient thermal stress intensity factors for a circumferential crack in a hollow cylinder based on generalized fractional heat conduction. *International Journal of Thermal Sciences*, 121, pp.336-347.
125. Kaminski, W., 1990. Hyperbolic heat conduction equation for materials with a nonhomogeneous inner structure. *Journal of heat transfer*, 112(3), pp.555-560.
126. Babaei, M.H. and Chen, Z., 2010. Transient hyperbolic heat conduction in a functionally graded hollow cylinder. *Journal of Thermophysics and Heat Transfer*, 24(2), pp.325-330.
127. Keles, I. and Conker, C., 2011. Transient hyperbolic heat conduction in thick-walled FGM cylinders and spheres with exponentially-varying properties. *European Journal of Mechanics-A/Solids*, 30(3), pp.449-455.
128. Eshraghi, I., Soltani, N. and Dag, S., 2018. Hyperbolic heat conduction based weight function method for thermal fracture of functionally graded hollow cylinders. *International Journal of Pressure Vessels and Piping*, 165, pp.249-262.
129. F. Erdogan, "Continuum physics," in *Complex Function Technique*, A. C. Eringen, Ed. vol. 2. New York, NY: Academic Press, 1975, pp. 523–603.
130. Herwig, H. and Beckert, K., 2000. Fourier versus non-Fourier heat conduction in materials with a nonhomogeneous inner structure. *J. Heat Transfer*, 122(2), pp.363-365.
131. Körner, C. and Bergmann, H.W., 1998. The physical defects of the hyperbolic heat conduction equation. *Applied Physics A*, 67(4), pp.397-401.
132. Anisimov, S.I., Kapeliovich, B.L. and Perelman, T.L., 1974. Electron emission from metal surfaces exposed to ultrashort laser pulses. *Zh. Eksp. Teor. Fiz*, 66(2), pp.375-377.
133. Elsayed-Ali, H.E., Norris, T.B., Pessot, M.A. and Mourou, G.A., 1987. Time-resolved observation of electron-phonon relaxation in copper. *Physical Review Letters*, 58(12), p.1212.
134. Liu, K.C. and Chen, H.T., 2009. Analysis for the dual-phase-lag bio-heat transfer during magnetic hyperthermia treatment. *International Journal of Heat and Mass Transfer*, 52(5-6), pp.1185-1192.
135. Othman, M.I., Ezzat, M.A., Zaki, S.A. and El-Karamany, A.S., 2002. Generalized thermo-viscoelastic plane waves with two relaxation times. *International journal of engineering science*, 40(12), pp.1329-1347.
136. Ezzat, M.A. and El-Karamany, A.S., 2003. On uniqueness and reciprocity theorems for generalized thermo-viscoelasticity with thermal relaxation. *Canadian journal of physics*, 81(6), pp.823-833.
137. Ezzat, M.A., Othman, M.I. and El-Karamany, A.S., 2002. State space approach to generalized thermo-viscoelasticity with two relaxation times. *International journal of engineering science*, 40(3), pp.283-302.
138. Othman, M.I. and Song, Y., 2008. Effect of rotation on plane waves of generalized electro-magneto-thermoviscoelasticity with two relaxation times. *Applied Mathematical Modelling*, 32(5), pp.811-825.

139. Ezzat, M.A., El-Karamany, A.S. and El-Bary, A.A., 2015. On thermo-viscoelasticity with variable thermal conductivity and fractional-order heat transfer. *International Journal of Thermophysics*, 36(7), pp.1684-1697.
140. Zhang, X.Y., Chen, Z.T. and Li, X.F., 2018. Thermal shock fracture of an elastic half-space with a subsurface penny-shaped crack via fractional thermoelasticity. *Acta Mechanica*, 229(12), pp.4875-4893.
141. Han, Y., Yang, Y., Li, B. and Feng, Z., 1995. Temperature and strain-rate dependence of fracture toughness of phenolphthalein polyether ketone. *Journal of materials science*, 30(14), pp.3658-3661.
142. Lim, W.W. and Mizumachi, H., 1995. Fracture toughness of adhesive joints. II. Temperature and rate dependencies of mode I fracture toughness and adhesive tensile strength. *Journal of applied polymer science*, 57(1), pp.55-61.
143. Araki, W., Shintaku, H., Ohashi, H., Horiuchi, Y. and Arai, Y., 2011. Temperature dependence and fracture criterion of mixed mode I/II fracture toughness of phenolic resin for friction material. *Journal of Applied Polymer Science*, 121(4), pp.2301-2309.
144. Rukolaine, S.A., 2014. Unphysical effects of the dual-phase-lag model of heat conduction. *International Journal of Heat and Mass Transfer*, 78, pp.58-63.
145. Shen, B. and Zhang, P., 2008. Notable physical anomalies manifested in non-Fourier heat conduction under the dual-phase-lag model. *International Journal of Heat and Mass Transfer*, 51(7-8), pp.1713-1727.
146. Wang, M., Yang, N. and Guo, Z.Y., 2011. Non-Fourier heat conductions in nanomaterials. *Journal of Applied Physics*, 110(6), p.064310.
147. Hu, K.Q. and Chen, Z.T., 2013. Transient heat conduction analysis of a cracked half-plane using dual-phase-lag theory. *International Journal of Heat and Mass Transfer*, 62, pp.445-451.
148. Tzou, D.Y., 1990. The singular behavior of the temperature gradient in the vicinity of a macrocrack tip. *International journal of heat and mass transfer*, 33(12), pp.2625-2630.
149. Delale, F. and Erdogan, F., 1979. Effect of transverse shear and material orthotropy in a cracked spherical cap. *International Journal of solids and structures*, 15(12), pp.907-926.
150. I.S. Gradshteyn, I.M. Ryzhik. Tables of integrals, series and product. New York, 1965
151. Kuang, Z.B., 2014. Discussions on the temperature wave equation. *International Journal of Heat and Mass Transfer*, 71, pp.424-430.
152. Antaki, P.J., 2005. New interpretation of non-Fourier heat conduction in processed meat. *Journal of Heat Transfer*, 127(2), pp.189-193.
153. Mingo, N., 2003. Calculation of Si nanowire thermal conductivity using complete phonon dispersion relations. *Physical Review B*, 68(11), p.113308.
154. Asheghi, M., Leung, Y.K., Wong, S.S. and Goodson, K.E., 1997. Phonon-boundary scattering in thin silicon layers. *Applied Physics Letters*, 71(13), pp.1798-1800.
155. Ju, Y.S. and Goodson, K.E., 1999. Phonon scattering in silicon films with thickness of order 100 nm. *Applied Physics Letters*, 74(20), pp.3005-3007.
156. Liu, W. and Asheghi, M., 2004. Phonon-boundary scattering in ultrathin single-crystal silicon layers. *Applied Physics Letters*, 84(19), pp.3819-3821.

157. Ju, Y.S., 2005. Phonon heat transport in silicon nanostructures. *Applied Physics Letters*, 87(15), p.153106.
158. Flik, M.I. and Tien, C.L., 1990. Size effect on the thermal conductivity of high-Tc thin-film superconductors. *Journal of Heat Transfer*, 112, pp.872-881.
159. McGaughey, A.J., Landry, E.S., Sellan, D.P. and Amon, C.H., 2011. Size-dependent model for thin film and nanowire thermal conductivity. *Applied Physics Letters*, 99(13), p.131904.
160. Majumdar, A.S.M.E., 1993. Microscale heat conduction in dielectric thin films. *Journal of Heat Transfer*, 115, pp.7-16.
161. Ma, Y., 2012. Size-dependent thermal conductivity in nanosystems based on non-Fourier heat transfer. *Applied Physics Letters*, 101(21), p.211905.
162. Li, D., Wu, Y., Kim, P., Shi, L., Yang, P. and Majumdar, A., 2003. Thermal conductivity of individual silicon nanowires. *Applied Physics Letters*, 83(14), pp.2934-2936.
163. Jeong, C., Datta, S. and Lundstrom, M., 2012. Thermal conductivity of bulk and thin-film silicon: A Landauer approach. *Journal of Applied Physics*, 111(9), p.093708.
164. Dames, C. and Chen, G., 2004. Theoretical phonon thermal conductivity of Si/Ge superlattice nanowires. *Journal of Applied Physics*, 95(2), pp.682-693.
165. Brancik, L., 1999, November. Programs for fast numerical inversion of Laplace transforms in MATLAB language environment. In *Proceedings of the 7th Conference MATLAB*(Vol. 99, pp. 27-39). Czech Republic Prague.
166. Ezzat, M.A. and El-Karamany, A.S., 2003. The relaxation effects of the volume properties of viscoelastic material in generalized thermoelasticity. *International journal of engineering science*, 41(19), pp.2281-2298.
167. Dong, Z.L., Khor, K.A. and Gu, Y.W., 1999. Microstructure formation in plasma-sprayed functionally graded NiCoCrAlY/yttria-stabilized zirconia coatings. *Surface and Coatings Technology*, 114(2-3), pp.181-186.
168. Kokini, K., DeJonge, J., Rangaraj, S. and Beardsley, B., 2002. Thermal shock of functionally graded thermal barrier coatings with similar thermal resistance. *Surface and Coatings Technology*, 154(2-3), pp.223-231.
169. Ghannadpour, S.A.M., Karimi, M. and Tornabene, F., 2019. Application of plate decomposition technique in nonlinear and post-buckling analysis of functionally graded plates containing crack. *Composite Structures*, 220, pp.158-167.
170. Gayen, D., Tiwari, R. and Chakraborty, D., 2019. Static and dynamic analyses of cracked on functionally graded structural components: A review. *Composites Part B: Engineering*, p.106982.
171. Sedighi, H.M., Keivani, M. and Abadyan, M., 2015. Modified continuum model for stability analysis of asymmetric FGM double-sided NEMS: corrections due to finite conductivity, surface energy and nonlocal effect. *Composites Part B: Engineering*, 83, pp.117-133.
172. Erdogan, F., 1998. Interface cracking of FGM coatings under steady-state heat flow. *Engineering Fracture Mechanics*, 59(3), pp.361-380.
173. Jin, Z.H., 2004. Effect of thermal property gradients on the edge cracking in a functionally graded coating. *Surface and Coatings Technology*, 179(2-3), pp.210-214.

174. Rangaraj, S. and Kokini, K., 2003. Multiple surface cracking and its effect on interface cracks in functionally graded thermal barrier coatings under thermal shock. *J. Appl. Mech.*, 70(2), pp.234-245.
175. Yildirim, B.O.R.A., Dag, S. and Erdogan, F., 2005. Three dimensional fracture analysis of FGM coatings under thermomechanical loading. *International journal of Fracture*, 132(4), pp.371-397.
176. Jin, Z.H. and Feng, Y.Z., 2008. Thermal fracture resistance of a functionally graded coating with periodic edge cracks. *Surface and Coatings Technology*, 202(17), pp.4189-4197.
177. Choi, H.J. and Paulino, G.H., 2010. Interfacial cracking in a graded coating/substrate system loaded by a frictional sliding flat punch. *Proceedings of the Royal Society A: Mathematical, Physical and Engineering Sciences*, 466(2115), pp.853-880.
178. Isaksson, P. and Hägglund, R., 2009. Structural effects on deformation and fracture of random fiber networks and consequences on continuum models. *International Journal of Solids and Structures*, 46(11-12), pp.2320-2329.
179. Chang, D.M. and Wang, B.L., 2015. Surface thermal shock cracking of a semi-infinite medium: a nonlocal analysis. *Acta Mechanica*, 226(12), pp.4139-4147.
180. Aifantis, E.C., 1992. On the role of gradients in the localization of deformation and fracture. *International Journal of Engineering Science*, 30(10), pp.1279-1299.
181. Zhou, Z.G., Du, S.Y. and Wu, L.Z., 2007. Investigation of anti-plane shear behavior of a Griffith permeable crack in functionally graded piezoelectric materials by use of the non-local theory. *Composite structures*, 78(4), pp.575-583.
182. Zhou, Z.G., Zhang, P.W. and Wu, L.Z., 2007. Investigation of the behavior of a mode-I crack in functionally graded materials by non-local theory. *International journal of engineering science*, 45(2-8), pp.242-257.
183. El-Borgi, S., Erdogan, F. and Hatira, F.B., 2003. Stress intensity factors for an interface crack between a functionally graded coating and a homogeneous substrate. *International Journal of Fracture*, 123(3-4), pp.139-162.
184. Erdogan, F. and Wu, B.H., 1996. Crack problems in FGM layers under thermal stresses. *Journal of thermal stresses*, 19(3), pp.237-265.